

NAGW-1905  
IN-46-CR  
©OVERRIDE-  
154691  
p- 114

LOW-FREQUENCY SOURCE PARAMETERS  
OF TWELVE LARGE EARTHQUAKES

by

PAOLO HARABAGLIA

Laurea in Scienze Geologiche  
Universita' degli Studi di Trieste - Italy  
(1987)

Submitted to the Department of Earth,  
Atmospheric and Planetary Sciences  
in Partial Fulfillment of the Requirements  
for the Degree of

MASTER OF SCIENCE  
in Geophysics  
at the

Massachusetts Institute of Technology

June 1993

© Massachusetts Institute of Technology 1993  
All rights reserved.

N93-25202

Unclas

G3/46 0154691

(NASA-CR-192806) LOW-FREQUENCY  
SOURCE PARAMETERS OF TWELVE LARGE  
EARTHQUAKES M.S. Thesis (MIT)  
114 p

Signature of Author

Department of Earth, Atmospheric and Planetary

March 15, 1993

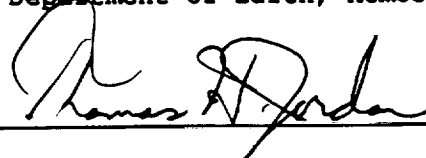
Certified by



Professor Thomas H. Jordan

Department of Earth, Atmospheric and Planetary Sciences  
Thesis Supervisor

Accepted by



Professor Thomas H. Jordan  
Department Head



LOW-FREQUENCY SOURCE PARAMETERS  
OF TWELVE LARGE EARTHQUAKES

by

PAOLO HARABAGLIA

Submitted to the Department of Earth,  
Atmospheric and Planetary Sciences on March 15, 1993  
in partial fulfillment of the requirements  
for the Degree of Master of Science  
in Geophysics

ABSTRACT

This thesis is part of a larger study by the author, P. Ihmle and T. Jordan toward a global survey of the low-frequency (1-21 mHz) source characteristics of large events. We are particularly interested in events unusually enriched in low-frequency and in events with a short-term slow precursor (Jordan, 1991).

We model the source time function of 12 large earthquakes using teleseismic data at low frequency. For each event we retrieve the source amplitude spectrum in the frequency range between 1 and 21 mHz with the Silver and Jordan method (Silver and Jordan, 1982) and the phase-shift spectrum in the frequency range between 1 and 11 mHz with the Riedesel and Jordan method (Riedesel et al., 1986). We then model the source time function by fitting the two spectra.

Two of these events, the 1980 Irpinia, Italy, and the 1983 Akita-Oki, Japan, are shallow-depth complex events that took place on multiple faults. In both cases the source time function has a length of about 100 seconds. By comparison Westaway and Jackson (1987) find 45 seconds for the Irpinia event and Houston and Kanamori (1986) about 50 seconds for the Akita-Oki earthquake.

The three deep events and four of the seven intermediate-depth events are fast rupturing earthquakes. A single pulse is sufficient to model the source spectra in the frequency range of our interest. Two other intermediate-depth events have slower rupturing processes, characterized by a continuous energy release lasting for about 40 seconds.

The last event is the intermediate-depth 1983 Peru-Ecuador earthquake. It was first recognized as a precursive event by Jordan (1991). We model it with a smooth rupturing process starting about 2 minutes before the high frequency origin time superimposed to an impulsive source.

Thesis Supervisor : Dr. Thomas H. Jordan  
Title: Robert R. Schrock Professor of Earth and Planetary Sciences and  
Department Head



## ACKNOWLEDGMENTS

The temptation would be to remember everybody I met here in America and this is an almost impossible task. I will limit myself to those with whom I worked closely. I owe a large part of my results to Pierre Ihmle, my best friend for the past three years. I also have a large debt with Tom Jordan who has given me the opportunity to live and learn in a vibrant place like MIT. Finally I want to remember Beverly Kozol-Tattenbaum who has always given me easy access to a very busy Tom Jordan and has tried to help me as much as she could.



To my staunchest supporter, my father.





## TABLE OF CONTENTS

<b>ABSTRACT</b>	<b>3</b>
<b>ACKNOWLEDGMENTS</b>	<b>5</b>
<b>DEDICATION</b>	<b>7</b>
<b>TABLE OF CONTENTS</b>	<b>9</b>
<b>1 - INTRODUCTION</b>	<b>11</b>
<b>2 - THEORY</b>	<b>15</b>
2.1 INTRODUCTION	15
2.2 SOURCE PARAMETERIZATION	15
2.3 PHASE-DELAY AND AMPLITUDE SPECTRA	16
2.4 THE RIEDESEL AND JORDAN METHOD	18
2.5 THE SILVER AND JORDAN METHOD	21
2.6 SYNTHETIC GREEN FUNCTIONS AND EARTH MODELS	22
2.7 CENTROID DEPTH	23
2.8 SOURCE MODELING	24
<b>3 - DATA EDITING AND OPTIMIZATION</b>	<b>27</b>
3.1 INTRODUCTION	27
3.2 DATA EDITING	28

3.3 DATA DETIDING	30
3.4 DATA OPTIMIZATION	30
<b>4 - SOUTH-EAST ASIA AND PACIFIC</b>	<b>35</b>
4.1 EVENTS DISCUSSION	35
<b>5 - JAPAN</b>	<b>49</b>
5.1 EVENTS DISCUSSION	49
<b>6 - PERU</b>	<b>55</b>
6.1 INTRODUCTION	55
6.2 INFLUENCE OF EARTH AND Q MODELS	55
6.3 THE 1989/12/03 PERU-BRAZIL EARTHQUAKE	56
6.4 THE 1986/11/23 PERU-ECUADOR EARTHQUAKE	57
6.5 THE 1983/04/12 PERU-ECUADOR EARTHQUAKE	58
<b>7 - IRPINIA, ITALY</b>	<b>77</b>
7.1 EVENT DISCUSSION	77
<b>8 - DISCUSSION</b>	<b>87</b>
8.1 PARAMETERS REVIEW	87
8.2 EVENTS REVIEW	88
8.3 METHOD ASSESSMENT	89
<b>REFERENCES</b>	<b>95</b>
<b>APPENDIX</b>	<b>99</b>

## CHAPTER 1 - INTRODUCTION

Most earthquakes are relatively fast rupturing events with rupture velocity greater than 1 km/s, and broadband methods with optimal frequency range between 15 mHz and 1 Hz are adequate to study them. However there are events, enriched in low-frequency, that are known to be slow-rupturing earthquakes (e.g. Beroza and Jordan, 1990; Kanamori and Stewart, 1976; Okal and Stewart, 1982). We are interested in investigating the properties of these events and to do so we need to study their source spectra at very low frequency. "Broad-band" time domain methods normally have a practical lower limit of about 10 mHz. The use of appropriate spectral techniques allows us to lower this limit to 1 mHz. In this thesis we present the source characteristics of a set of 12 events in the frequency range between 1 and 11 mHz. We extend our analysis up to about 20 mHz to provide a link with studies at higher frequencies.

A spectral anomaly of the kind mentioned above means a large characteristic duration (Silver and Jordan, 1983; Beroza and Jordan, 1990; Jordan, 1991) and this in turn translates into an unusually slow earthquake. If this is the case, the technique developed by Jordan (1991) allows us to assess if the event has a short-term low frequency precursor.

There are many reasons why it is important to focus our attention on this frequency band. Currently we do not really understand some important aspects of the rupture dynamics,

especially the nucleation and the end of the rupture. Many theories have been developed (see for example Scholz 1990) but we still lack a large data-base to categorize the various events according to their geographical and tectonic setting and their source characteristics. If we could distinguish which earthquakes are slow and which are "precursive", in the sense formulated by Jordan (1991), we might gain a better understanding of the source mechanics. The ideal way of studying these processes would be by near-field geodetic methods: unfortunately this is impossible because many events occur either at too great depth or in inaccessible areas, like the oceans. We believe that the best way to gather enough data to improve our knowledge of the rupture is by conducting some global study with teleseismic data. The practical implication of such an approach is that it might also lead to important clues to the unanswered question of which earthquakes are short-term predictable. The idea of a short-term slow precursor large enough to be detected by teleseismic methods is not new; it has been presented, among others, by Kanamori and Cipar (1974), Dziewonski and Gilbert (1974), Cifuentes and Silver (1989). However a group at MIT, comprising the author, P. Ihmle and T. Jordan is applying the methods developed by Jordan (1991) in a first attempt to conduct a global survey. In this thesis we present a subset of 12 events out of the approximately 100 that has been processed up to now at MIT. Most of them are rather fast-rupturing events, but there are some that are slow and one, the intermediate focus event of 12 April 83 along the border between Peru and Ecuador that seems to have a very large precursor. This is not the only precursive event we have

found yet (see, for example, Ihmle et al. 1993) but is the only one we describe in detail in this study.



## CHAPTER 2 - THEORY

### 2.1 INTRODUCTION

Our aim is to investigate the source behavior at frequencies as low as 1 mHz for earthquakes with total moment larger than  $5 \cdot 10^{18}$  N-m.

We use a combination of spectral techniques: we employ the method developed by Riedesel and Jordan (Riedesel et al., 1986; Riedesel and Jordan, 1989) in the frequency band between 1 and 11 mHz and a modified version of the method developed by Silver and Jordan (1982) in the frequency band between 1 and 21 mHz.

### 2.2 SOURCE PARAMETERIZATION

An earthquake is an extremely complex phenomenon. The complete description of it, even in the case of a very simple event, would actually require an enormous (infinite) number of parameters. It is possible however to greatly simplify the parameterization whenever we are interested in describing only a subset of specific characteristics.

If we limit our investigation of the source at sufficiently low-frequencies, we can ignore any space related term altogether as long as we perform a proper spatial average (Silver and Jordan, 1983) and concentrate on the "temporal" aspects of the source. A further simplification is to assume that the orientation of the source mechanism is constant with respect to time. Although this is not

generally true, it is an acceptable approximation as long as we perform a proper spatial average (Silver and Jordan, 1983).

We can conveniently describe such a source by a stress glut of the form  $\Gamma(\mathbf{r}, t) \approx \sqrt{2} M_T^0 \hat{\mathbf{M}} \delta(\mathbf{r} - \mathbf{r}_0) F(t)$  (Jordan 1991), where  $M_T^0$  is the total (static) scalar moment,  $\hat{\mathbf{M}}$  is a time-independent tensor with unit Euclidean norm ( $\hat{\mathbf{M}}:\hat{\mathbf{M}} = 1$ ) representing the source mechanism,  $\mathbf{r}_0$  is the spatial centroid of the stress glut and  $F(t)$  is a scalar-valued moment release function, assumed to be zero prior to a starting time  $t_*$  (one-sided) and non-decreasing for  $t \geq t_*$  (monotone). We assume it monotone to insure that slip reversals are not possible. A further requirement,  $\lim_{t \rightarrow \infty} F(t) = 1$ , is necessary to specify  $M_T^0$ .

### 2.3 PHASE-DELAY AND AMPLITUDE SPECTRA

If we can model an event in the above terms, it is possible to retrieve a series of parameters that will describe some important source features without having to model it. We can in fact infer the total energy release, its time centroid, its characteristic duration, and its skewness.

To retrieve these parameters, we rewrite the source spectrum in the polar form  $f(\omega) = |f(\omega)| e^{-i\phi(\omega)}$ , where the phase is  $\phi(\omega) \equiv \omega \Delta t(\omega)$ . Both the spectral modulus  $|f(\omega)|$  and the phase-delay function  $\Delta t(\omega)$  are real-valued, even functions of frequency and their expansions about zero frequency can be written

$$|f(\omega)| = 1 + f_2 \omega^2 / 2! + \dots + f_{2n} \omega^{2n} / (2n)! + \dots \quad (2.1)$$

$$\Delta t(\omega) = \Delta t_1 + \Delta t_3 \omega^2 / 2! + \dots + \Delta t_{2n+1} \omega^{2n} / (2n)! + \dots \quad (2.2)$$

(Jordan, 1991).



Following Silver and Jordan (1983) and Jordan (1991), we describe the coefficients in (2.1) and (2.2) in terms of polynomial moments. The polynomial moments

$$\mu_p = \int_{t_*}^{\infty} (t - t_*)^p dF(t), \quad p = 0, 1, 2, \dots \quad (2.3)$$

of  $F(t)$  are positive given its non-decreasing property.

By definition,  $\mu_0 = 1$ . The source centroid time is  $t_1 \equiv t_* + \mu_1$ . It follows that the source central moments are defined as

$$\hat{\mu}_p = \int_{t_*}^{\infty} (t - t_1)^p dF(t) \quad (2.4)$$

and are related to the ordinary moments in (2.2) by

$$\mu_p = \sum_{q=0}^p \binom{p}{q} (t_1 - t_*)^{p-q} \hat{\mu}_q. \quad (2.5)$$

The source characteristic duration (Silver and Jordan, 1983) is therefore defined as a function of the second central moment  $\tau_c = 2\hat{\mu}_2^{1/2}$ . Finally, taking into account the third central moment  $\hat{\mu}_3 = \mu_3 - 3(t_1 - t_*)\mu_2 + 2(t_1 - t_*)^3$ , it is possible to measure the source skewness (Jordan, 1991) as  $3t_3 - t_1^3 = -\hat{\mu}_3 + 3t_*\hat{\mu}_2 - \mu_1^3$ . Following Jordan(1991), it is convenient to introduce the skewness parameter  $\alpha \equiv -\frac{3}{2} t_3/t_1^3$ , a dimensionless quantity. Let us assume that the event duration is sufficiently short that the first two terms in (2.1) and (2.2) will dominate the spectral shape out to  $\omega_{max}$ . Let also  $M_T(\omega) \equiv M_T^0 |f(\omega)|$  be the total moment spectrum. It follows from (2.1), that  $M_T^0$  is the spectral value at zero-frequency and the characteristic duration is

given by the spectral curvature at the same zero-frequency. Similarly, from (2.2), it follows that the intercept at zero-frequency will yield the centroid time  $t_1$  and the source skewness will be proportional to the spectral curvature.

## 2.4 THE RIEDESEL AND JORDAN METHOD

We make use of a modified version of a special procedure initially developed by Riedesel et al. (1986) to estimate both  $|f(\omega)|$  and  $\Delta t(\omega)$ . This procedure actually combines two different methods: one introduced by Silver and Jordan (1982, 1983) and the other by Riedesel and Jordan (Riedesel et al., 1986; Riedesel and Jordan, 1989).

The Riedesel and Jordan method allows us to estimate both  $|f(\omega)|$  and  $\Delta t(\omega)$  but is not particularly reliable for  $|f(\omega)|$ . It also gives a good solution for  $\hat{M}(\omega)$ . The frequency range we consider is between 1 and 11 mHz, typically subdivided into ten 1-mHz disjunct bands. We discussed the lower limit in chapter 1. The upper limit is also practical: our ability to properly model surface waves at higher frequencies decreases rapidly because of the greater role of lateral heterogeneities. Since most of the signal in the 1 to 11 mHz band is due to fundamental modes, we compute narrow-band integrals of the complex Fourier spectrum centered at the average eigenfrequency  $\bar{\omega}_k$  of the  $k$ th fundamental spheroidal modes both for observed and synthetic seismograms, the latter computed assuming an a priori mechanism. We multiply the complex conjugate of the synthetic integral times the observed integral and a phase factor  $\exp(i\bar{\omega}_k t)$ , and sum the result over the modes in the 1-mHz bands, usually about 10 modes per band. The maxima of the resulting cross-correlation functions occur at the times

which best equalize, in the least-squares sense, the phase of the data relative to the synthetic. The next step consists in retrieving  $M_T^0 \hat{M}(\omega)$ . We perform this on a band by band basis, inverting the above mentioned integrals with a standard least-square technique. The synthetic integrals are appropriately shifted in time according to the values retrieved during the first step.

The first step yields  $\Delta t(\omega)$  and the second  $|f(\omega)|$  but, as we will see,  $|f(\omega)|$  is normally estimated with a different and more robust method developed by Silver and Jordan (1982, 1983).

The non-linearity in the above mentioned technique is rather weak. In theory we should iterate over the two steps until the solution converges. In practice, if we start from a good initial mechanism, such as the one provided for example by the CMT catalog, there is no need for any iteration. If by any chance, the starting mechanism were unknown, a very simple starting model would do the job in most cases in a maximum of four to five iterations; if it were to fail, we would notice it by the unrealistic time-shifts we would retrieve. Each band would have time-shift jumps of the order of hundreds of seconds due to severe phase skipping problems. A new starting model would be required.

To retrieve the time shift spectrum, we average, band by band, the correlation times obtained in the first step. They can have RMS scatters of the order of 10 seconds or more, mostly due to imperfect modeling of aspherical heterogeneities, but the uncertainty from this effect is substantially reduced by averaging over all the seismograms in the network. It is also noteworthy that since we are dealing with very long wave-periods, we must look at many hours of signal (usually

about six) and consequently the waves can circle the whole earth a couple of times during this interval; this adds to the averaging effect, although it is not as dramatic as averaging over the network, because the first wave trains, less attenuated, carry most of the weight in the solution (on average even orbits surface waves must travel  $180^\circ$  more than odd orbits).

Once retrieved  $\Delta t(\omega)$ , we try to estimate time centroid and source skewness by fitting a standard spectrum that we define, following Jordan (1991), as

$$\Delta t(\omega) = (1 - \alpha) \Delta t_1 + \frac{\alpha}{\omega} \arctan \omega \Delta t_1, \quad 0 \leq \omega \leq \omega_{max} \quad (2.6)$$

If  $\Delta t(\omega)$  increases with frequency, then  $\alpha$  is negative, implying a negative skewness. Conversely if there is a decrease,  $\alpha$  is positive, implying a positive skewness.

The second step of this method yields mechanism and total-moment spectrum. The latter, however, is not particularly satisfactory since the cross-correlation technique does not take into account any portion of the signal that has been dephased by imperfect modeling of the earth. These effects are stronger at higher frequencies and consequently the spectrum could be highly biased by a larger than expected roll-off (Silver and Jordan, 1982).

As stated before, the band by band mechanism is instead a rather reliable measure. By averaging over the best bands we can compute an average moment tensor with a covariance matrix. Then we can use it as source mechanism to compute the total moment spectrum (see next section).

## 2.5 THE SILVER AND JORDAN METHOD

The total moment spectrum,  $M_T(\omega) \equiv M_T^0 |f(\omega)|$  is estimated using a modified version of the procedure developed by Silver and Jordan (1982, 1983). The original method employs values of both power spectra and cross spectra integrated over discrete frequency bands. The integrations are done over disjunct 1-mHz bands. We have recently extended the computation up to 21 mHz. The method is optimized to account for errors introduced by incorrect modeling of the earth structure (mostly aspherical heterogeneities), errors in the assumed source mechanism, and ambient seismic noise. It is noteworthy that this method does not make use of any phase information and is insensitive to biases in  $M_T(\omega)$  introduced by the dephasing of synthetics relative to data by unmodeled path effects. Cross spectra had originally been used together with power spectra because the source mechanism estimates  $\hat{\mathbf{M}}$  available at the time were not as well constrained as they are today. However, since they are fairly sensitive to aspherical heterogeneities, the version of the Silver-Jordan algorithm employed here uses only power spectra integrals. At the time the method was developed, the earth model currently used was 1066 (Gilbert and Dziewonski, 1975). Today better earth models, for example PREM SH8WM13, are available (see next section). By data analysis, we have determined a more appropriate value for the heterogeneities correction parameter. Now it is fixed to 0.2. Following Silver and Jordan (1983) and Riedesel et al. (1986), we recover the zero-frequency parameters  $M_T^0$  and  $\tau_c$  by fitting the observations in the investigated frequency window using a spectrum of the form

$$M_T(\omega) = M_T^0 / (1 + \omega^2 \tau_c^2 / 8) \quad (2.7)$$

Equation (2.7) is consistent with the definition of  $\tau_c$  and implies that  $\hat{\mu}_4 = 6\hat{\mu}_2^2$ . Source time functions of this type have been considered by Aki (1967) and Brune (1970) among others.

The curvature at zero-frequency cannot be negative. If (2.7) adequately describes the amplitude spectrum (see chapter 6), then when  $M_T(\omega)$  is flat, the source is an almost instantaneous process. When conversely the spectrum rolls-off, the source has a longer characteristic duration.

## 2.6 SYNTHETIC GREEN FUNCTIONS AND EARTH MODELS

The earth model we routinely employ is the radially anisotropic PREM (Dziewonski and Anderson, 1981). We compute the green functions using the great circle approximation (Woodhouse and Dziewonski, 1984) and incorporate asymptotic phase corrections generally for SH8WM13 (Woodward et al. 1992). We also routinely compute the green functions for the spherical PREM (Dziewonski and Anderson, 1981), 1066A (Gilbert and Dziewonski, 1975) and Core11, the latter being an unpublished model developed at Scripps (Guy Masters, personal communication). The Q model we normally use is the one of PREM but we also compute synthetics for PREM and PREM SH8WM13 with the QM1 model (Widmer et al., 1991) and a low Q model we made up to have a lower Q comparison term (Fig. 2.1). The reason is that we want to assess the influence of the earth parameterization on the solution. Typically the phase spectrum, the one we obtain with the Riedesel and Jordan method, is influenced mostly

by the choice of the earth model, while the amplitude spectrum, obtained through the Silver and Jordan method, is mostly affected by the  $Q$  model. The higher the  $Q$ , the more the spectrum will roll-off, giving a slower apparent rupture velocity.

Our preferred earth model is PREM SH8WM13. The Riedesel and Jordan method gives an estimate of the quality of the solution expressed as variance reduction. The heterogeneous PREM does not yield a significant improvement at lower frequencies (1-5 mHz) over the other models but gives a better variance reduction at higher frequencies, of the order of 20% over both the spherical PREM and CORE 11 and sometimes even 100% over 1066A.

Our favourite  $Q$  model is PREM, that seems to better represent the true earth  $Q$  in the frame of our investigation. We assess the quality of the  $Q$  model for a given event-network geometry and its influence on the source solution by a sliding time window. If the  $Q$  model is satisfactory, an amplitude spectrum obtained using the first three hours of signal is comparable to the one obtained using the following three hours. If the roll-off of the spectrum increases, it means that  $Q$  is too high and the opposite if it decreases. This also allows us to put a qualitative bound on the effect of the source solution in those cases where the  $Q$  model is not satisfactory.

## 2.7 CENTROID DEPTH

Our technique does not automatically invert for the centroid depth but we can relocate it by systematic search. There are two different way to proceed: Silver and Jordan (1983) showed that the 1977 Sumbawa event amplitude spectrum changed conspicuously by

varying the centroid depth. Their aim was to look for a spectrum that was monotonically decreasing with frequency. A more rigorous assessment comes from the variance reduction between data and synthetic integrals we obtain with the Riedesel and Jordan method. This is particularly advantageous because we can quantify an eventual frequency dependence.

## 2.8 SOURCE MODELING

The above methods do not specifically invert for the time source function. Consequently we also routinely attempt a forward modeling of it. We have found that the model for a source function proposed by Jordan and Frazer (1975)

$$s(a,b,t_*) = \exp [-a/(t-t_*) - (t-t_*)/b] H(t-t_*) \quad (2.8)$$

appropriately describes most of the events we have investigated.  $H$  is the step function,  $a$  is the rise time,  $b$  the decay time. In some of the earthquakes we have studied, the sources are complex and cannot be satisfactorily described by (2.8) alone. In such cases we combine several (2.8), one for each subevent.

There are also earthquakes with slower components. We have found that cosine (Hanning) bells are appropriate to describe such slower episodes.



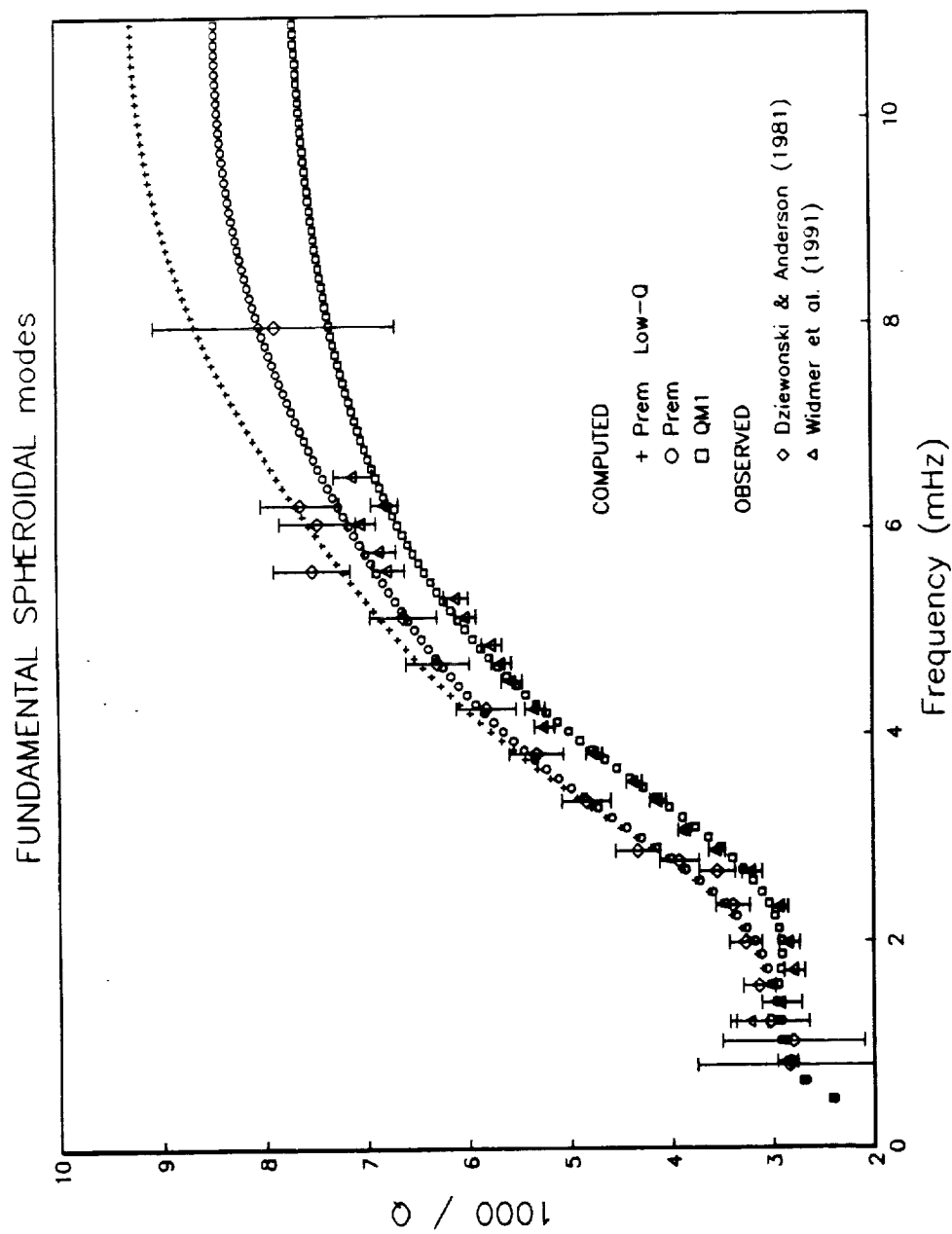


**Fig. 2.1 - Frequency dependence of modal-Q for three different radial Q-models. Only fundamental spheroidal modes up to 11 mHz are shown.**



## CHAPTER 3 - DATA EDITING AND OPTIMIZATION

### 3.1 INTRODUCTION

As previously stated, we employ two different methods, one of which, the Silver and Jordan method, does not make use of any phase information: a correct choice of data becomes of primary concern. This process of selection can be subdivided in two main steps.

The first and most basic one consists in the elimination of non-linearities as well as transient noise since they affect the amplitude spectra in an unpredictable way. To accomplish it, we have developed a complex screening and editing procedure. We try to follow a conservative approach to "clean" the data: interpolation is preferred to "editing out", and "editing out" is preferred to discarding a trace altogether. In this context "editing out" means flagging a certain portion of the signal so that it will not be used throughout the whole inversion procedure.

The second step is in fact intimately related to the inversion itself and consists in selecting the time interval, according to the magnitude of the earthquake, and the traces to be used. Stations that are identified as outliers, usually because of instrument problems, are discarded. This second selection is performed inverting iteratively on the basis of the knowledge acquired in the previous iterations and is probably the most subjective part of the whole procedure.

### 3.2 DATA EDITING

We found that the best way to proceed is first to filter the "raw data" at low frequency, namely with a low-pass butterworth filter with a cut off frequency of 2 mHz and a band-pass cosine filter starting at 0.8 mHz, lower corner frequency of 1 mHz, higher corner frequency of 3 mHz and cutoff at 3.2 mHz. The butterworth-filtered trace gives us a good indication of where any non-linearity starts and ends. The cosine-filtered one shows the effect of the non-linearity on the lower frequency bands and allows for a quick assessment of the signal to noise ratio.

We start to screen out our data looking at all three traces. We discard traces according to the following criteria:

- 1) Traces where the instrument is clearly not working properly.
- 2) Traces where the event is not visible at all.
- 3) Records with high ambient noise, mostly on islands, typically RAR and RPN. For these stations the signal to noise ratio can be so small that the weight of the station in the final solution becomes negligible. A station is discarded under these assumptions if, at most, only R1 is visible on the unfiltered trace and there is no visible signal in the cosine filtered (1-3 mHz) trace.
- 4) The instrument gain is too low (generally some Geoscope stations) and only a few major waveforms are recorded.
- 5) The event induced non-linearity is so strong that most of the signal is lost.
- 6) Near-site induced non-linearities and/or strong red noise are spaced in such a way that it is not possible to have at least four or five hours of uninterrupted signal. They can be in the form of large glitches

spaced by a couple of hours or in the form of low-frequency transient noise lasting many hours (notably in CMO). They are discarded only if a significant effect is visible on the cosine filtered (1-3 mHz) signal.

7) There are too many spikes (typically hundreds over a 48 hours interval). It is easy to pinpoint and eliminate them in the "noise" portion of the trace but not in the "event" part and this could bias our spectral analysis.

Once we have decided to use a trace, we start to process it. The aim is to have a chunk of uninterrupted data, possibly starting at the origin time and whose total length is at least six hours. We first eliminate any event induced non-linearity by editing out from the event origin time up to the end of the non-linearity itself. We have found that to avoid truncation effects, it is better to edit out up to a point where there are no large arrivals both at high and low frequency.

It is also useful to have a segment of data in front of the event to perform the noise analysis. This segment must be comparable in length to the one used in the inversion. Although it is important to perform an accurate noise analysis, there are a series of cases when it is advisable to edit out the noise portion of the trace and use the reference curves instead. This happens when:

- 1) There is some event large enough to alter significantly the spectral characteristics of the noise portion of the record respect to the event one.
- 2) Some instrument related problems (usually mass resets and instrument induced non-linearities) trash the record.

3) There is some strong non-stationary noise. The noise is modulated with a period of the order of 10 or more hours. This case is extremely tricky and if in doubt, its better not to use the trace at all.

Finally we try to clean the trace, interpolating spikes, glitches and even small events. If the interpolation interval becomes too large, more than five minutes, the alternative is editing out. As a rule of the thumb to decide whether to interpolate or edit out, we must remember that our procedure requires a segment of uninterrupted data, ideally for at least six hours. It is preferable to try to interpolate over longer time intervals if the interpolation is at the end of the segment we would like to use, while it is somewhat better to edit out if 1) the portion to be edited out is at the beginning of the segment and 2) the portion immediately preceding it, has already being edited out due to event induced non-linearity.

### 3.3 DATA DETIDING

After editing the data we proceed to remove the tide signature. We do not calculate the tide effect for any given date and any given site but we simply strip the typical tide harmonics from the signal. This operation has the desirable effect that if the elimination of non-linearities has not been carried on properly, it will show up with a kink at the beginning or at the end of the trace. Otherwise the record will have no appreciable harmonic trend.

### 3.4 DATA OPTIMIZATION

The next step is intimately related to the inversion itself and consists in a series of iterations to compute phase-shift and amplitude

spectra. During these iterations we try to identify the various outliers and to optimize the time window over which we perform our inversion.

We start by computing a tentative phase-delay spectrum applying the Riedesel and Jordan method (from here onward RJ) described in chapter 2.4. Our initial mechanism is the CMT one. We obtain a series of time-shifts, one for each station and for each frequency band, as resulting from the cross correlation between data and synthetics. The procedure yields also a band inversion of the moment tensor. Moreover we obtain the individual values of the variance reduction resulting by the inversion, station by station and band by band.

The mechanisms we compute with RJ do not normally show any significant frequency dependent variation. In general the bands with the best variance reduction are the fourth, fifth and sixth. We compute our "best" mechanism by averaging over these bands. It is almost always very similar to the CMT one, so there is no need to iterate, as previously stated in chapter 2.4. In trial cases we have seen that whenever we iterate, the individual time-shifts vary by less than a second and the time-shift spectrum shows no practical difference at all. We also need an input mechanism to compute the amplitude spectrum with the Silver and Jordan method (from here onward SJ) described in chapter 2.5. We might use our "best" mechanism, but for consistency with the phase-delay spectrum we normally prefer to use the CMT one. The SJ method requires also a covariance matrix for the input mechanism and the CMT does not provide one, We construct it on the basis of the one we get computing our solution.

If an earthquake is shallow, the RJ method has difficulty determining  $m_{r\phi}$  and  $m_{r\theta}$  due to the boundary conditions: we have the option of projecting them out (Riedesel and Jordan, 1989).

Certain stations, like RAR or RPN, on average have poor values of variance reduction (about 50%). These are extremely noisy sites, and low values are normal. Similar variance reduction for another higher gain station, would suggest that something is not properly modeled. In such a case we should further investigate the possible cause. If we identify the station as an outlier, we discard it and repeat the whole process. In fact if the data have been properly edited, outliers are rather rare and mostly confined to cases of incorrect instrument response. They can be detected by anomalous pattern in the variance reduction with respect to other stations and by their eventual influence on the amplitude spectra. In the late seventies, for example, the gain for SUR was not properly calibrated. We discovered it when we noticed that whenever we included the station in the inversion the amplitude spectra of various events changed drastically. The RJ inversion moreover had the tendency to fit that record at the expense of the others; its variance reduction was usually above the average. As a counter example the instrument response for the Geoscope station SSB has the opposite problem for most of the eighties. This is easy to identify; the station carries almost no weight in the amplitude spectrum inversion and the variance reduction for this station is extremely poor. The more tricky case is when there is a record that is not properly modeled due to some path effect. This is in general the case of one record out of fifteen. The most usual situation is a case of focusing and defocusing effects. This is not a problem in the



computation of the amplitude spectrum because the SJ method does not make use of any phase information and we select our time window so to have an even number of Rayleigh waves orbits. The time-shift spectrum is seriously affected instead since the individual time-shifts can jump by more than 30 seconds from one band to another; it is always better not to include the station in the computation of this spectrum. Finally there is a very small number of records, about one out of forty, that strongly affects the amplitude spectrum without any apparent reason. If the event is covered by a large number of stations, we simply discard it. If the number of available seismograms is small, eight or nine, and we find one of these records, we do not typically process the event.

In recent years we often have multiple records at various sites (different networks and/or instruments) so it is important to define a selection criterion for each event and apply it to all the duplicates. We give preeminence to the traces with the less amount of truncation. If both traces have similar truncations or no truncation at all, we prefer the IDA instruments over the GDSN and Geoscope stations since they have better characteristics at low frequencies (1-3 mHz).

Another problem we face is the selection of an optimal time window. We normally use six hours after the first good data point but for smaller events we prefer only three hours. A three hours interval roughly covers two Rayleigh waves orbits. It is important to consider an even number of orbits. We must remember that RJ and SJ methods are actually weighting the signal in a different way. The signal treated by SJ is convolved with a Hanning taper, so most of the weight of the solution is carried on by the central portion of the time window. RJ

conversely is mostly controlled by the first good orbit and to a lesser extent by the second one. Other contributions are often insignificant. The choice of three hours versus six is therefore the result of a complex trade-off between signal to noise ratio and amount of truncations, both related to the event size. Smaller events, less than  $1 \cdot 10^{19}$  N-m, have usually fewer truncations but also decay below noise level rather soon. In this case we use three hours. Events larger than  $5 \cdot 10^{19}$  N-m are large enough that we can use our optimal interval of six hours. For events that fall in between, we must weight whether to use the full six hours interval or not, by assessing the signal to noise ratio and the number of traces that are truncated.

Due to the strong ambient noise, the first two frequency bands (1-3 mHz) normally are not distinct for earthquakes below  $1 \cdot 10^{19}$  N-m, and we do not use them. We usually disregard only the first band for earthquakes up to  $3 \cdot 10^{19}$  N-m while we use all the bands for events of more than  $1 \cdot 10^{20}$  N-m. In the range between  $3 \cdot 10^{19}$  and  $1 \cdot 10^{20}$  N-m the situation may vary from event to event. In fact the decision of which band to use is not arbitrary; it comes from the analysis performed by the SJ method that quantifies the correction applied to each band. If the total correction is more than 30 to 40% of the moment in a given band, that band is not particularly meaningful and we do not use it.

In the computation of the phase-delay spectrum we do not consider individual time shifts if they are larger than 30 seconds or if the associated variance reduction is less than 20%. As stated before, we also eliminate stations with strong focusing and defocusing effects.

## CHAPTER 4 - SOUTH-EAST ASIA AND PACIFIC

### 4.1 EVENTS DISCUSSION

The first group of earthquakes we will focus on, comprises six events along the margin between the Indo-Australian and the Pacific Plate. This is a representative subset of a group of 15 events we have investigated in the area up to now. We chose to present only the earthquakes with good azimuthal coverage.

The seismograms used for each earthquake are shown in Appendix. The CMT, NEIC and ISC parameters are reported in Table 8.1. The parameters computed fitting the spectra with (2.6) and (2.7) are shown in Table 8.2. For each event we show a plot with both spectra as obtained by the RJ and SJ methods and the source used to model them (Figs. 4.1-4.6).

Four of the these events are thrust earthquakes, while the other two have a mixed thrust/strike-slip mechanism.

If we consider the scaling relationship between total scalar moment and source duration (Kanamori and Given, 1981), we see that all but one have rather fast rupturing processes, the notable exception being the 29 October 87, Talaud Islands event (Fig. 8.1).

The 23 September 78, New Hebrides earthquake source model has negative  $t_*$  but this is only a numerical artifact induced by the small centroid time-shift. The uncertainty of the time shifts is within a couple of seconds.

The large rise time of the 23 February 87, Vanuatu Islands and the 11 November 83, Banda Sea event are more significant. In both

cases the time centroid values we recover are rather large. For Banda Sea especially, we obtain a value that is almost 5 seconds larger than the CMT. The Vanuatu Islands earthquake is also noteworthy; we improve the residual variance by about 10% if we select the NEIC depth as centroid depth.

The last event we will focus on, is the above mentioned Talaud Islands earthquake. The theoretical spectrum does not provide a good fit to the data. Most of the moment must be released in the first few seconds, to account for the centroid time-shift, but some of the residual moment have to be released by a relatively long lasting coda to account for the large characteristic duration. We chose to model it by superimposing a half cosine (Hanning) bell to (2.8) Moreover also in this case  $t_*$  has negative values due to numerical uncertainties in the model.

type	start	durat.	moment	rise	decay
dbexp	-1.00	31.00	0.17	0.10	4.00

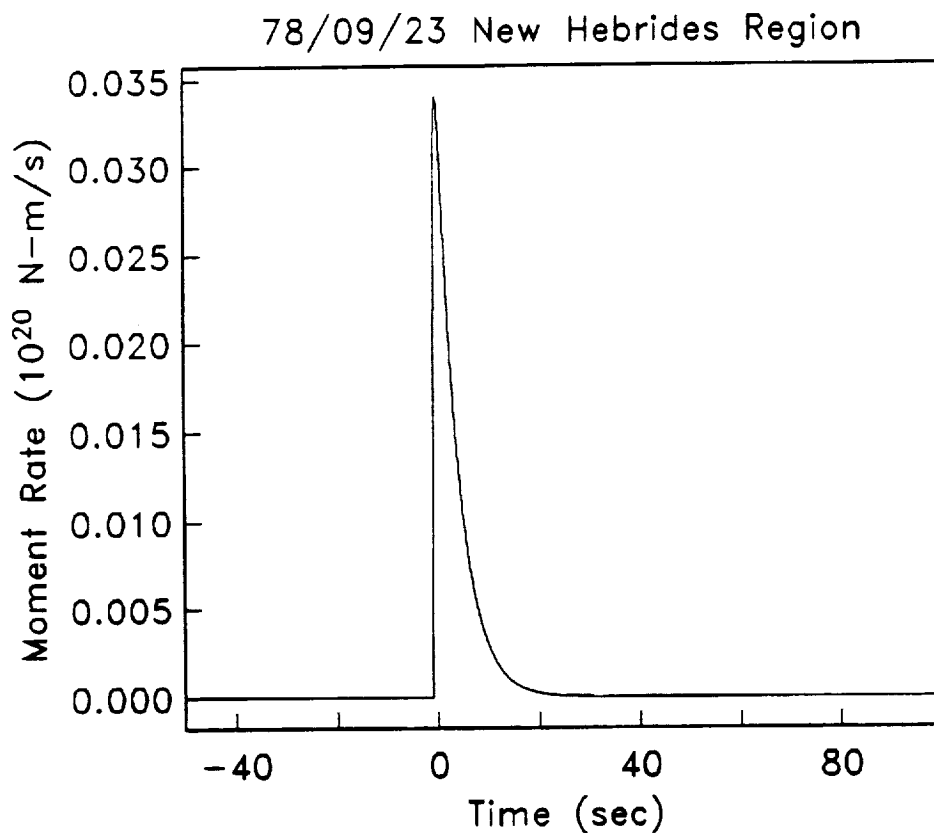


Fig. 4.1 - a) Source model for the 79/09/23 New Hebrides event. b) Amplitude spectra: observed (dots) and modelled (solid line). c) Phase-delay spectra: observed (dots) and modelled (solid line). Error bars represent one standard deviation.  $M_T^0$ ,  $t_1$ ,  $\tau_c$ ,  $\alpha$  are computed from the source time function in a)

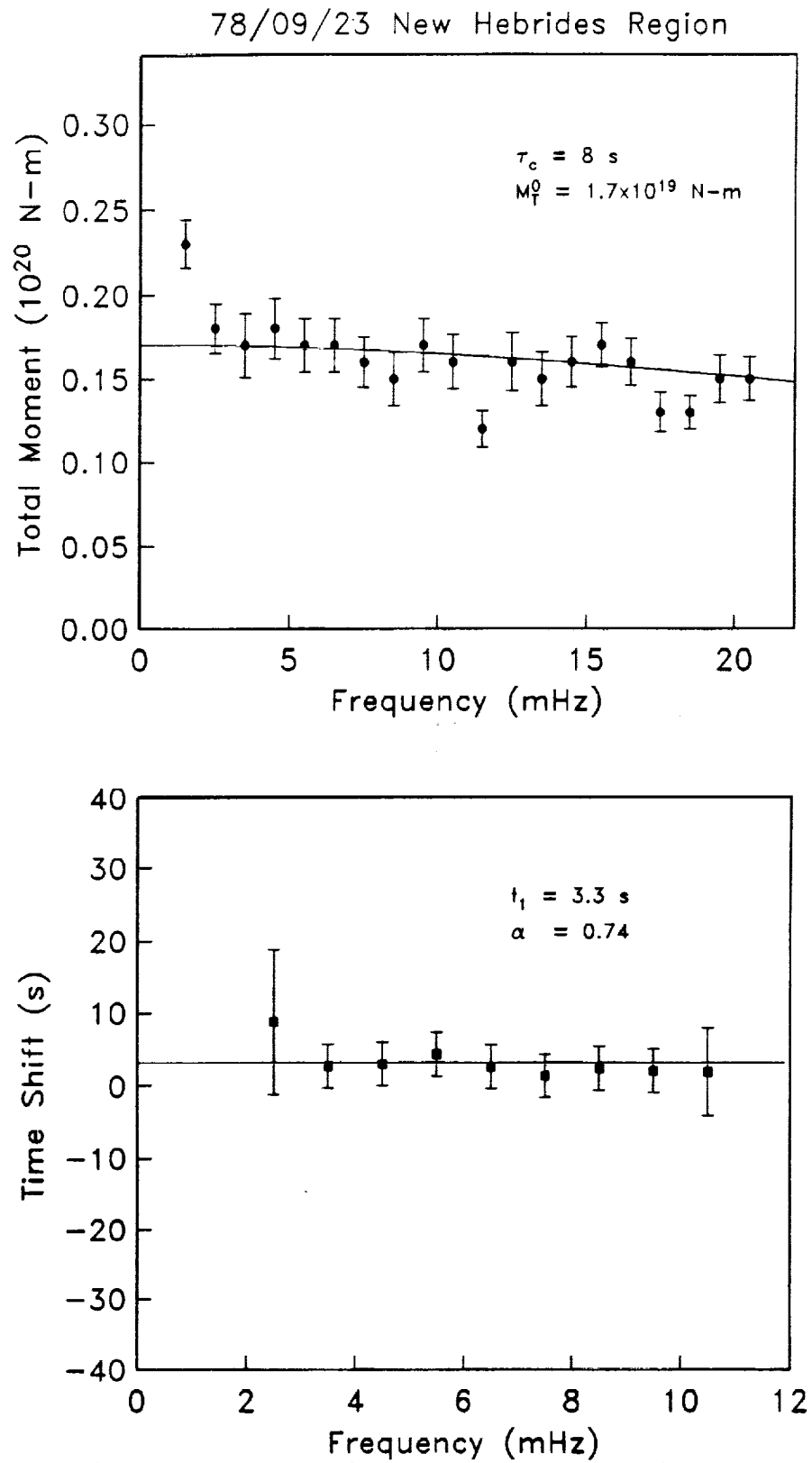


Fig 4.1 continued

type	start	durat.	moment	rise	decay
dbexp	0.00	50.00	0.33	10.00	3.00

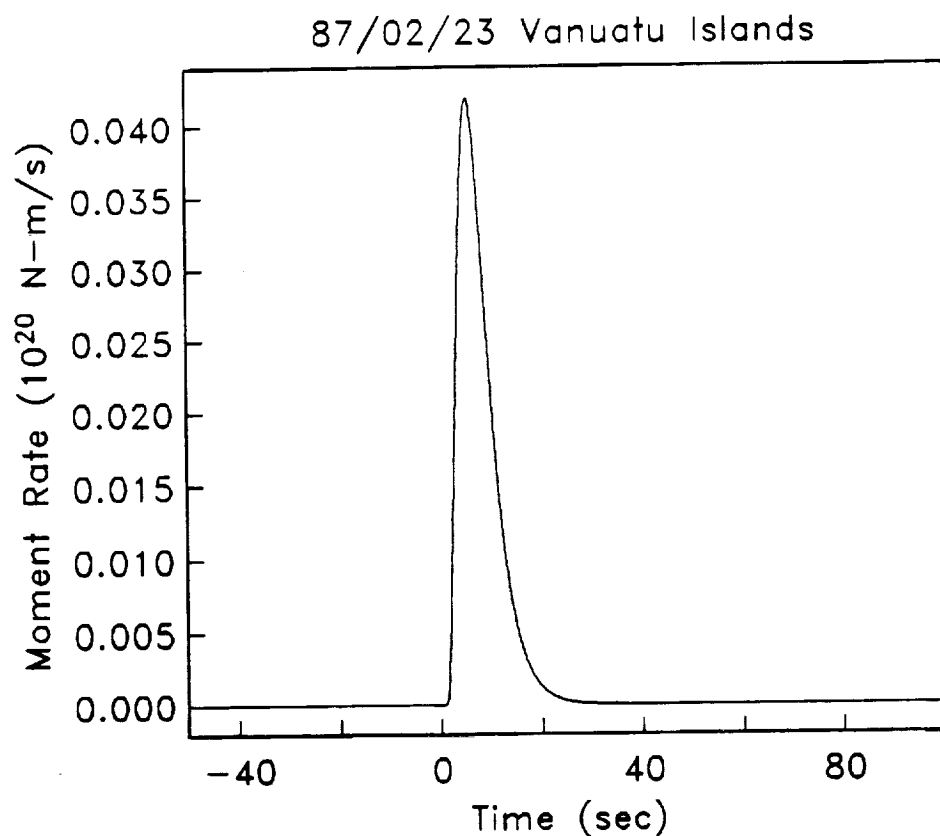


Fig. 4.2 - a) Source model for the 87/02/23 Vanuatu event. b) Amplitude spectra: observed (dots) and modelled (solid line). c) Phase-delay spectra: observed (dots) and modelled (solid line). Error bars represent one standard deviation.  $M_T^0$ ,  $t_1$ ,  $\tau_c$ ,  $\alpha$  are computed from the source time function in a)

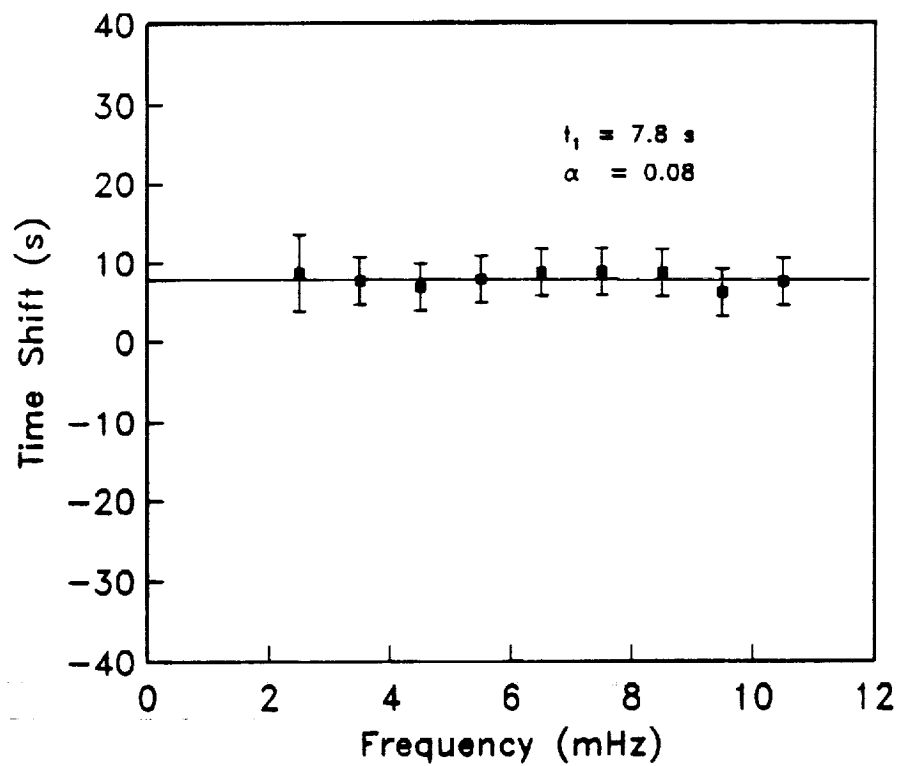
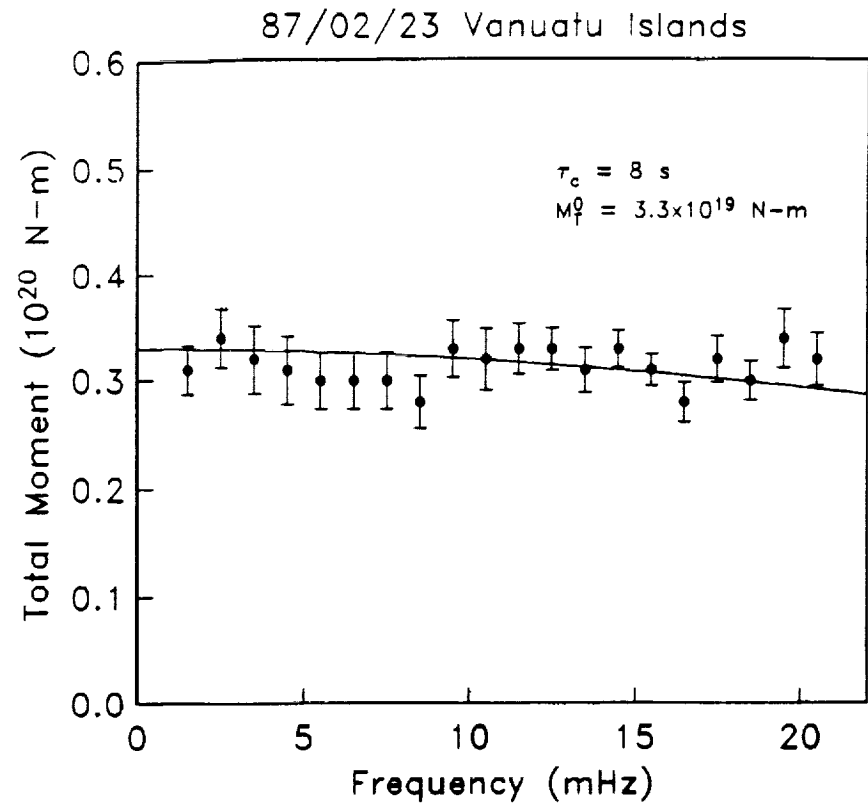


Fig 4.2 continued



type	start	durat.	moment	rise	decay
dbexp	0.00	100.00	2.00	8.00	8.00

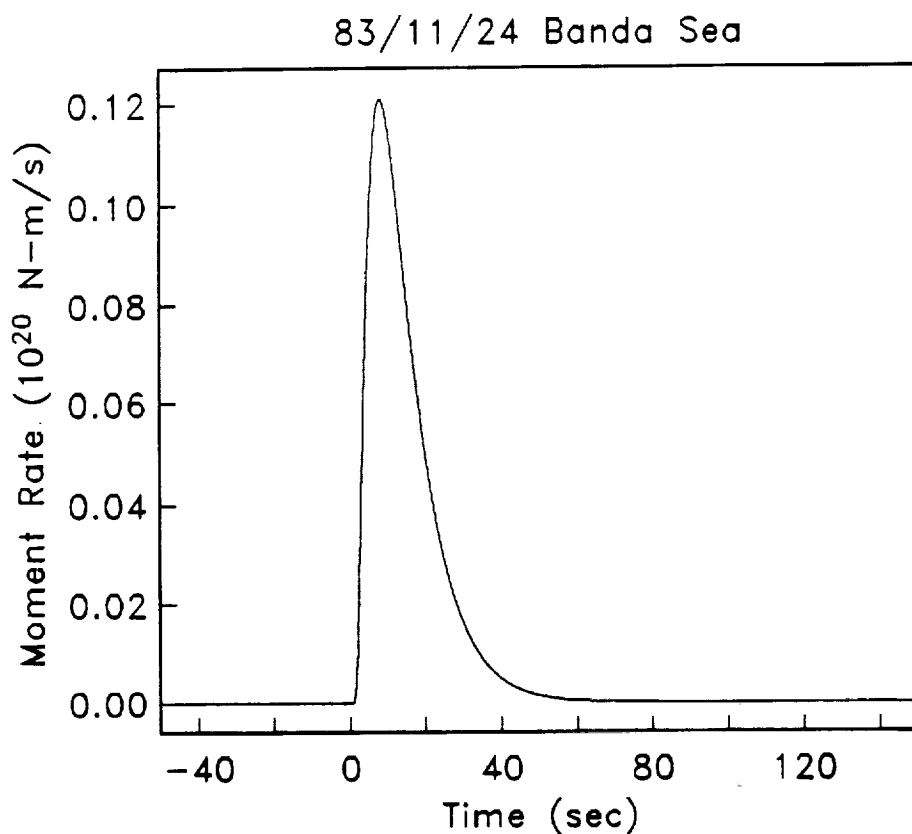
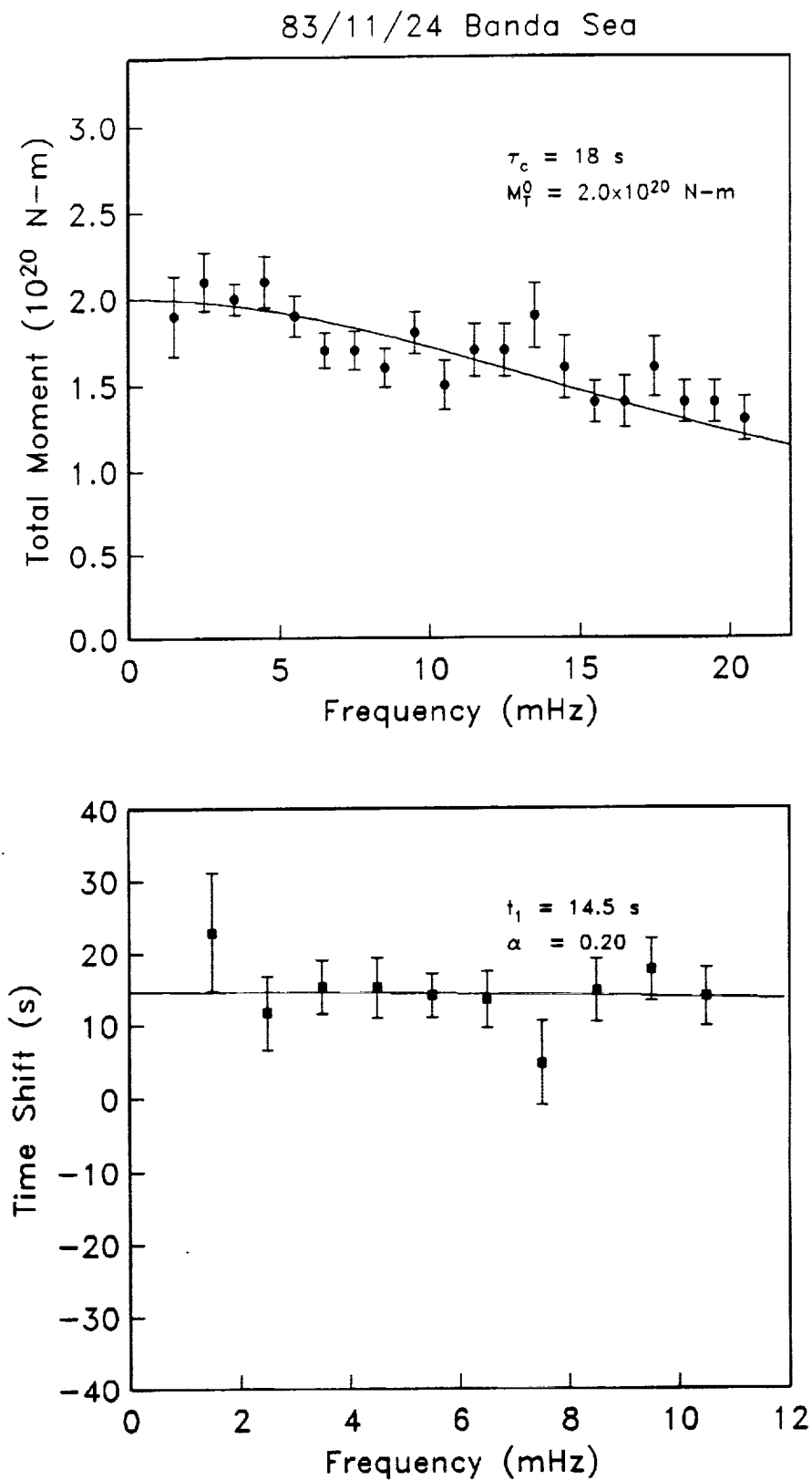


Fig. 4.3 - a) Source model for the 83/11/24 Banda Sea event. b) Amplitude spectra: observed (dots) and modelled (solid line). c) Phase-delay spectra: observed (dots) and modelled (solid line). Error bars represent one standard deviation.  $M_T^0$ ,  $t_1$ ,  $\tau_c$ ,  $\alpha$  are computed from the source time function in a)

**Fig 4.3 continued**

type	start	durat.	moment	rise	decay
dbexp	0.00	15.00	0.06	0.50	0.50

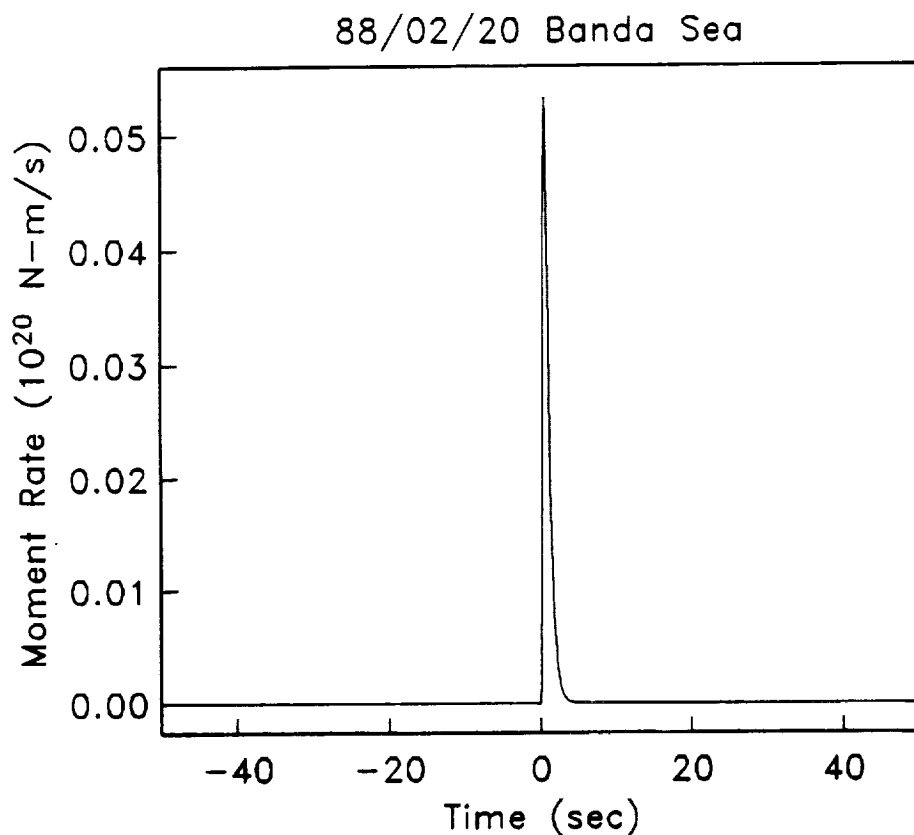


Fig. 4.4 - a) Source model for the 88/02/20 Banda Sea event. b) Amplitude spectra: observed (dots) and modelled (solid line). c) Phase-delay spectra: observed (dots) and modelled (solid line). Error bars represent one standard deviation.  $M_T^0$ ,  $t_1$ ,  $\tau_c$ ,  $\alpha$  are computed from the source time function in a)

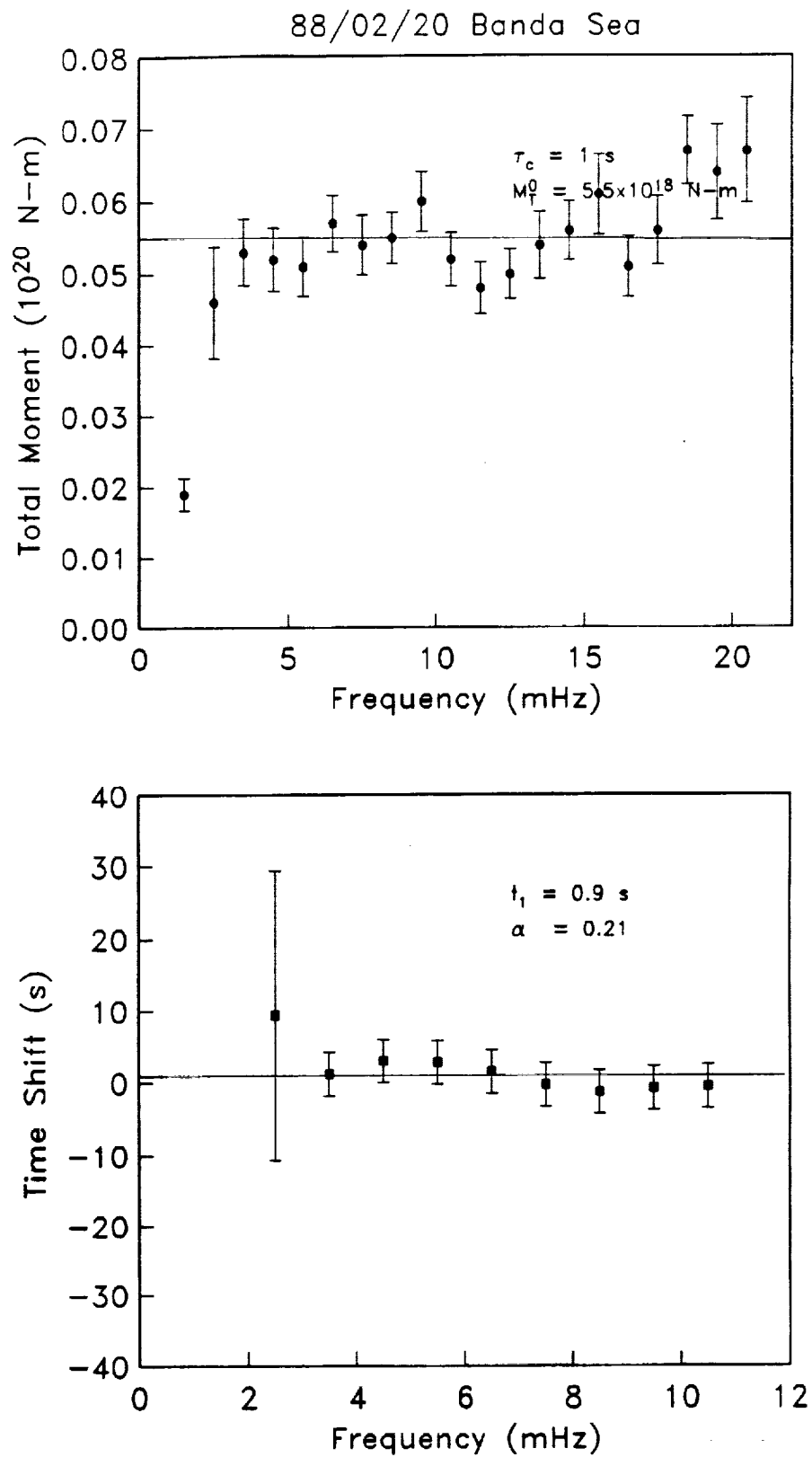


Fig 4.4 continued

type	start	durat.	moment	rise	decay
dbexp	0.00	50.00	0.13	1.00	3.00

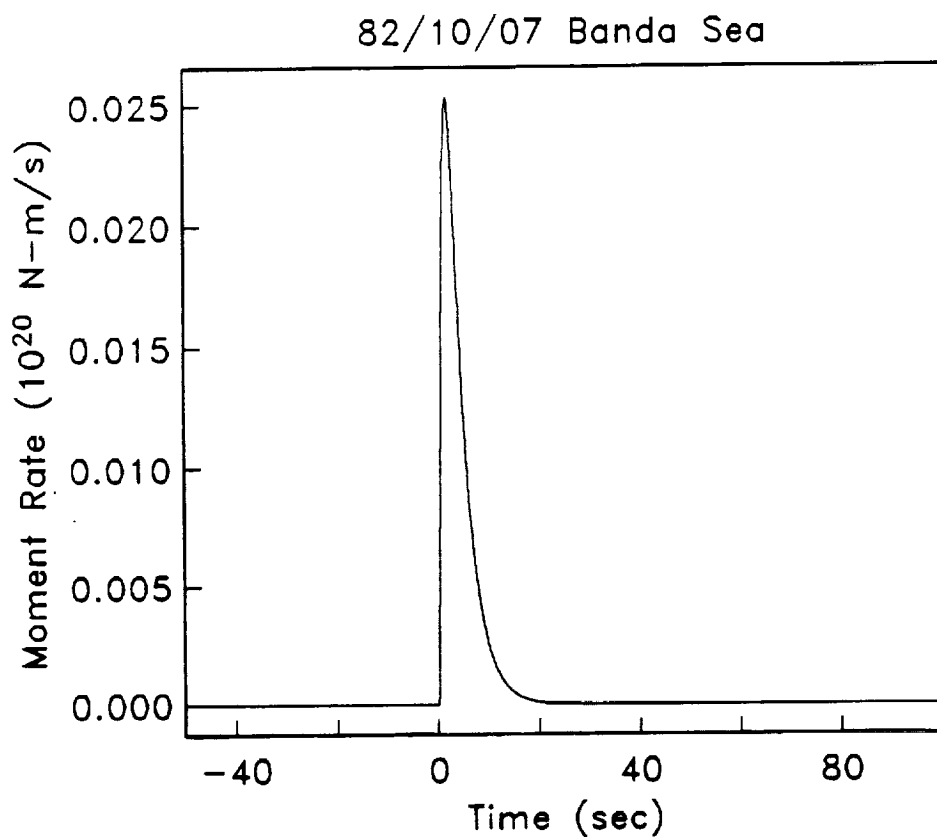
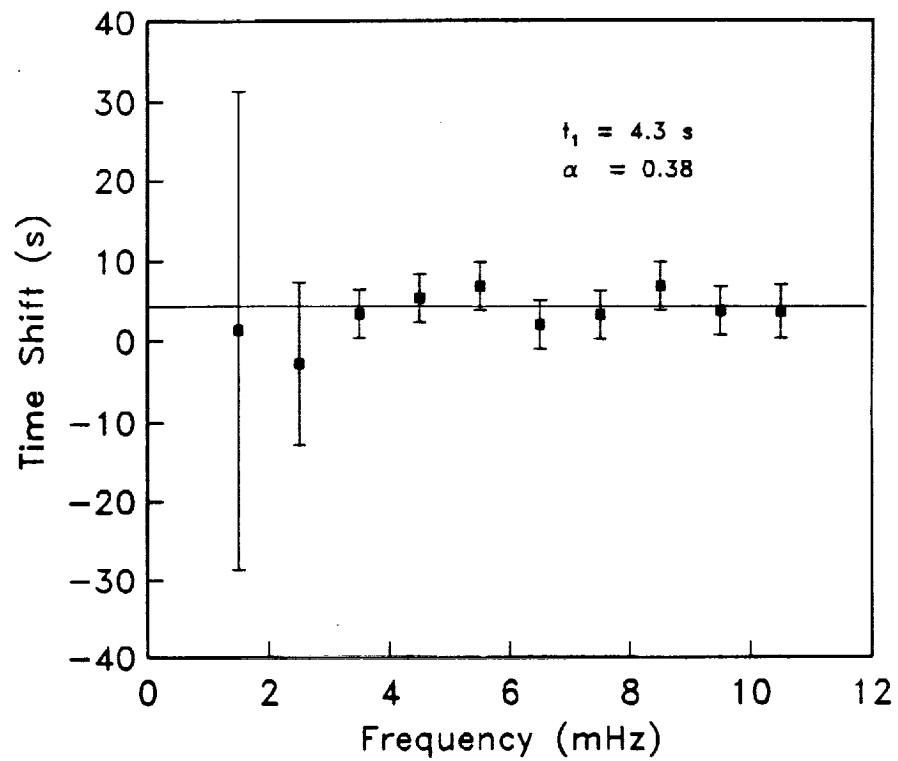
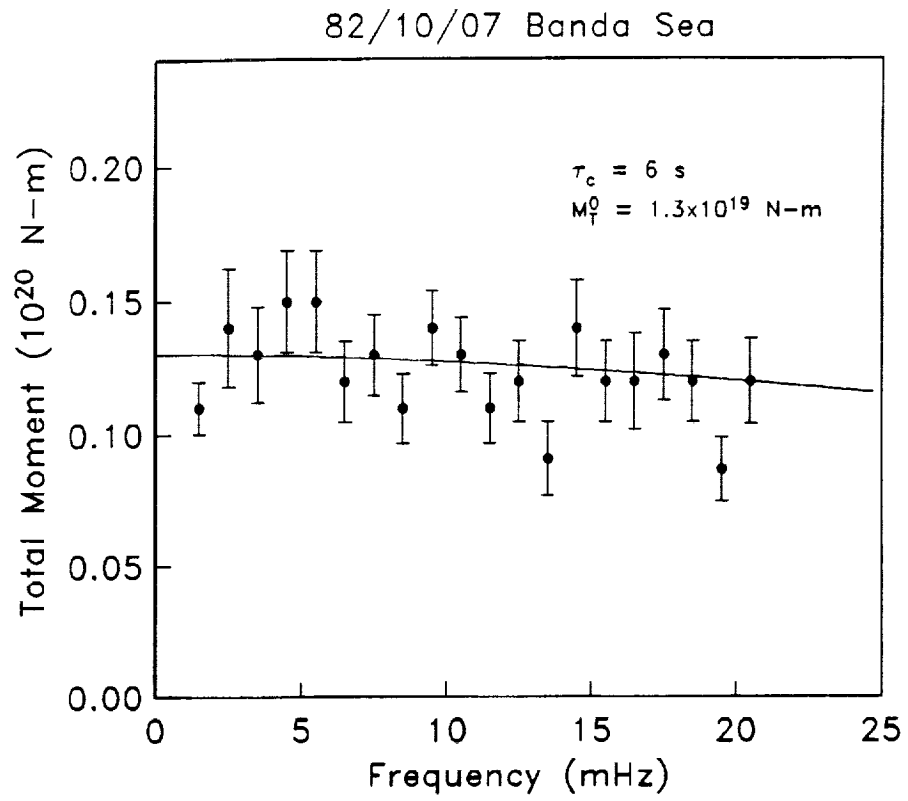


Fig. 4.5 - a) Source model for the 82/10/07 Banda Sea event. b) Amplitude spectra: observed (dots) and modelled (solid line). c) Phase-delay spectra: observed (dots) and modelled (solid line). Error bars represent one standard deviation.  $M_T^0$ ,  $t_1$ ,  $\tau_c$ ,  $\alpha$  are computed from the source time function in a)

**Fig 4.5 continued**

type	start	durat.	moment	rise	decay
dbexp	-2.00	17.00	0.11	0.10	1.00
slow	-2.00	47.00	0.06	1.00	46.00

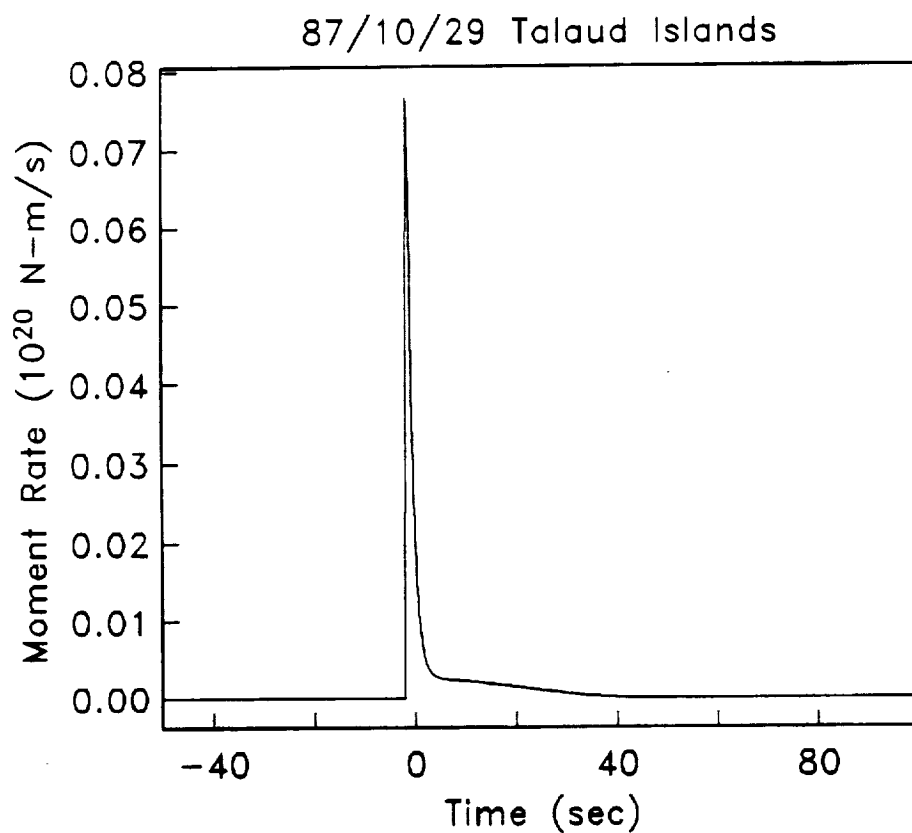


Fig. 4.6 - a) Source model for the 87/10/29 Talaud Islands event. b) Amplitude spectra: observed (dots) and modelled (solid line). c) Phase-delay spectra: observed (dots) and modelled (solid line). Error bars represent one standard deviation.  $M_T^0$ ,  $t_1$ ,  $\tau_c$ ,  $\alpha$  are computed from the source time function in a)

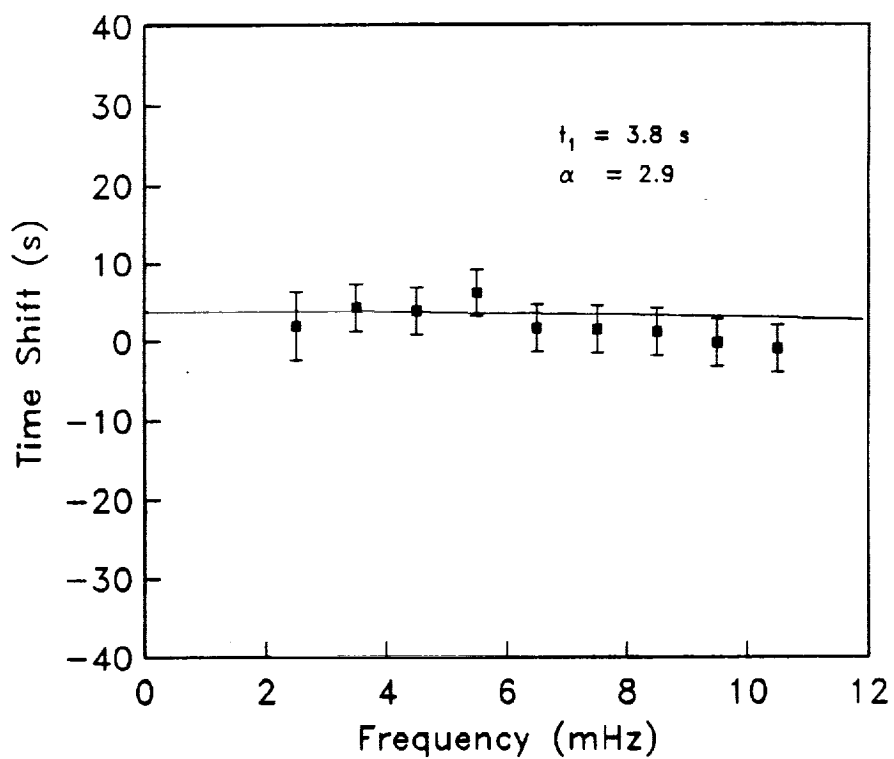
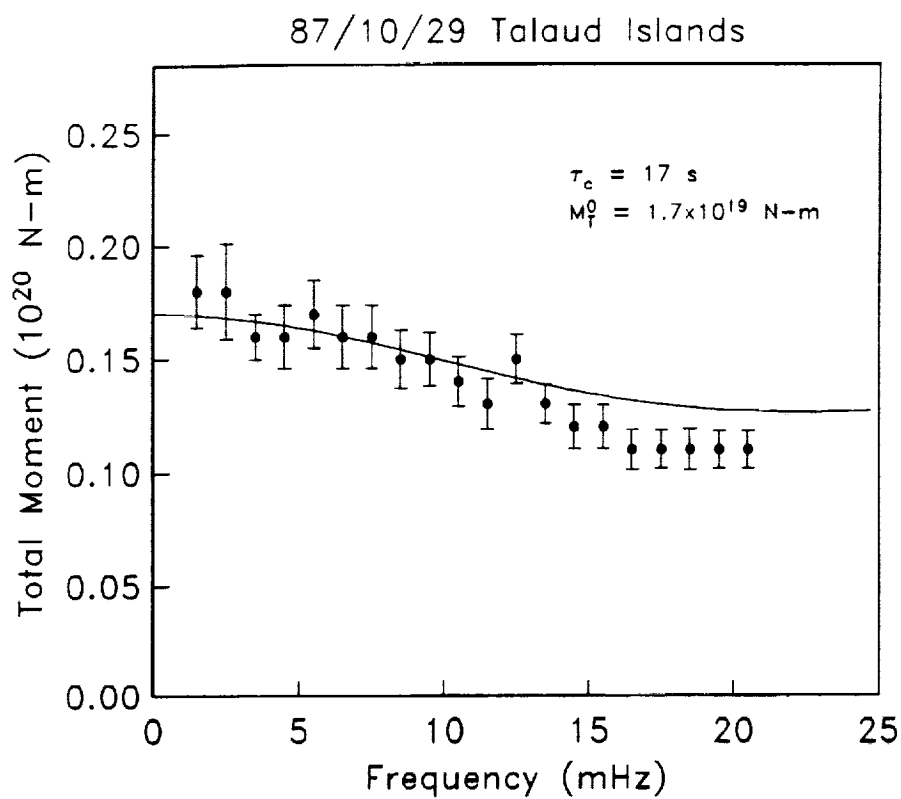


Fig 4.6 continued



## CHAPTER 5 - JAPAN

### 5.1 EVENTS DISCUSSION

Here we briefly examine a deep event, the 7 September 88, South of Honshu event, and in greater detail the 26 May 83, Akita-Oki earthquake.

The seismograms used for the two earthquakes are shown in Appendix. The CMT, NEIC and ISC parameters are reported in Table 8.1. The results of the inversion with respect to (2.6) and (2.7) are shown in Table 8.2.

The deep event is a fast rupturing earthquake. We show a plot with both spectra as obtained by the RJ and SJ methods and the source used to model them (Fig 5.1).

The 1983 Akita-Oki earthquake is more interesting. This very large event was recognized by various authors, Houston and Kanamori (1986) among others, to have ruptured along two distinct fault segments. The second rupture took place about 25 seconds after the first one on a fault about 50 km further to the north and with a slightly different strike (Fukuyama and Irikura, 1986). The latter authors also infer a slower rupture velocity for the second segment, about 2 km/s versus 2.5 km/s. In their inversion they use empirical green functions but for the second sub-event they use an especially large earthquake ( $M_s=7$ ) that could significantly bias their results.

The spectra and a tentative model based on Fukuyama and Irikura, (1986) with a two sub-events model are presented in Fig. 5.2 (model, dashed line). There are two striking features. First, we recover

a total scalar moment that is 33% larger than the CMT. Second, a two episodes model does not explain the kind of roll-off in the amplitude spectrum we observe at high frequency.

Comparing other larger events we have studied in MIT, we have noticed that the discrepancy in moment with the CMT is rather common. In this case it is probably caused by the CMT simpler modeling of the source (boxcar).

The spectral roll-off is a more interesting feature. To model it we need to add a further rupture episode with a moment that is about 8% of the total, 80 seconds after the initial rupture (Fig 5.2, solid line).

We do not know yet what is the nature of this episode. To further investigate this event the best alternative will probably be to include the GDSN stations available at the time. We do not use them routinely because their lower frequency limit is about 4 mHz but in a case like this where the uncertainty is in the 10 to 20 mHz band they might be very useful.

type	start	durat.	moment	rise	decay
dbexp	0.00	20.00	0.11	3.00	1.00

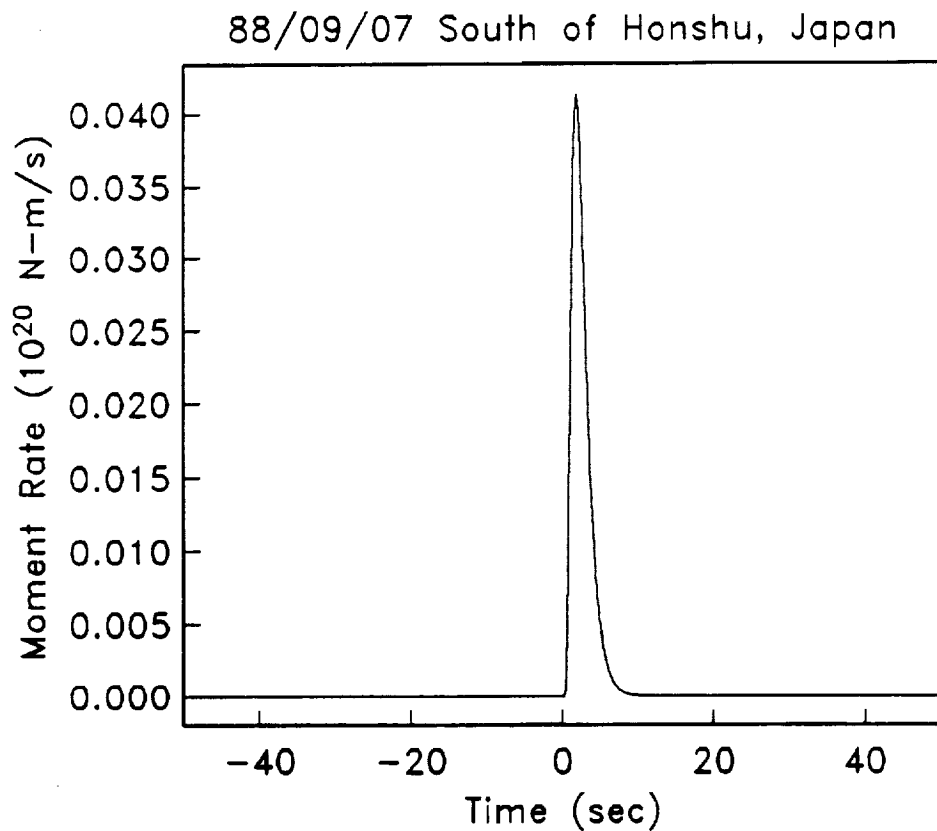


Fig. 5.1 - a) Source model for the 88/09/07 South of Honshu, Japan, event. b) Amplitude spectra: observed (dots) and modelled (solid line). c) Phase-delay spectra: observed (dots) and modelled (solid line). Error bars represent one standard deviation.  $M_T^0$ ,  $t_1$ ,  $\tau_c$ ,  $\alpha$  are computed from the source time function in a)

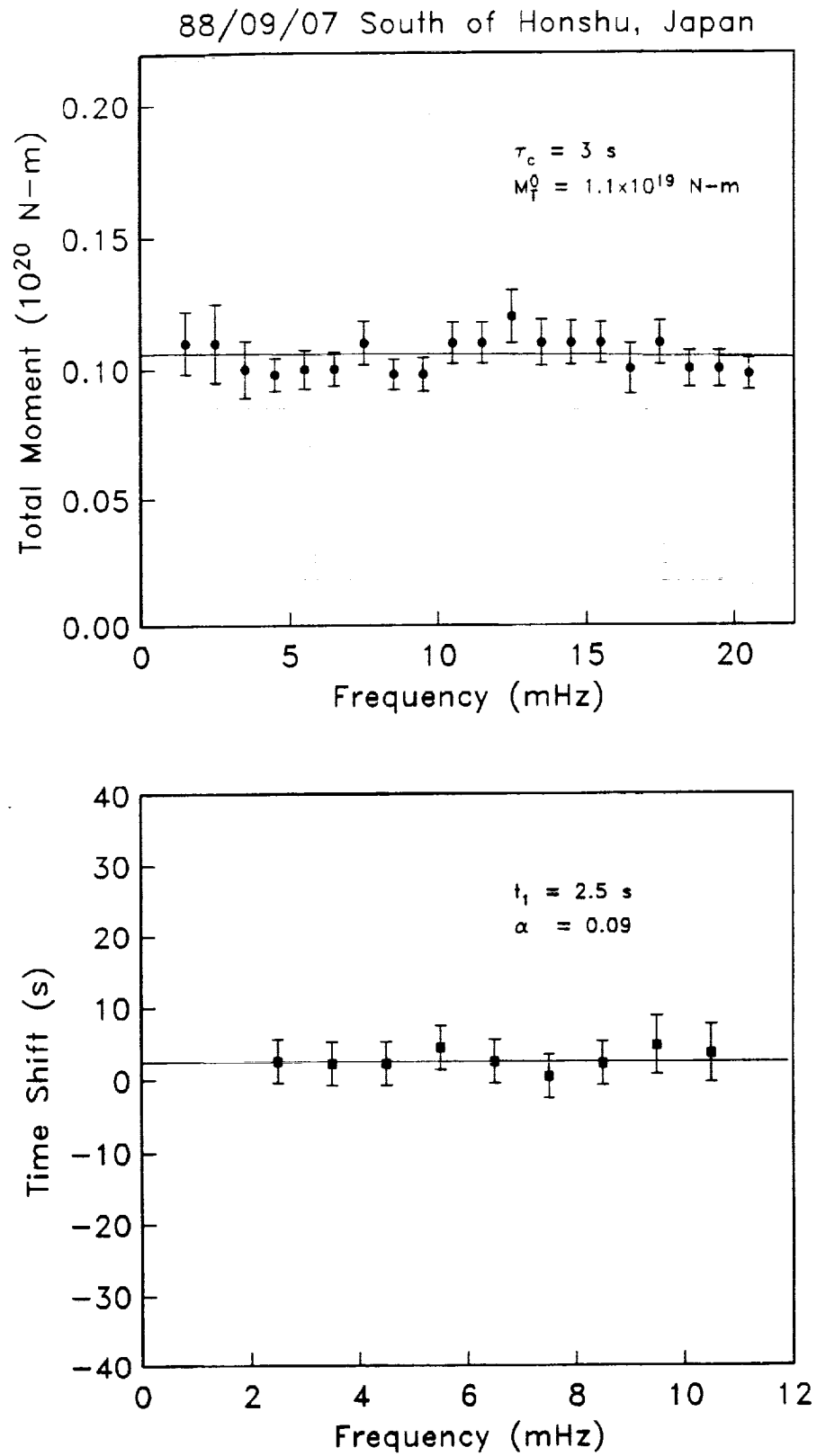


Fig 5.1 continued

type	start	durat.	moment	rise	decay
dbexp	0.00	60.00	4.00	1.00	8.00
dbexp	20.00	50.00	1.50	2.00	8.00
dbexp	80.00	30.00	0.50	2.00	4.00

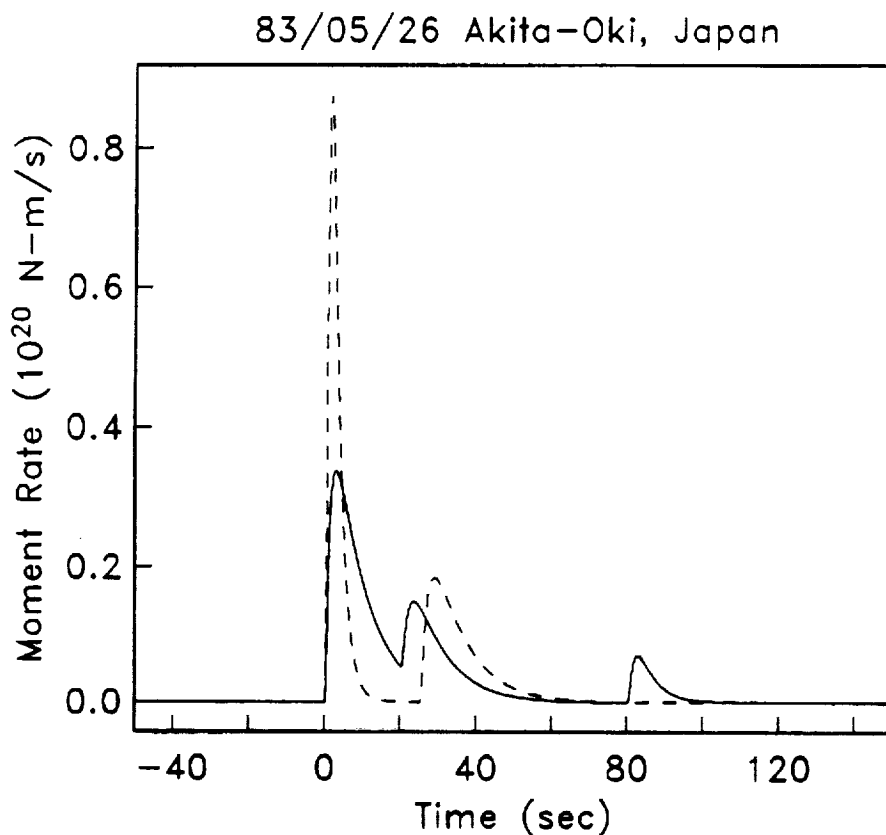


Fig. 5.2 - a) Source model for the 83/05/25 Akita-Oki event. b) Amplitude spectra: observed (dots) and modelled (solid line - this study; dashed - derived from Fukuyama and Irikura). c) Phase-delay spectra: observed (dots) and modelled (solid line, dashed line). Error bars represent one standard deviation.  $M_T^0$ ,  $t_1$ ,  $\tau_c$ ,  $\alpha$  are those of the source time function presented in this study)

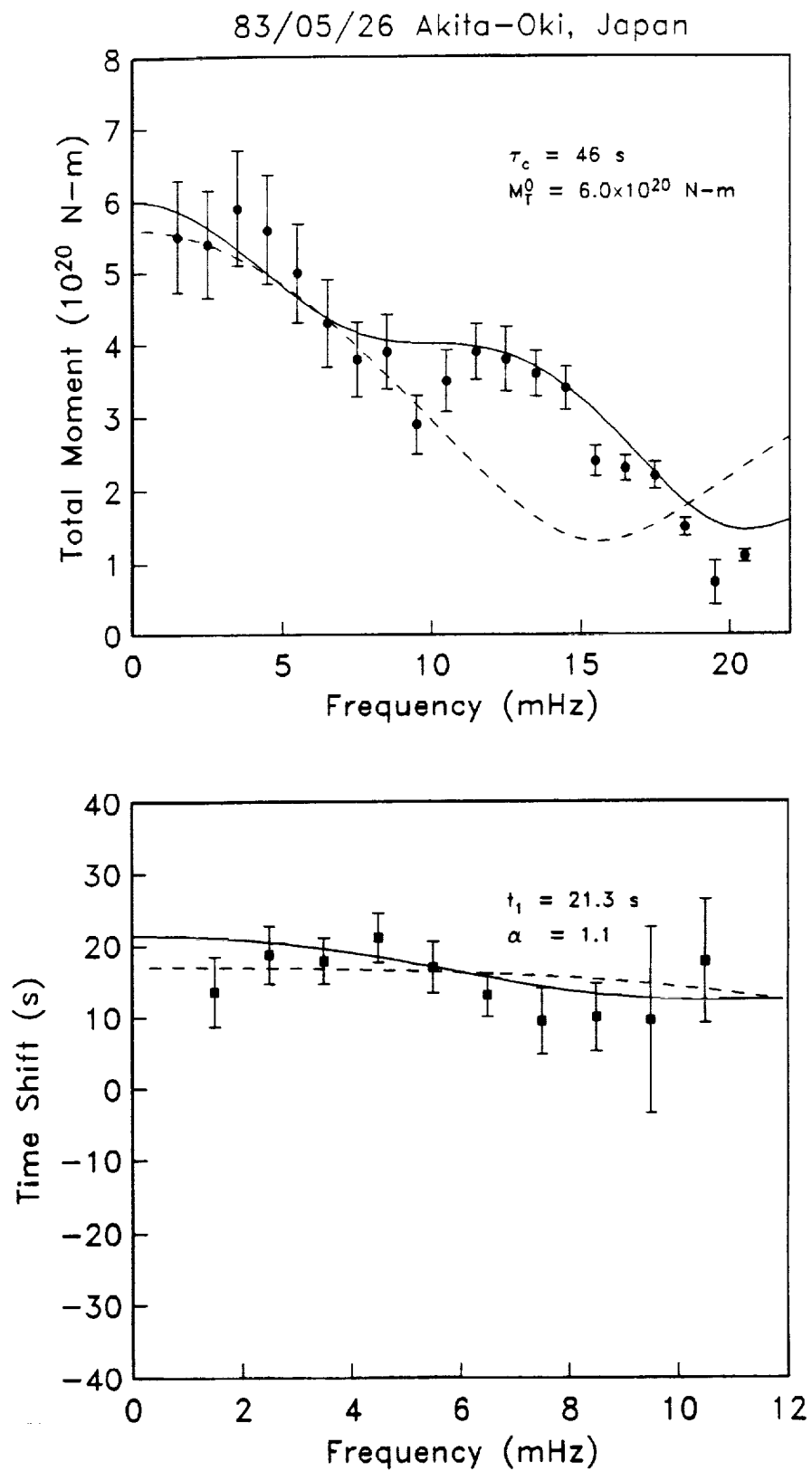


Fig 5.2 continued

## CHAPTER 6. - PERU

### 6.1 INTRODUCTION

The following three events are very similar for various aspects: focal depths ranging from 90 to 150 km, normal faulting mechanisms, relatively close epicentral locations. Nonetheless their source time functions are remarkably different. One, the 3 December 89 Peru-Brazil, is a fast rupturing earthquake, another, the 23 November 86 Peru-Ecuador, is much slower and the third one, the 12 April 1983 Peru-Ecuador, is an event with what we believe to be a short-term low-frequency precursor. Their CMT, NEIC and ISC parameters are reported in Table 8.1 and the records used in the inversion for the three events are shown in Appendix.

### 6.2 INFLUENCE OF EARTH AND Q MODELS

Since one of these earthquakes is of particular interest, we conducted extensive tests to assess the influence of our elastic and anelastic parameterization on the spectra. We have systematically varied the time window and the set of records used in the inversion so to have independent spectral estimates. In the frequency interval between 1 and 11 mHz, the stability of both spectra is remarkable for all three events. At higher frequencies (11-21 mHz) the amplitude spectra of the two smaller events are more sensitive to changes in the time window.

We recover basically the same features even if we use a different model like Core11.

Different Q models, namely those described in chapter 2, still yield the same basic trend for the 1983 Peru-Ecuador amplitude spectrum, large characteristic duration and small centroid time shift, although they are not as insensitive as those derived from the PREM Q model to variations in the time window.

In Fig. 6.1 we show the amplitude spectrum for the 1983 Peru-Ecuador, using the three different Q models and Core11. In Fig. 6.2 we show how the spectrum computed using five untruncated records with a time window of three hours compares with the one obtained with nine different records with a time window of six hours starting three hours after the origin time.

We have also conducted cross-tests between the various events, using for comparison a common time window and data set. Once again the spectra do not vary significantly respect to the inversion with optimal time window and full data set. This is an indication that the differences we observe are mostly due to the source. This is especially true for the two Peru-Ecuador earthquakes that have similar locations and mechanisms.

### 6.3 THE 1989/12/03 PERU-BRAZIL EARTHQUAKE

This is a normal faulting event with a depth of about 150 km. According to the NEIC bulletin, a first subevent was followed 3.8 seconds later by a second one. No estimate of the relative magnitude is available.

We show the time-shift and the amplitude spectrum in Fig. 6.3. We did not use BJI and LHI in determining the phase-shift spectrum since there are rather strong phase jumps across the



frequency bands. The characteristic duration indicates a very fast rupturing episode and this partially contrasts with a rather large centroid time. Since the earthquake is relatively small, only slightly above the minimum threshold for our method, we might have some problem in determining the characteristic duration, that might be as high as 8 or 10 seconds. Nonetheless even allowing for such errors, it would still be a fast event.

We model the source with a single pulse, since we cannot distinguish two pulses spaced 4 seconds apart, but we require a very large group delay (Fig. 6.3).

#### 6.4 THE 1986/11/23 PERU-ECUADOR EARTHQUAKE

This is also a normal faulting event with depth of about 100 km. There is a certain disagreement on this value (see Table 8.1)

The CMT depth is 102 km but we improve our variance reduction by about 20% in the frequency interval between 2 and 10 mHz if we set it at 92 km. The resulting time-shift and amplitude spectrum are shown in Fig. 6.4. Both of these spectra are well constrained: there are 23 records and the event is well above the noise level.

We determined that it has a centroid time-shift of only about 4 seconds and a large characteristic duration. An adequate model would require a source with an almost instantaneous rise time, an equally fast decay time but it should also have a relatively long lasting coda. To represent it, we superimpose a slowly decaying source to our usual function and we model it with a half cosine (Hanning) bell.

### 6.5 THE 1983/04/12 PERU-ECUADOR EARTHQUAKE

This event was first recognized by Jordan (1991) as a precursive event. We investigated it in detail and believe that it is a compound event. Its source associates a slow-rupturing low-frequency episode to a regular fast rupturing one. The slow episode might start as early as 2 minutes before the fast episode.

The phase-shift and amplitude spectra are presented in Fig. 6.5. The time-shift spectrum is typical of a fast rupturing earthquake while the amplitude spectrum is typical of a very slow one. Since there is a marked difference in slope after 6 mHz, we determine the characteristic duration taking into account only the lower frequencies. The RJ method yields also a moment tensor for each of the 10 frequency bands. We show them in Fig. 6.6. It is noteworthy that the mechanism is extremely stable across all the bands. This seems to guarantee that one of our assumptions, that the mechanism does not have frequency dependence, is respected.

To understand the relationship between the two spectra we recall that Jordan (1991) identifies a set inequalities

$$\Delta t_1 > 0 \quad (6.2)$$

$$\alpha > -1/8 \quad (6.2)$$

$$\tau_c < \tau_c^{max}(H_0) \equiv \Delta t_1 \sqrt{2(1 + \sqrt{1 + 8\alpha})} \quad (6.3)$$

assuming  $t_*$  to be the origin time, that hold for any monotone one-sided source time function and regardless of their characteristics;

they are not required to be smooth or even have a finite duration. Inequality (6.3) depends only weakly on the skewness.

Let  $t_0$  be the high frequency ( $P$ -wave) origin time. For most real earthquakes,  $t_0 \approx t_*$ . There are cases however (Dziewonski and Gilbert, 1974; Kanamori and Cipar, 1974; Cifuentes and Silver, 1989; Ihmle et al., 1993) where there are indications that  $t_0 > t_*$ . Following Jordan (1991), let us assume an hypothetical source time function where  $t_0 > t_*$ . Then we can think of the source in the time interval  $t_* - t_0$  as a seismic precursor to the main rupture. The spectrum of the rupture process normally is rich enough to radiate at all frequencies in the seismic band; high-frequency waves, emitted instantly, mark the initiation of crack propagation ( $P$ -wave origin time,  $t_0$ ). We observe a consistent delay of  $t_0$  respect to  $t_*$  if the source does not radiate high frequency energy in that interval, that is, if the process is smooth.

Using the above mentioned inequalities we can try to detect slow precursors. The null hypothesis is  $H_0 \equiv \{\text{the earthquake is ordinary}\}$ , the alternative is  $H_1 \equiv \{\text{the earthquake has a short-term slow precursor}\}$ .  $H_0$  implies that  $t_0 \approx t_*$ . If it can be demonstrated that the data are inconsistent with any one of the above inequalities then we can reject  $H_0$  in favor of  $H_1$ .

Jordan (1991) states that if  $H_0$  is true, then  $\Delta t_1$  and  $\alpha$  cannot be arbitrarily chosen; causality requires that the source group delay,  $d\phi/d\omega$ , must be greater than zero for  $\omega \leq \omega_{max}$ . If (2.6) satisfactory describes the time-shift spectrum, then the causality constraint is satisfied if  $\Delta t_1 > 0$  and

$$\alpha < 1 + \frac{1}{\omega_{max}^2 \Delta t^2} \quad (6.4)$$

Jordan (1991) argument that the Peru-Ecuador event is precursive, is based on the assumption that if a seismic source is a "reasonable" function of limited duration, at most hundreds of seconds, than it can be described by the first two terms in (2.1) and (2.2). If this is true, then (6.4) also holds. This allows us to compute (6.3) using the upper bound value of  $\alpha$  instead of the poorly determined one we get from the time-shift spectrum. Consequently taking into account the uncertainties on the time centroid, we obtain a one-sided 99% confidence interval of  $\tau_c^{max}(H_0) < 28$  seconds. Our estimate of the characteristic duration exceeds 70 seconds and this violates the inequality.

An explanation for this earthquake is a "compound" source. The slow rupture starts first and "drives" the whole process. The mounting stress caused by this rupture causes at a certain point the failure of an asperity and this in turn gives origin to the high frequency source. Consequently we model our spectra as a combination of a fast rupturing source superimposed to a slower one. We chose to describe the slow episode as a cosine (Hanning) bell starting about 110 seconds before the high frequency origin time and lasting for about 220 seconds. Our model requires a moment release of  $5.4 \cdot 10^{19}$  N-m, equally distributed between the 2 episodes (Fig. 6.7).

A couple of facts add to the consistency of our hypothesis. First the amplitude spectrum beyond 6 mHz is almost flat. This means that above that frequency it is impossible to observe any

contribution of the slow source to the incoming waves. Synthetic seismograms for the 14 stations used in the inversion show that the amplitude of the fast component is about a thousand times larger than the slow one in the seismograms filtered with a band-pass cosine filter between 8 and 22 mHz. Only at very low frequencies (synthetic seismograms band-pass filtered from 0.5 to 3 mHz) the slow component becomes comparable to the fast one (Fig. 6.8 for ALE).

To interpret these unusual spectra in terms of a source process, we must show that they are not the result of some kind of bias owing to unmodeled propagation effects or source mislocation. As shown before the elastic and anelastic parameterization cannot cause the huge spectral roll-off we observe. We also conducted an extensive search to determine if a depth mislocation might affect our results. A depth of about 90 km (20 km shallower), makes the event look faster (Fig. 6.9). The requirement for a precursor becomes more questionable since  $\tau_c^{max}(H_0) < 28$  seconds and the characteristic duration we obtain is about 30 seconds. However, the total variance reduction in this case decreases by about 20% in the range between 2 and 10 mHz and this leads us to think that it is not a credible alternative. Nonetheless even if depth of the event happened to be about 90 km, it would still be difficult to model it without a considering a precursor. The model that fits better the data has a cosine (Hanning) bell starting 60 seconds before the high frequency origin time and lasting for 2 minutes with a total moment release of  $2.0 \cdot 10^{19}$  N-m superimposed to the same high frequency

source we had before. It seems to satisfactory explain the two spectra. The source and the spectra are shown in Fig. 6.10.

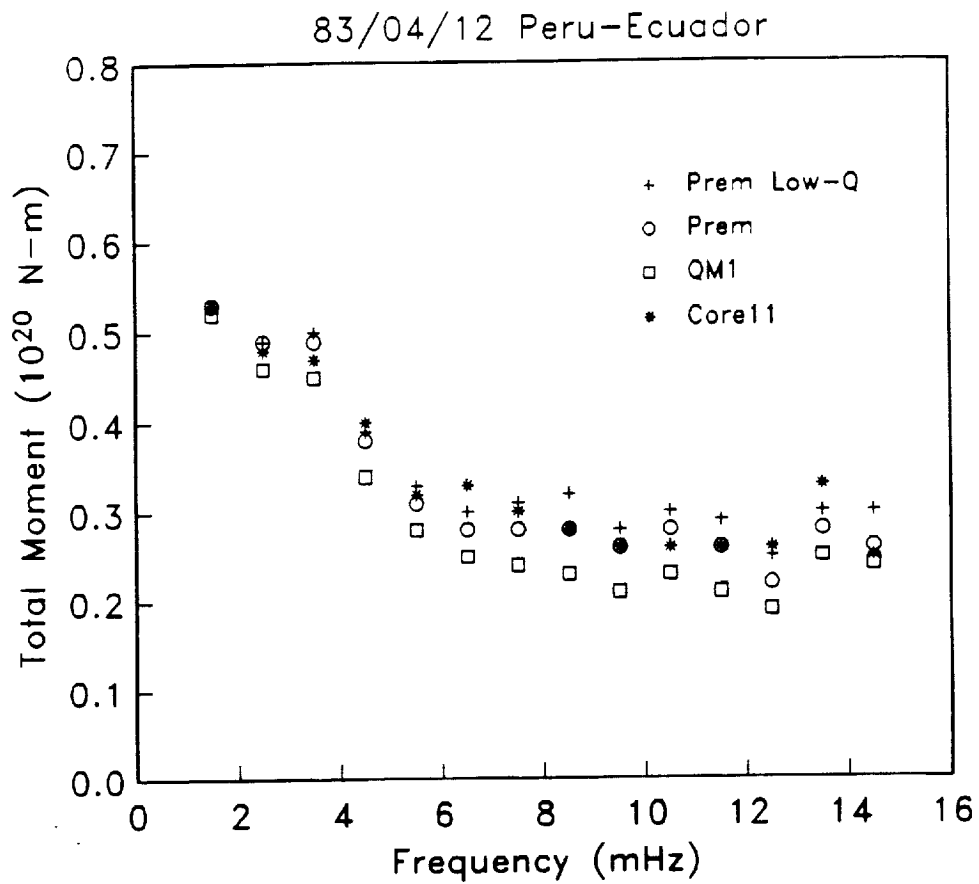


**Fig. 6.1 - Amplitude spectra for the 83/04/12 Peru-Ecuador event using three different Q models (Q-Prem; L-Q; QM1) one different spherical earth model (CORE11)**

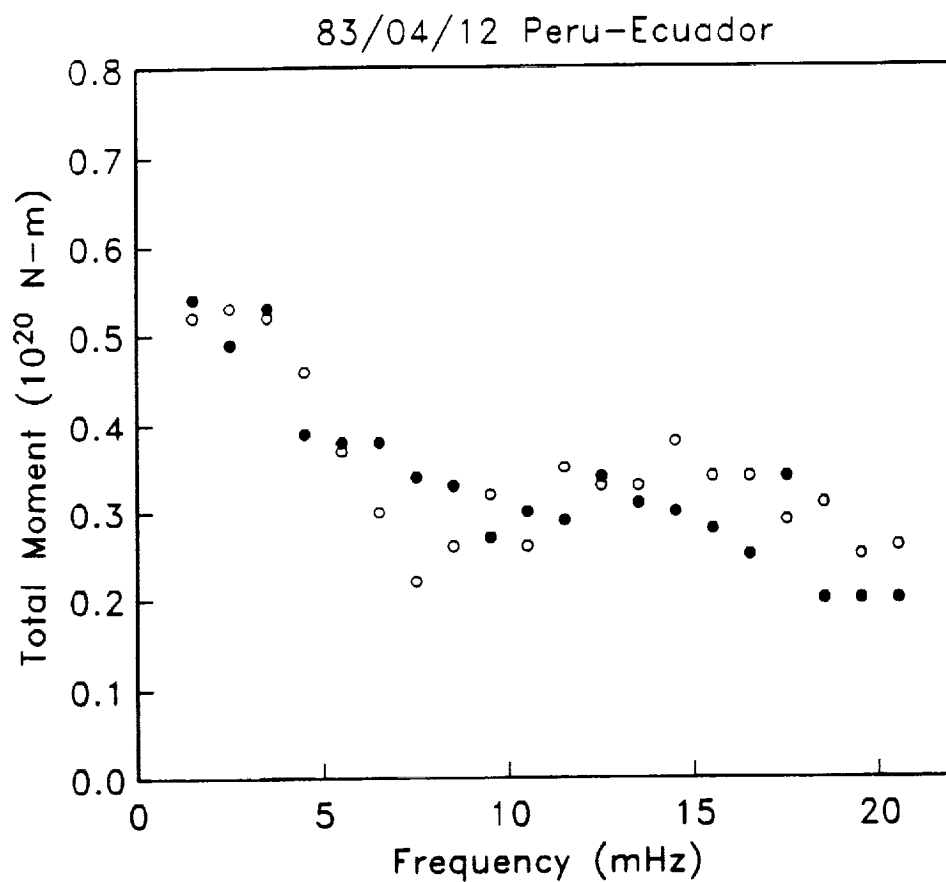


**Fig. 6.2 - Amplitude spectra for the 83/04/12 Peru-Ecuador event using a time window of three hours for five stations (ALE, GUA, SPA, SSB, PCR) and a time window of six hours, starting three hours after the event with the remaining nine stations.**



type	start	durat.	moment	rise	decay
dbexp	0.00	25.00	0.07	20.00	1.00

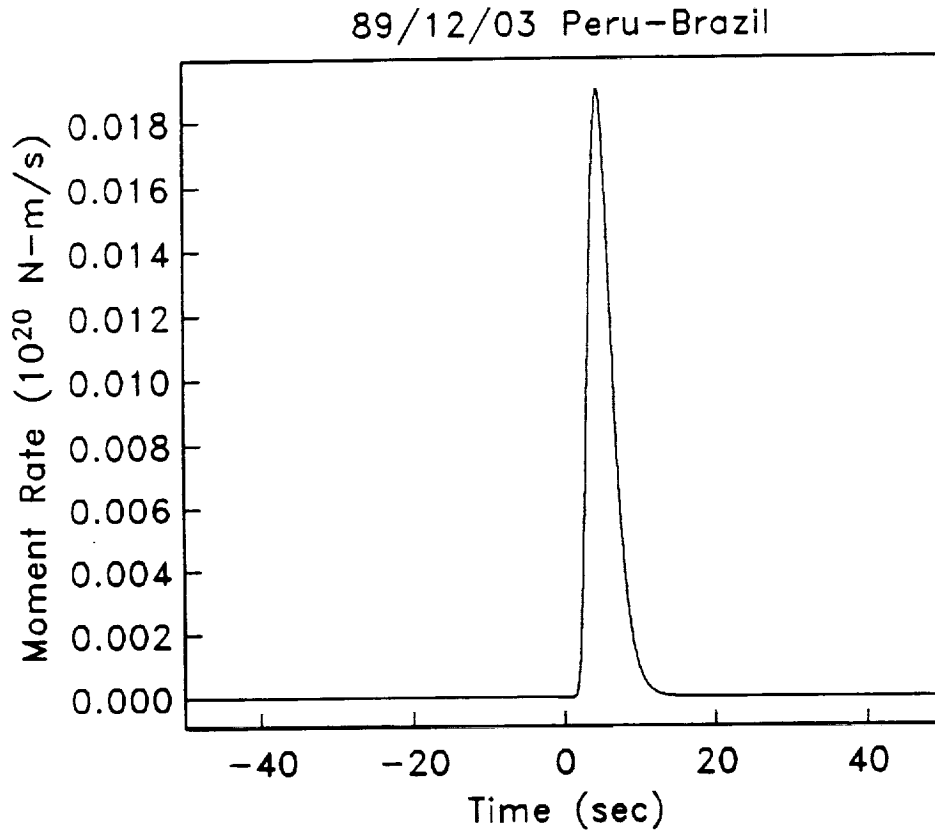


Fig. 6.3 - a) Source model for the 89/12/03 Peru-Brazil event. b) Amplitude spectra: observed (dots) and modelled (solid line). c) Phase-delay spectra: observed (dots) and modelled (solid line). Error bars represent one standard deviation.  $M_T^0$ ,  $t_1$ ,  $\tau_c$ ,  $\alpha$  are computed from the source time function in a)

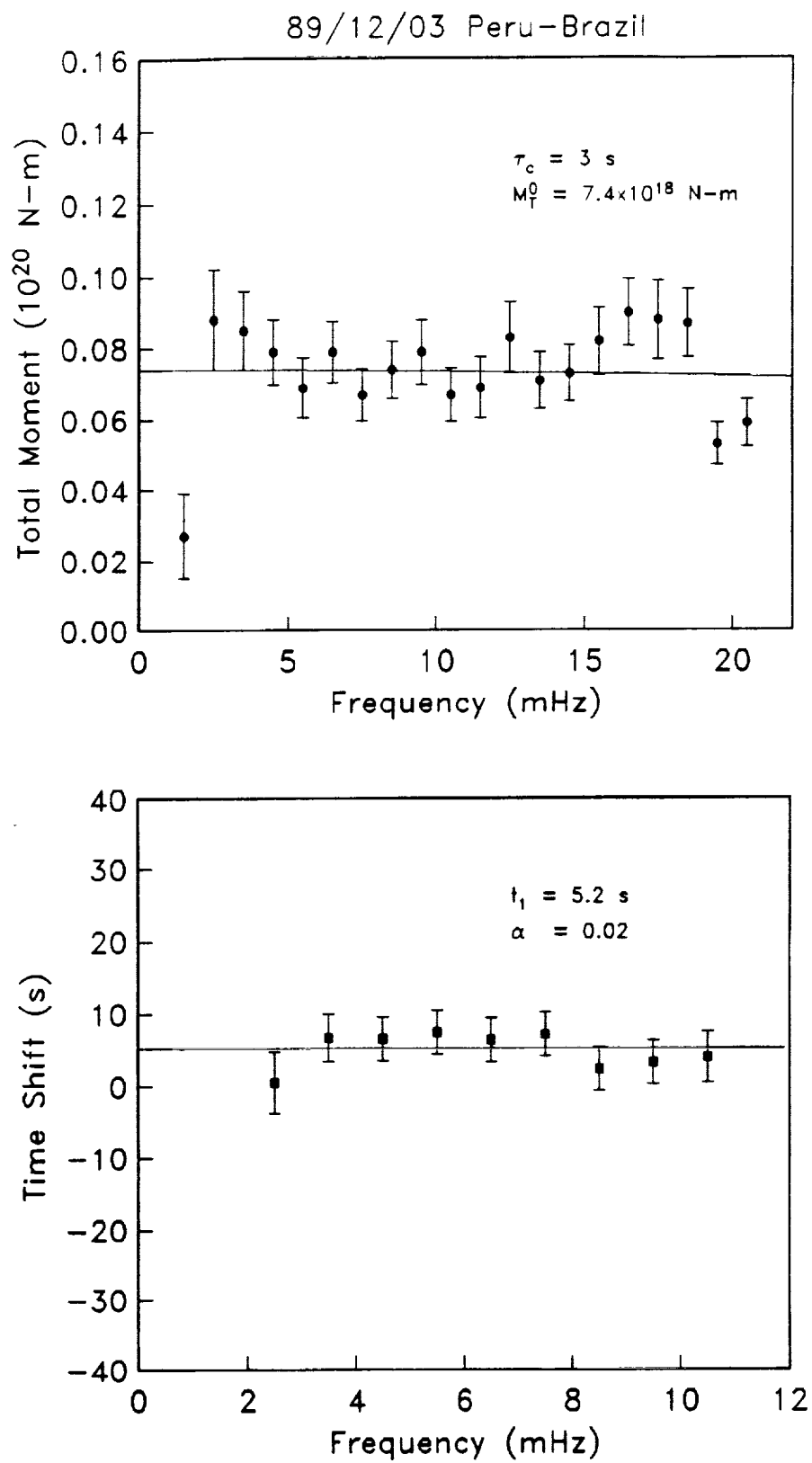


Fig 6.3 continued

type	start	durat.	moment	rise	decay
dbexp	0.00	40.00	0.14	0.10	2.00
slow	0.00	40.00	0.05	0.10	39.00

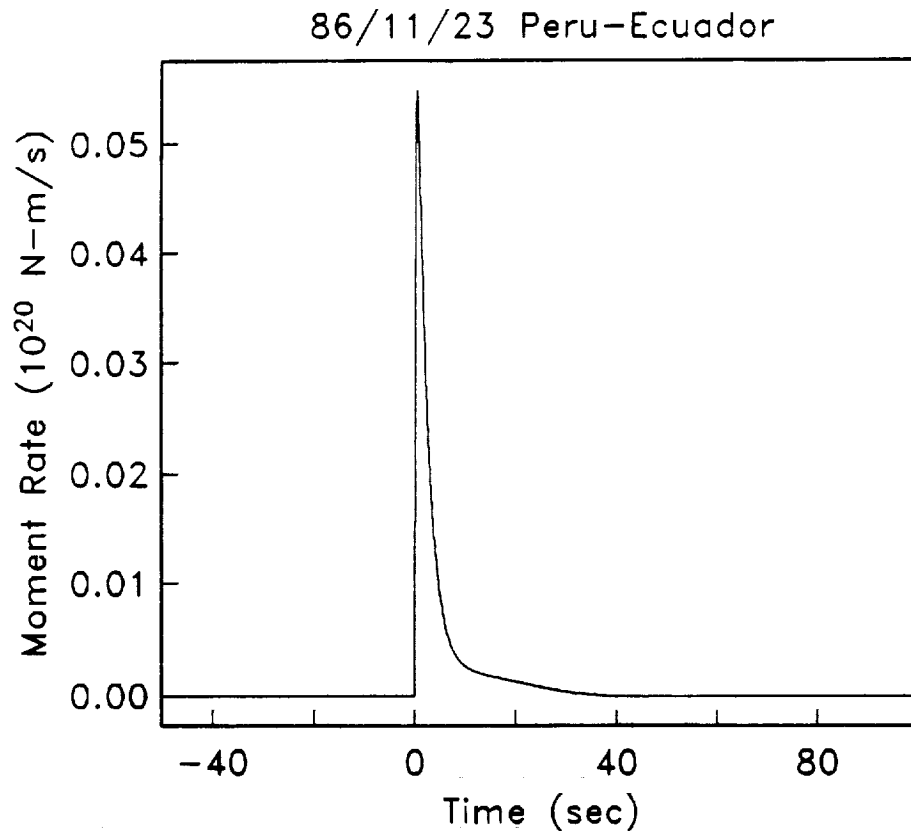


Fig. 6.4 - a) Source model for the 86/11/23 Peru-Ecuador event. b) Amplitude spectra: observed (dots) and modelled (solid line). c) Phase-delay spectra: observed (dots) and modelled (solid line). Error bars represent one standard deviation.  $M_T^0$ ,  $t_1$ ,  $\tau_c$ ,  $\alpha$  are computed from the source time function in a)

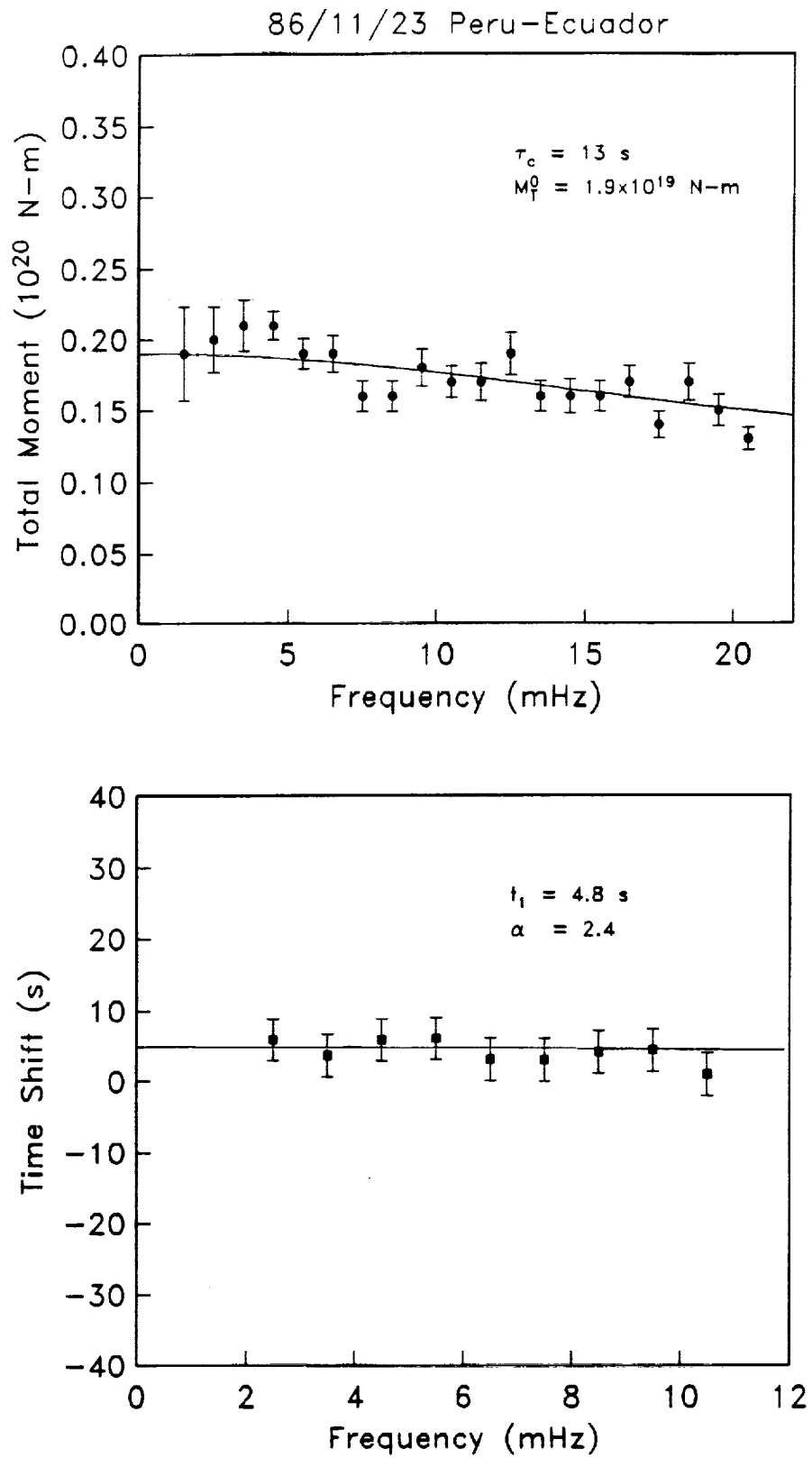
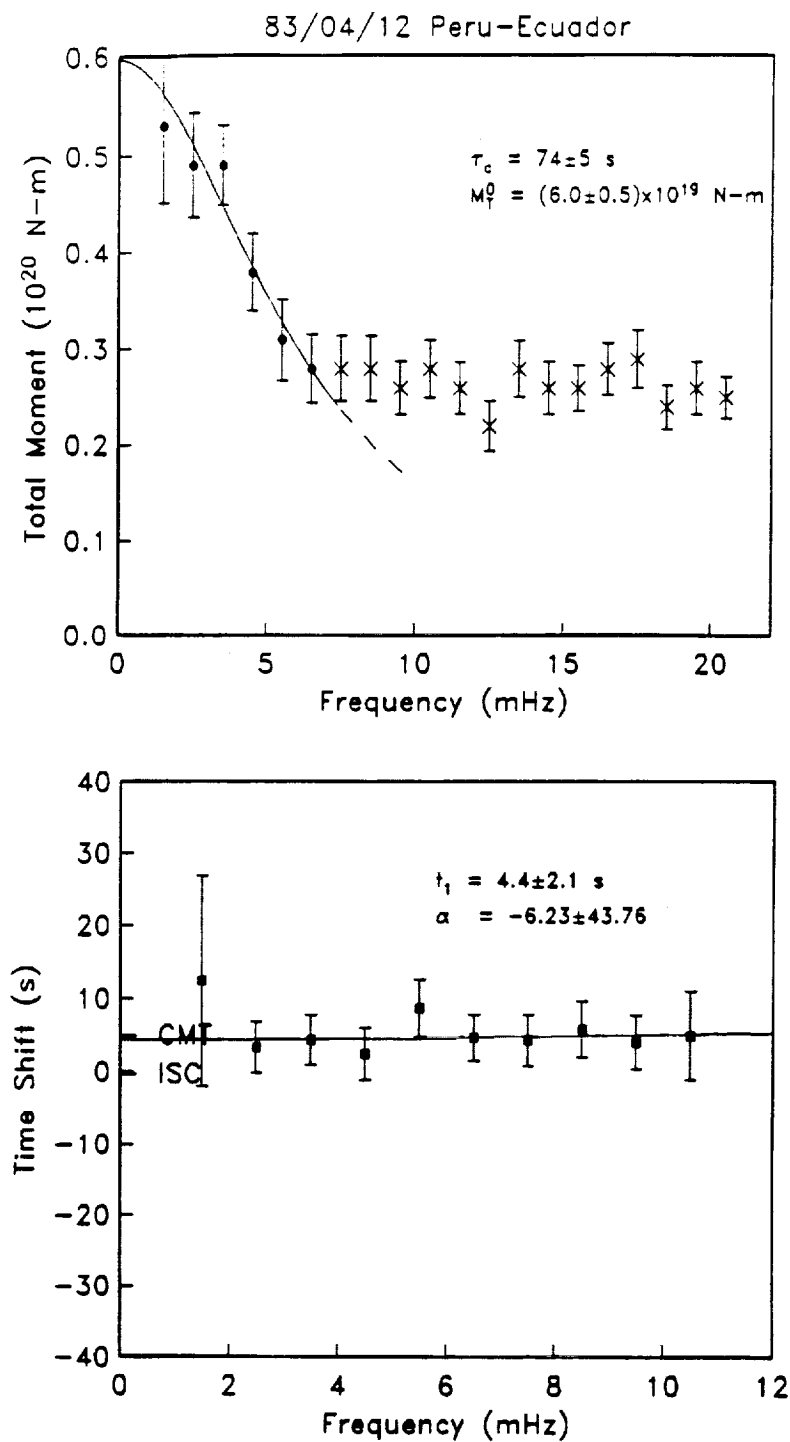


Fig 6.4 continued



**Fig. 6.5 - 89/04/12 Peru-Ecuador event. a) Amplitude spectra: observed (dots) and modelled (solid line). b) Phase-delay spectra: observed (dots) and modelled (solid line). Error bars represent one standard deviation.  $M_T^0$ ,  $t_1$ ,  $\tau_c$ ,  $\alpha$  are computed by least square fitting of (2.6) and (2.7)**

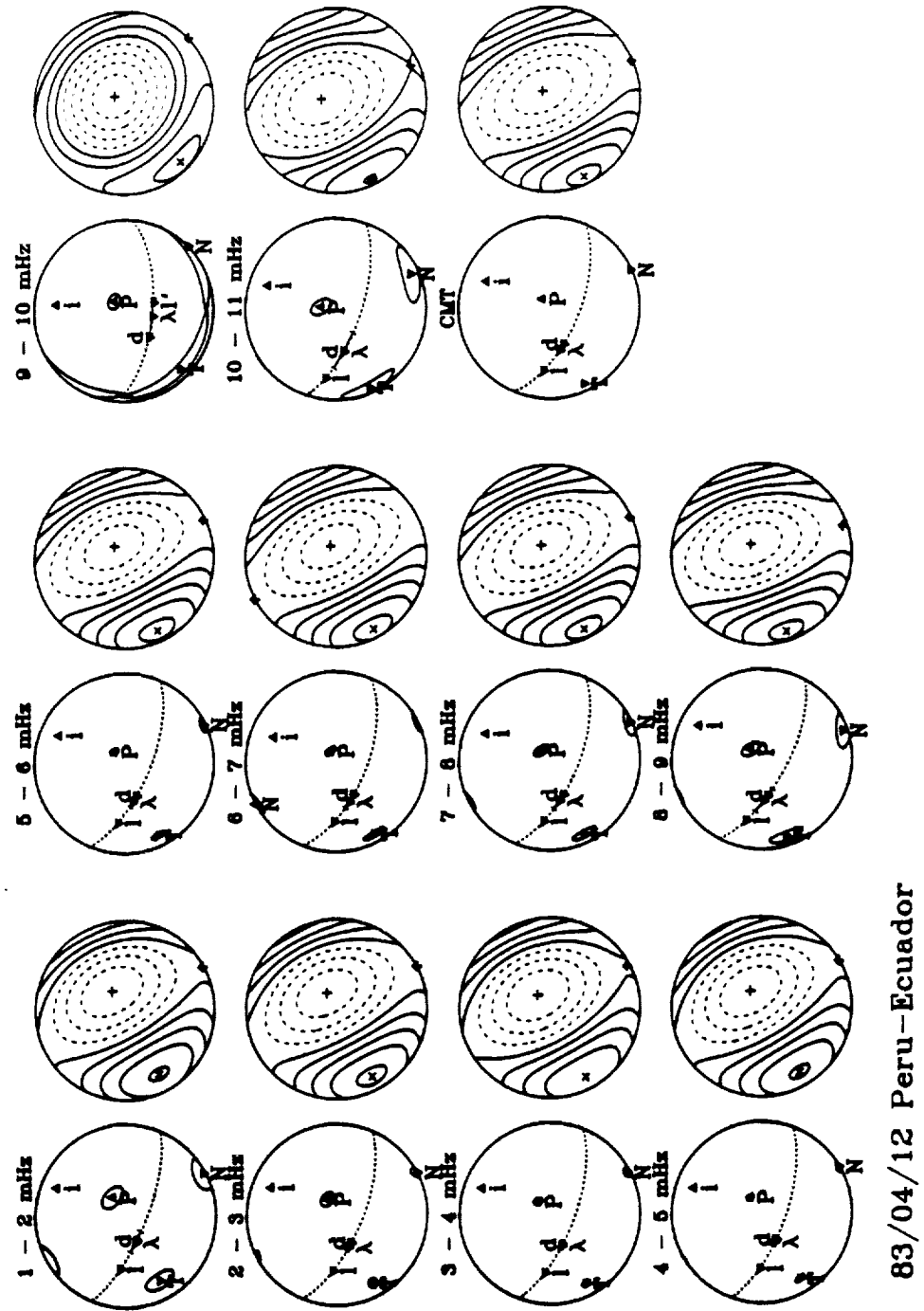
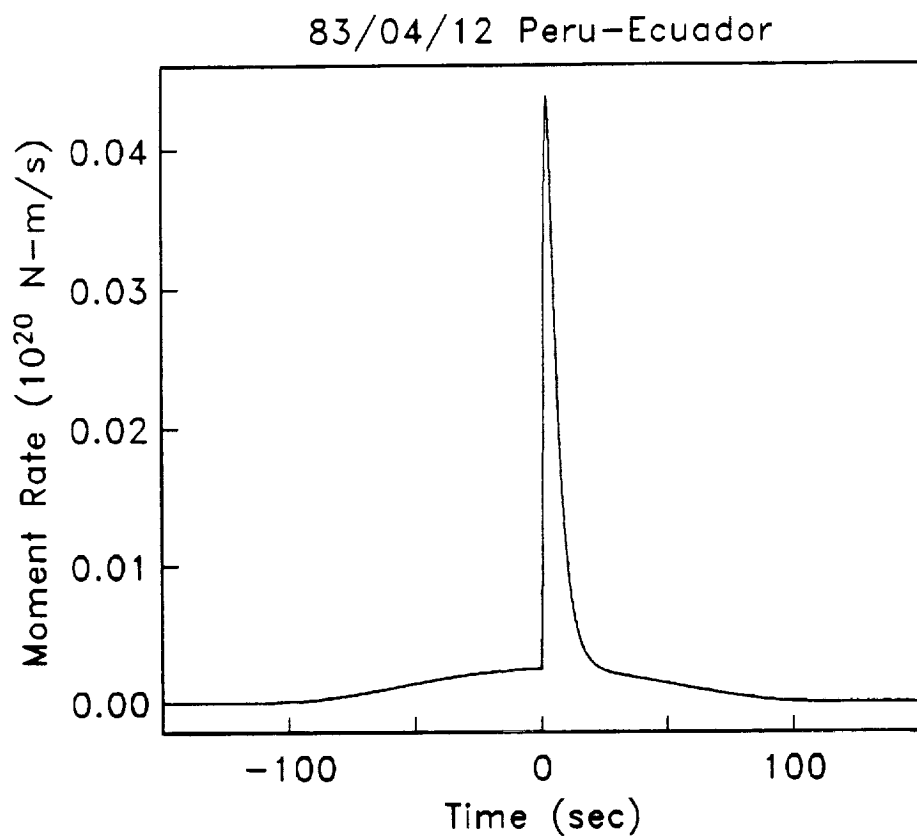


Fig 6.6 - Source-mechanism spectra  $\hat{M}(\omega)$  for the 89/04/12 Peru-Ecuador event. For details on the plotting convention see Riedesel and Jordan (1989)

type	start	durat.	moment	rise	decay
dbexp	0.00	40.00	0.27	1.00	4.00
hann	-110.00	220.00	0.27		



**Fig. 6.7 - a) Source model for the 83/04/12 Peru-Ecuador event. b) Amplitude spectra: observed (dots) and modelled (solid line). c) Phase-delay spectra: observed (dots) and modelled (solid line). Error bars represent one standard deviation.  $M_T^0$ ,  $t_1$ ,  $\tau_c$ ,  $\alpha$  are computed from the source time function in a)**

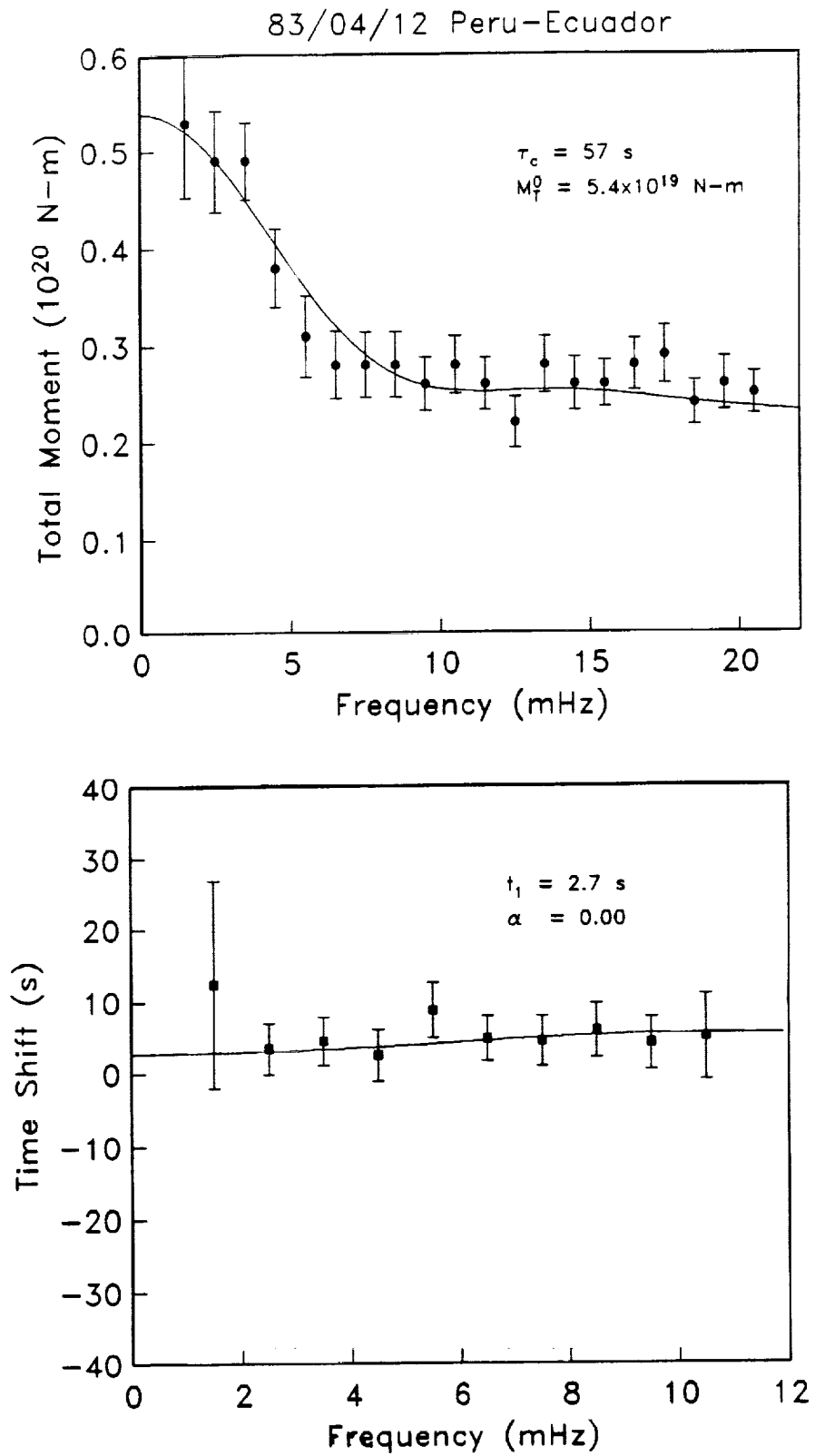


Fig 6.7 continued



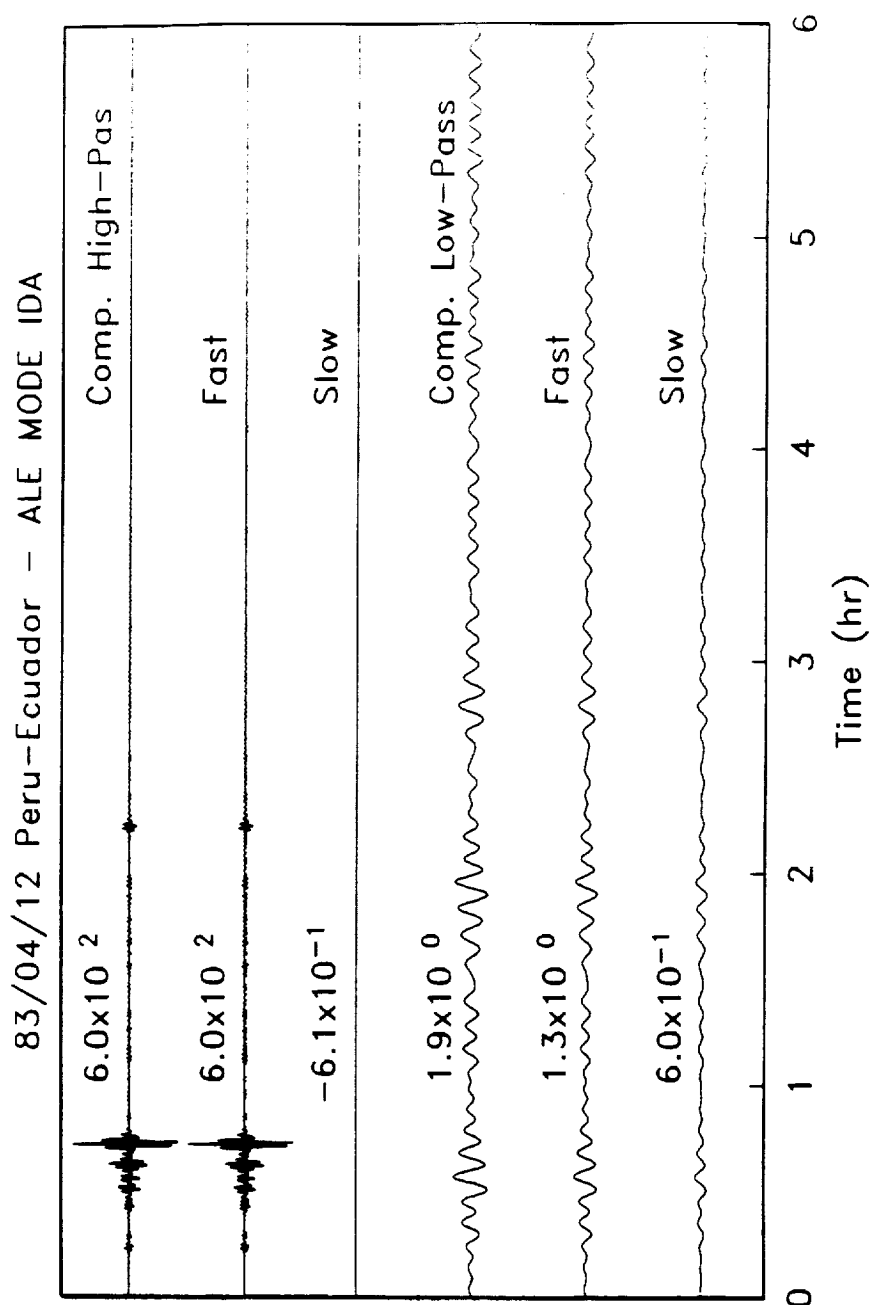


Fig 6.8 - synthetic seismograms of ALE computed using the source of Fig. 6.7a (compound) and its components (fast and slow). The three traces above are band-pass filtered with a cosine filter between 8 and 22 mHz. The three traces below are band-pass filtered with a cosine filter between 0.5 and 3 mHz. A scaling factor of 100 is applied to low-pass filtered traces.

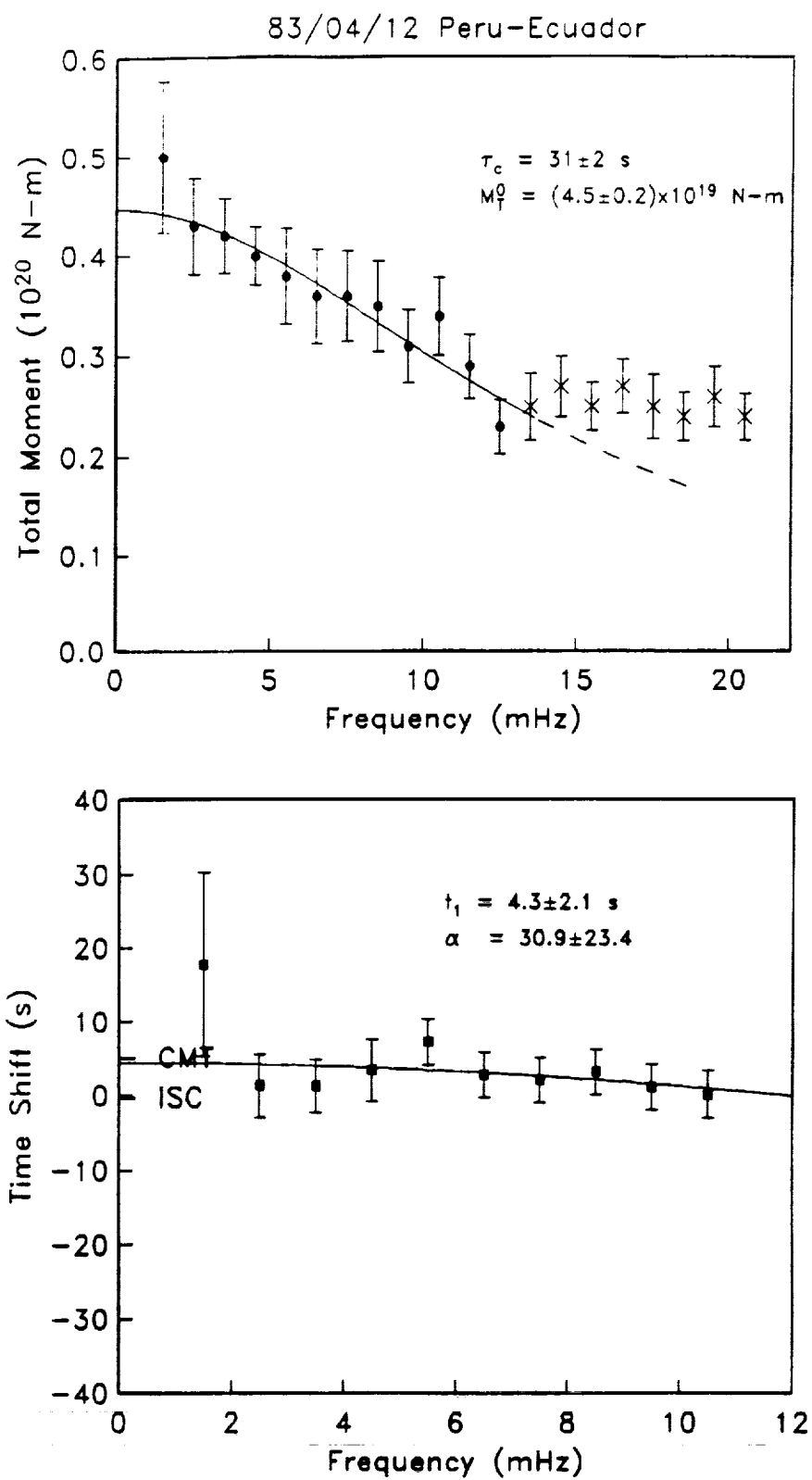


Fig. 6.9 - as in Fig 6.5 but with a centroid depth of 91 km

type	start	durat.	moment	rise	decay
dbexp	0.00	40.00	0.27	1.00	4.00
hann	-60.00	120.00	0.20		

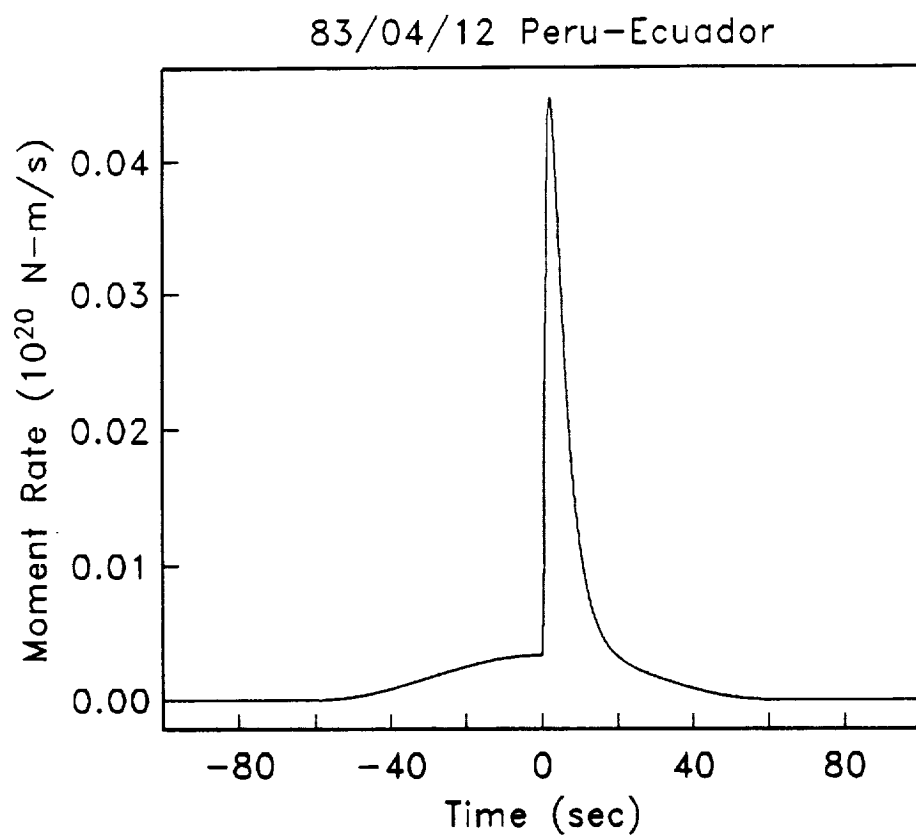


Fig. 6.10 - as in Fig 6.7 but with a centroid depth of 91 km

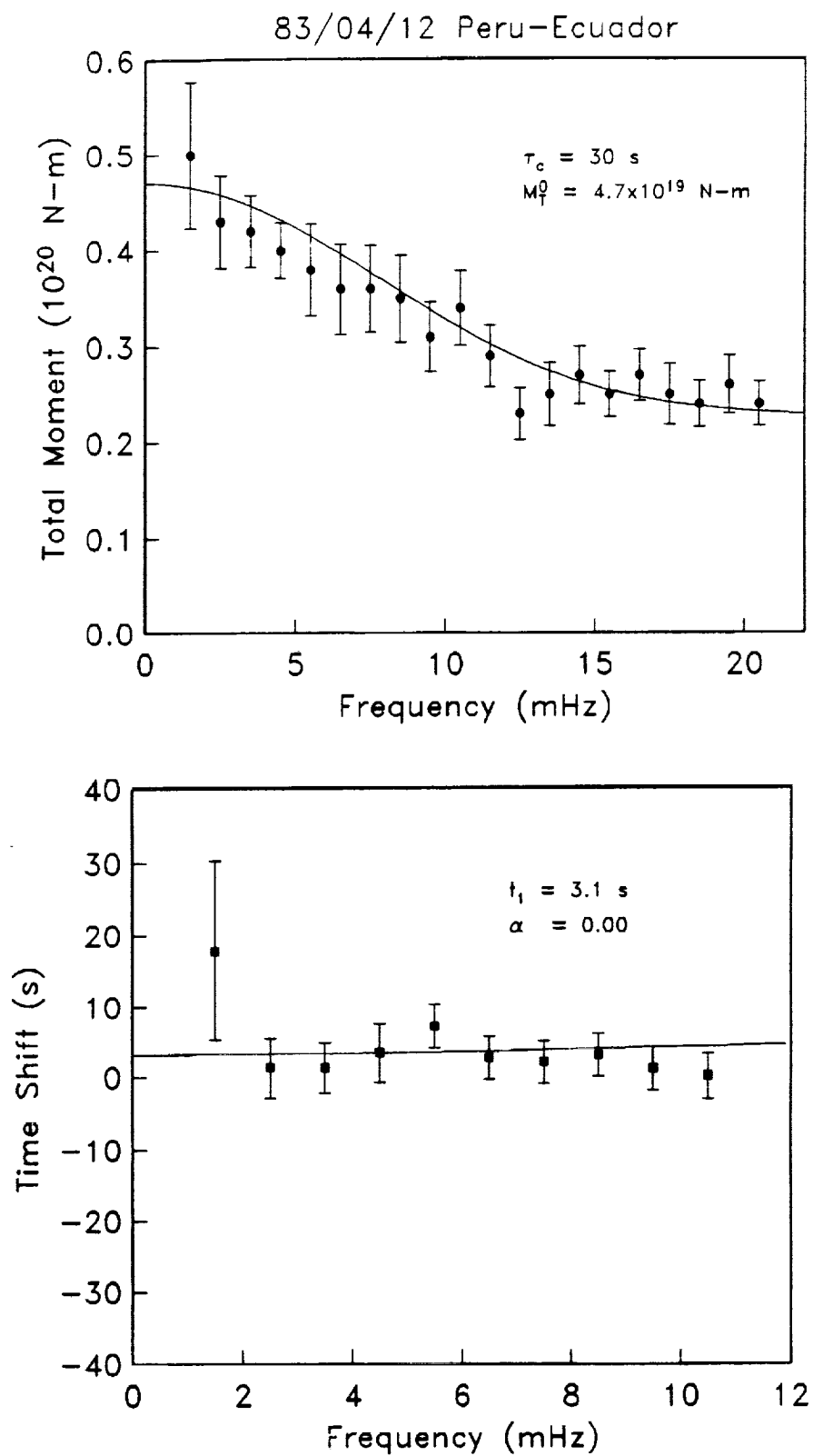


Fig 6.10 continued

## CHAPTER 7 - IRPINIA, ITALY

### 7.1 EVENT DISCUSSION

This is one the best studied events ever. It is a normal earthquake that developed on at least three, and possibly as many as five, different faults. The process lasted at least 45 seconds. There is agreement between the various researchers on the time source function but there is no agreement on the precise location of each fault involved and on the dip of some of them; only the model for the first seven seconds of rupture is rather undisputed. Fig 7.1 shows the model proposed by Bernard and Zollo (1989). The rupture started at a depth of about 12 km (Westaway and Jackson, 1987) on a fault dipping  $70^\circ$  and initially developed to the south-east. It then started to propagate north-west. The next major episode known as the "20-second" subevent is more controversial. Some authors, following Westaway and Jackson (1987), think that there were two distinct ruptures. First a tiny rupture still with similar steeply-dipping mechanism occurred to the south of the nucleation point with a delay of about 12 seconds, followed by a rupture, possibly along a sub-horizontal plane, about 5 km north of the nucleation point with a delay of about 20 seconds. Other researchers, following Bernard and Zollo (1989), believe that the rupture to the south was indeed the "20-second" rupture, and, in accord with Westaway and Jackson, that it took place along a sub-horizontal fault. Harabaglia et al. (1990) believe that this triggered also some motion on a  $70^\circ$  dipping continuation to the south-east of the main fault. Finally the

third major episode, known as the "40-second" subevent, took place on a fault parallel to the main one, about 10 km to the north of the nucleation point. Its dip is poorly constrained; it might have been an antithetic fault or sub-horizontal or simply parallel to the main one.

The main disagreements between the various authors are on the precise location of some of these faults and on their dip. As stated before our method does not have a resolution of the order of 10 to 20 km on the horizontal plane. The uncertainty on the dip might be a more serious problem. Since the event is rather shallow, the  $m_{r\phi}$  and  $m_{r\theta}$  components of the moment tensor are very poorly constrained, and this reflects to a large uncertainty on the dip as well. If the event would have been deeper we could have not discounted this problem.

The earthquake triggered over 20 accelerographs of the ENEA-ENEL network, eight of which were within 50 km of the faults. Modeling the accelerograms requires a moment release of about  $1.5 \cdot 10^{19}$  to  $2 \cdot 10^{19}$  N-m depending on the different methods adopted. Teleseismic studies find higher values, between  $2.5 \cdot 10^{19}$  (CMT) and  $3 \cdot 10^{19}$  N-m (Boschi et al., 1981). In particular Kanamori and Given (1982) obtain  $2.8 \cdot 10^{19}$  N-m inverting surface waves at periods of 4 mHz using IDA records. The discrepancy between moment retrieved at teleseismic distances and moment determined in the near field, is rather high but still acceptable on the assumption that the accelerogram network did not properly cover the whole fault region. It is also noteworthy that the computed centroids have depths of 10 to 20 km while Harabaglia et al. (1990), among others, showed that the bulk of the rupture detected in the

near field occurred at very shallow depths, possibly between 2 and 6 km, such that 5 km seems to be a more realistic estimate for a centroid based exclusively on these data.

The 10 IDA stations used in our inversion are shown in Appendix. Table 8.1 shows the CMT, NEIC and ISC parameters. BDF is not included in this set since we believe its instrument response was not properly calibrated at the time. Two other IDA stations, ESK and PFO, are aligned along the fault strike and show very strong focusing and defocusing effects. Their inclusion on the amplitude spectrum inversion does not affect significantly the final outcome since we make use of about 4 Rayleigh wave orbits for each trace and any influence of such focusing and defocusing is averaged out. In similar cases the phase-delay spectrum is somewhat affected, so we tested their influence on the solution and found that their trend is consistent with that of the other stations. The time-shift and amplitude spectra are shown in Fig. 7.2, solid dots. The odd-looking phase-delay spectrum is the result of the same trend for eight out of the 10 stations used; RAR and TWO are the only one to show an opposite one. Another strange feature is the drop in energy visible on the amplitude spectrum between 7 and 9 mHz. This is also a common trend for most of the records.

The amplitude spectrum is similar to that of the Peru-Ecuador event although the phase-delay is not. This lead us to explore the possibility of a compound source. However, in this case we do not need any precursor to model the data.

As stated before, source models based on near-field data at high frequency (0.5-10 Hz) are shallower than the models obtained

using teleseismic data in frequency range between 4 and 20 mHz. This could be an indication of some frequency dependence of the centroid. It might also mean that the geometry of the near-field network was such that portion of the various faults were not properly recovered.

We tried an inversion with a centroid depth of 9 and 5 km (Fig. 7.2, open dots and triangles). The time-shift spectrum is not significantly affected but the amplitude spectrum has an overall drop across the bands. The RJ variance reduction improves slightly at higher frequencies and worsen in equally small amount at lower frequencies. If these changes in the residual variance were significant, an explanation would be that a rupture as the one modeled by the above mentioned authors, mainly a shallow one on steep dipping faults, was associated to a longer, slower and deeper rupture, possibly along a sub-horizontal plane. If this were the case, the slower rupture should be slow enough not to influence significantly the near field but fast enough to be detectable by CMT based methods. Unfortunately, we do not think that the difference in variance reduction across the bands obtained by RJ is really significant. The frequency dependence of the centroid is a possibility but is currently beyond the resolution of our method.

We see a marked change of slope at about 6 or 7 mHz. This leads us to believe that a "slow" source starting at about the origin time and lasting about 80 to 150 seconds with a moment release of about  $8 \cdot 10^{18}$  N-m associated to a fast rupture of about  $2 \cdot 10^{19}$  to  $2.4 \cdot 10^{19}$  N-m would explain the data reasonably well. Another reason why we think such a "slow" source is reasonable, is that the



triggered accelerographs kept on recording for as much as 90 seconds: the small amplitude phases after the first 50 seconds are usually discounted as lateral arrivals and reflections of various kind. This is certainly a possibility, but it is also possible that some of the background energy is given by the relatively slower rupturing fault at depth.

We are faced with one serious problem in trying to model the Irpinia source time function. We need a compact source to model an essentially flat amplitude spectrum beyond 8 mHz, and all the rupture models available have relevant characteristic durations, about 14 seconds. We also need an overall larger moment release. If we assumed a centroid depth of 9 km, we would still need an additional  $4 \cdot 10^{18}$  N-m release in the first few seconds. If we assumed a greater depth, 14 km as in the CMT for example, this value should be as high as  $6 \cdot 10^{18}$  N-m. Consequently on the assumption that the latter value is excessive, we prefer to set our centroid depth at 9 km and we use a modified version of the Bernard and Zollo source, adding a total of  $4 \cdot 10^{18}$  N-m to the rupture in the first 7 seconds. We superimpose to this source a slow component with a duration of a 100 seconds and a moment of  $8 \cdot 10^{18}$  N-m. The results are shown in Fig. 7.2

We believe that as a future development of this study, we should try to include the GDSN data in the inversion process and see if we can bound better our model: their lower frequency limit is about 4 mHz. Our experience tells us that the low frequencies measurements are very reliable even with few records available while higher frequencies are slightly less reliable and even with

that limit they could be of great utility at higher frequencies in trying to clarify if the compact high frequency source we observe with the current data set is the result of an insufficient number of records.

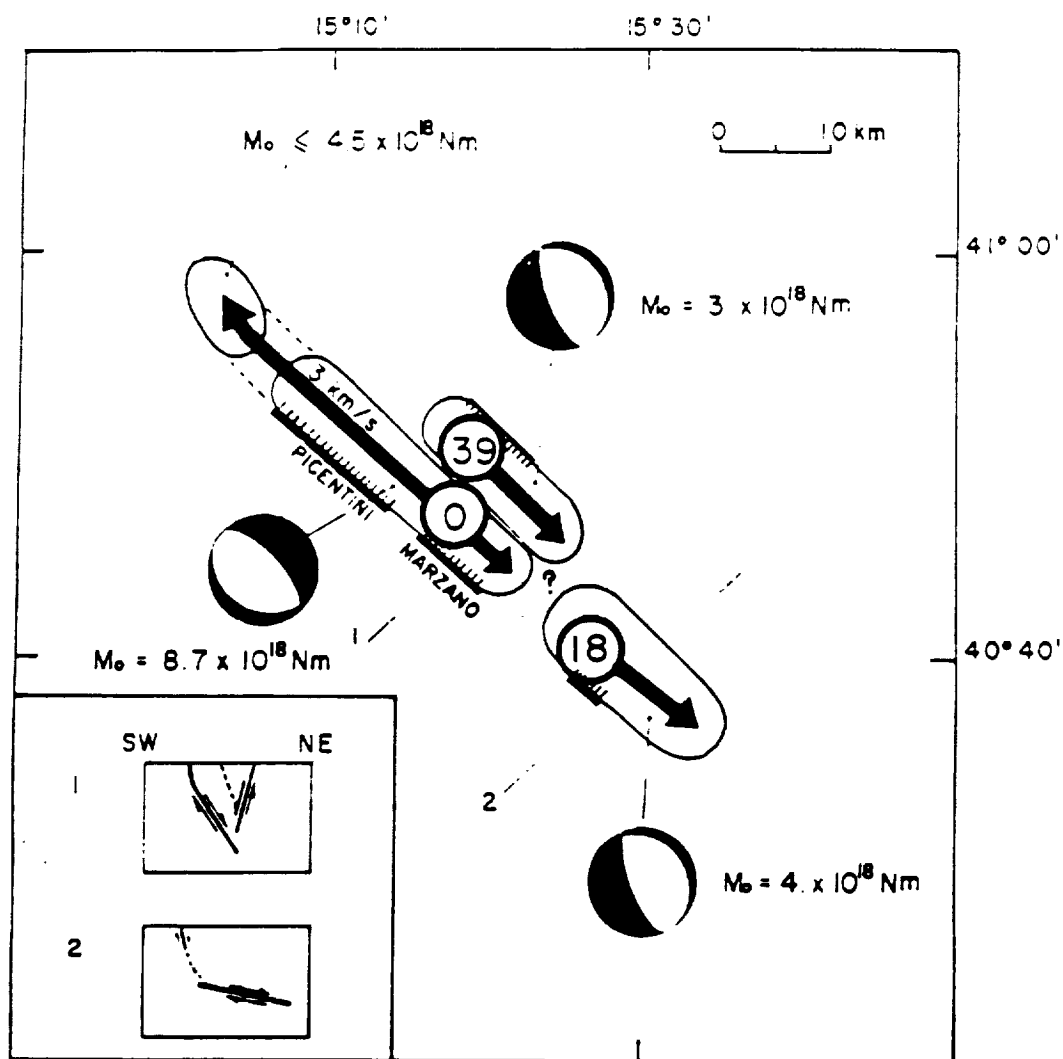


**Fig 7.1- Map of the source region for the 80/11/23 Irpinia event (from Bernard and Zollo, 1989)**

type	start	durat.	moment	rise	decay
dbexp	0.00	4.00	0.04	1.00	1.00
dbexp	2.00	5.00	0.09	1.00	1.00
dbexp	7.00	3.00	0.04	1.00	1.00
dbexp	18.00	7.00	0.04	1.00	1.00
dbexp	39.00	6.00	0.03	1.00	1.00
slow	0.00	100.00	0.08	1.00	30.00

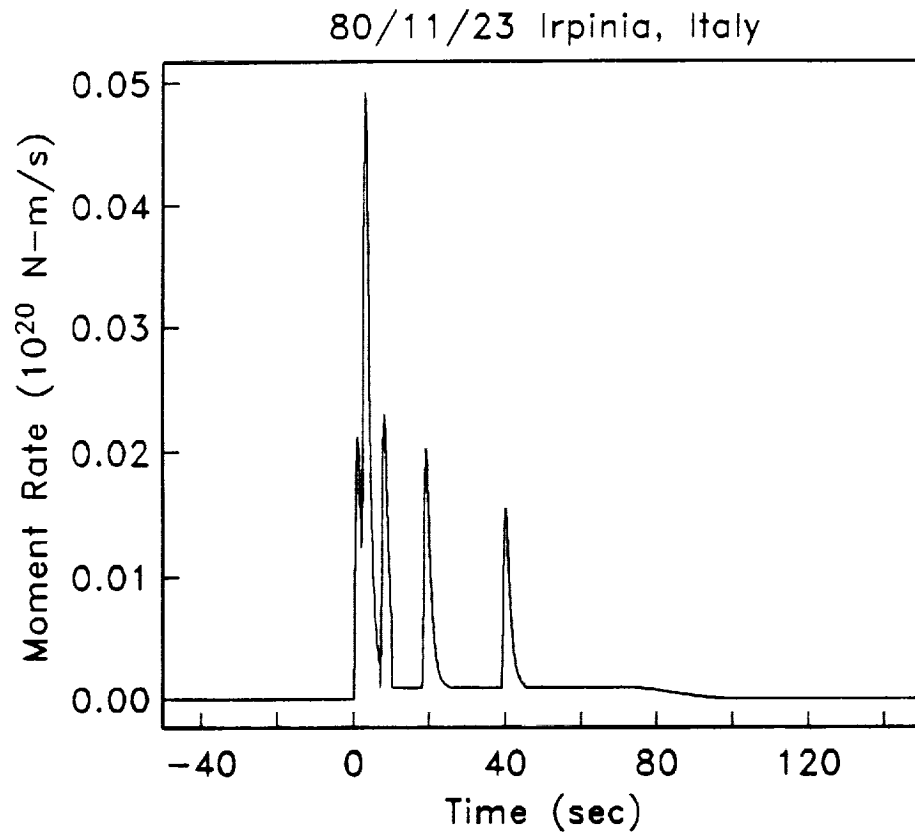


Fig. 7.2 - a) Source model for the 80/11/23 Irpinia event. b) Amplitude spectra: observed (dots, depth 14 km; circles, depth 9 km; triangles, depth 5 km) and modelled (solid line). c) Phase-delay spectra: observed (dots, depth 14 km; circles, depth 9 km; triangles, depth 5 km) and modelled (solid line). Error bars represent one standard deviation.  $M_T^0$ ,  $t_1$ ,  $\tau_c$ ,  $\alpha$  are computed from the source time function presented in this study)

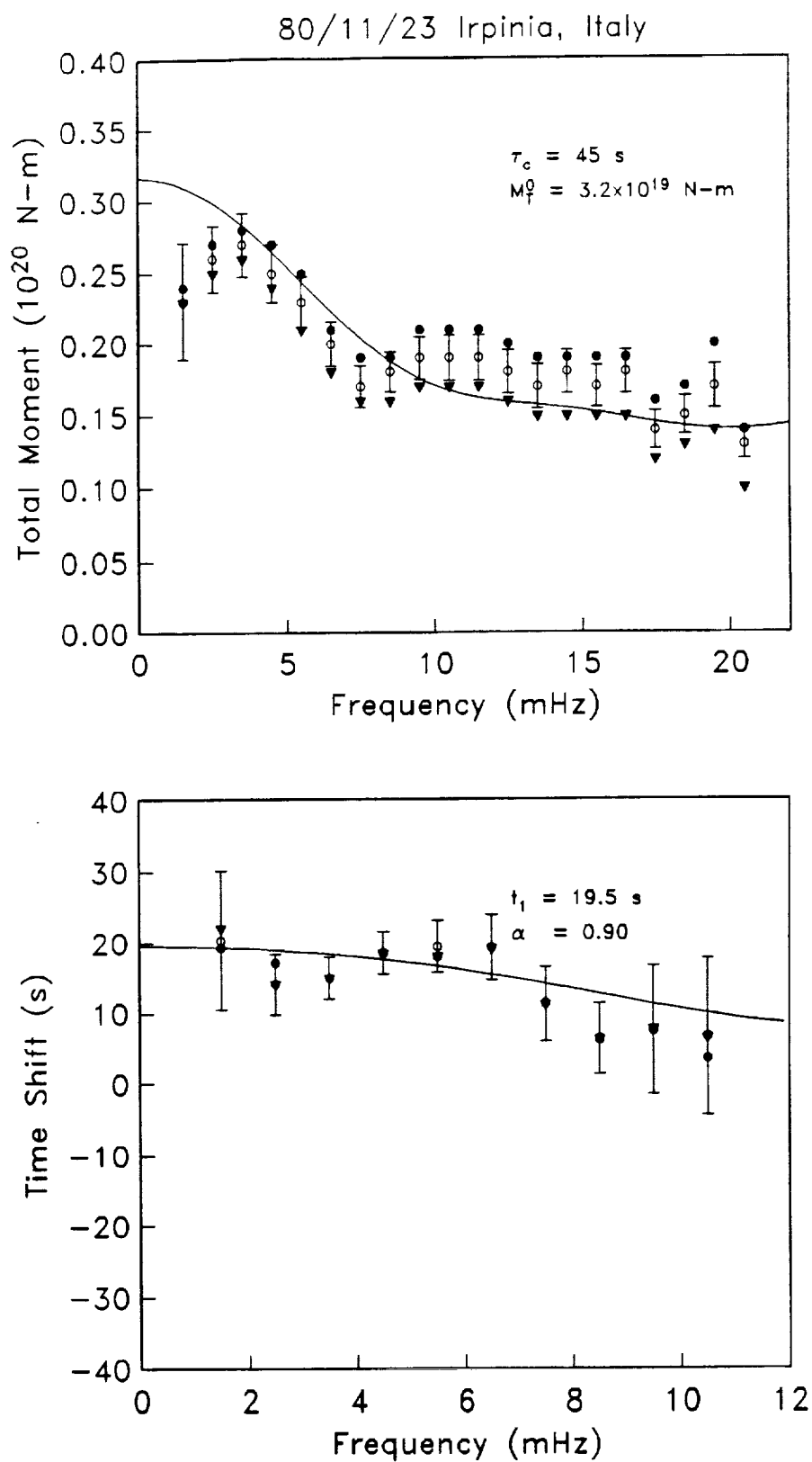


Fig 7.2 continued



## CHAPTER 8 - DISCUSSION

### 8.1 PARAMETERS REVIEW

We have examined in detail 10 intermediate and deep focus events and two shallow ones. Table 8.1 contains the parameters obtained with the RJ and SJ methods.

In Fig 8.1 we plot the total scalar moment with respect the characteristic duration. We use the scaling relationship between the above quantities and the rupture velocity proposed by Kanamori and Given (1981) to plot three velocity curves on the same figure.

We show in Fig. 8.2 the total moment we retrieve with respect to the CMT. Our values are consistent for 10 out of 12 events. The two earthquakes for which there is a sizeable difference are the 1983 Peru-Ecuador and Akita-Oki. We discussed the former in detail in chapter 6; the CMT value does not fully account for the slow precursor. The latter shows a trend that we have noticed to be true for most of the major events we have processed at MIT: the CMT moment seems to be systematically smaller than ours for events larger than  $1 \cdot 10^{20}$  N-m.

In Fig. 8.3 we show how our time centroid compares with the CMT. The values are within few seconds of each other, with the notable exceptions of the 1983 Banda Sea and 1980 Irpinia earthquakes. The Banda Sea is briefly discussed in chapter 4.2. To our knowledge this event has not been subject to any extensive investigation by other researchers, so it is not easy to formulate any hypothesis of why we observe such a large discrepancy. The other exception is the Irpinia earthquake. We have argued in chapter 7 that the event probably has

a slow component associated with the high frequency source and for this reason we observe larger time-shifts in the lower frequency bands.

## 8.2 EVENTS REVIEW

The deeper earthquakes (depth greater than 70 km) are a representative subset of a larger group of about 40 events with similar geographical locations, almost equally divided between deep and intermediate events, that we have investigated. The vast majority of these earthquakes, about 75%, have rather fast rupturing processes even in those cases where they are known to be complex events. We presented in this study nine typical examples of those fast events and two examples of earthquakes with slower sources. We model the slower ones by superimposing a relatively long coda to a fast rupturing source. Finally one earthquake, the 1983 Peru-Ecuador, seems to have a low-frequency slow precursor. Such event was originally identified by Jordan (1991). Precursive events have been observed elsewhere (Ihmle et al., 1993, for the shallow focus; Dziewonski and Gilbert, 1974, for the deep 1970 Colombia and 1963 Peru-Bolivia events), but since we have found no other occurrence in our set, we cannot estimate how common they could be within intermediate depth earthquakes. We have concentrated our search toward intermediate and deep events in three geographical locations, South America, Japan and the border between the Indo-Australian and the Pacific Plate in the time interval between 1977 and 1989. A more global survey will probably give us a better understanding. Nonetheless, it is noteworthy that the deep events we processed (depth greater than 300 km) are all fast.



The two shallow earthquakes we have examined in detail are rather complex. As with many other events of this nature their mechanism is time dependent and this adds to the difficulty of analyzing them. In the case of the Irpinia Earthquake in particular, the centroid depth is poorly constrained and our choice is bounded mostly by the models available from high-frequency studies. We model it by superimposing a slow component to a fast rupturing source obtained by inversion of near-field data. If the correct depth of the centroid turned out to be deeper than the 9 km we have selected (a rather shallow value compared to the 14 km of the CMT), then the whole amplitude spectrum would be shifted up and this would in turn mean that to model it, the fast rupturing source would have to be about 25% greater than the one inferred by the near-field data.

The other shallow earthquake, the Akita-Oki, has the amplitude spectrum characterized by a marked drop in the higher frequencies. To model it, we need to create an interference pattern by adding a third rupture episode 80 seconds after the origin time to the two subevents recognized in literature (example, Houston and Kanamori, 1986). We do not know yet if this feature is true or if it is the result of some unusual source-receiver geometry.

### 8.3 METHOD ASSESSMENT

The combined RJ and SJ technique is an extremely powerful tool and is very reliable if the azimuthal coverage is adequate (eight or more stations are desirable). The amplitude spectrum is affected by the ambient noise and consequently we obtain our most dependable results for larger events. The time-shift spectrum on the contrary is

almost unaffected by the ambient noise, so its estimate is as accurate for the smaller events as it is for the larger ones. Unfortunately the current models do not allow for time-shift measurements that have standard errors less than about three seconds. This means that parameters like  $\alpha$  are quite often poorly constrained.

The most serious limit we have experienced is that we cannot compute the time-shift up to the 21 mHz we would need for consistency with SJ. If we could compute a time-shift spectrum up to that frequency, our ability to model the source time function would greatly improve. Ihmle et al. (1993) have done this by cross-correlating Rayleigh and Love waves for the 1989 Macquarie Ridge earthquake. The method is extremely promising but requires untruncated data to work at its best. For older events like Akita-Oki and Irpinia it is therefore necessary to include some of the GDSN instruments available at the time. The dynamic range of these instruments limits their usage below 4 mHz but they should be adequate in the higher frequencies.

		$h$ km	$M_T^0$ $10^{20}$ N-m	$\tau_c$ s	$\Delta t_1$ s	$\alpha$
78/ 9/23	NEW HEBRIDES	207	$0.17 \pm 0.01$	$10 \pm 2$	$3.7 \pm 2.2$	$31 \pm 31$
80/11/23	IRPINIA	9	$0.31 \pm 0.02$	$47 \pm 4$	$19.1 \pm 2.9$	$1.8 \pm 0.7$
82/10/ 7	BANDA SEA	521	$0.13 \pm 0.01$	$12 \pm 2$	$4.3 \pm 2.1$	$0.9 \pm 31.6$
83/ 4/12	PERU-ECUADOR	111	$0.60 \pm 0.05$	$74 \pm 5$	$4.4 \pm 2.1$	$-6.2 \pm 43.7$
83/ 5/26	AKITA-OKI	13	$6.8 \pm 0.3$	$42 \pm 1$	$19.2 \pm 2.7$	$1.2 \pm 0.9$
83/11/24	BANDA SEA	142	$1.9 \pm 0.1$	$15 \pm 1$	$14.4 \pm 2.5$	$0.2 \pm 1.5$
86/11/23	PERU-ECUADOR	92	$0.19 \pm 0.01$	$14 \pm 1$	$5.7 \pm 1.8$	$14 \pm 8$
87/ 2/23	VANUATU ISL.	250	$0.31 \pm 0.01$	$1 \pm 10$	$8.1 \pm 2.0$	$0.8 \pm 4.7$
87/10/29	TALAUD ISL.	142	$0.17 \pm 0.01$	$18 \pm 1$	$5.0 \pm 2.0$	$35 \pm 25$
88/ 2/20	BANDA SEA	321	$0.055 \pm 0.001$	0 -	$2.9 \pm 2.0$	$128 \pm 184$
88/ 9/ 7	S. OF HONSHU	491	$0.10 \pm 0.01$	$1 \pm 10$	$2.4 \pm 1.7$	$-40 \pm 258$
89/12/ 3	PERU-BRAZIL	151	$0.074 \pm 0.004$	$3 \pm 16$	$6.5 \pm 2.0$	$7.6 \pm 5.5$

Table 8.1 - Parameters determined with the RJ and SJ methods.  
 $\Delta t_1$  is computed with respect to the NEIC origin time.

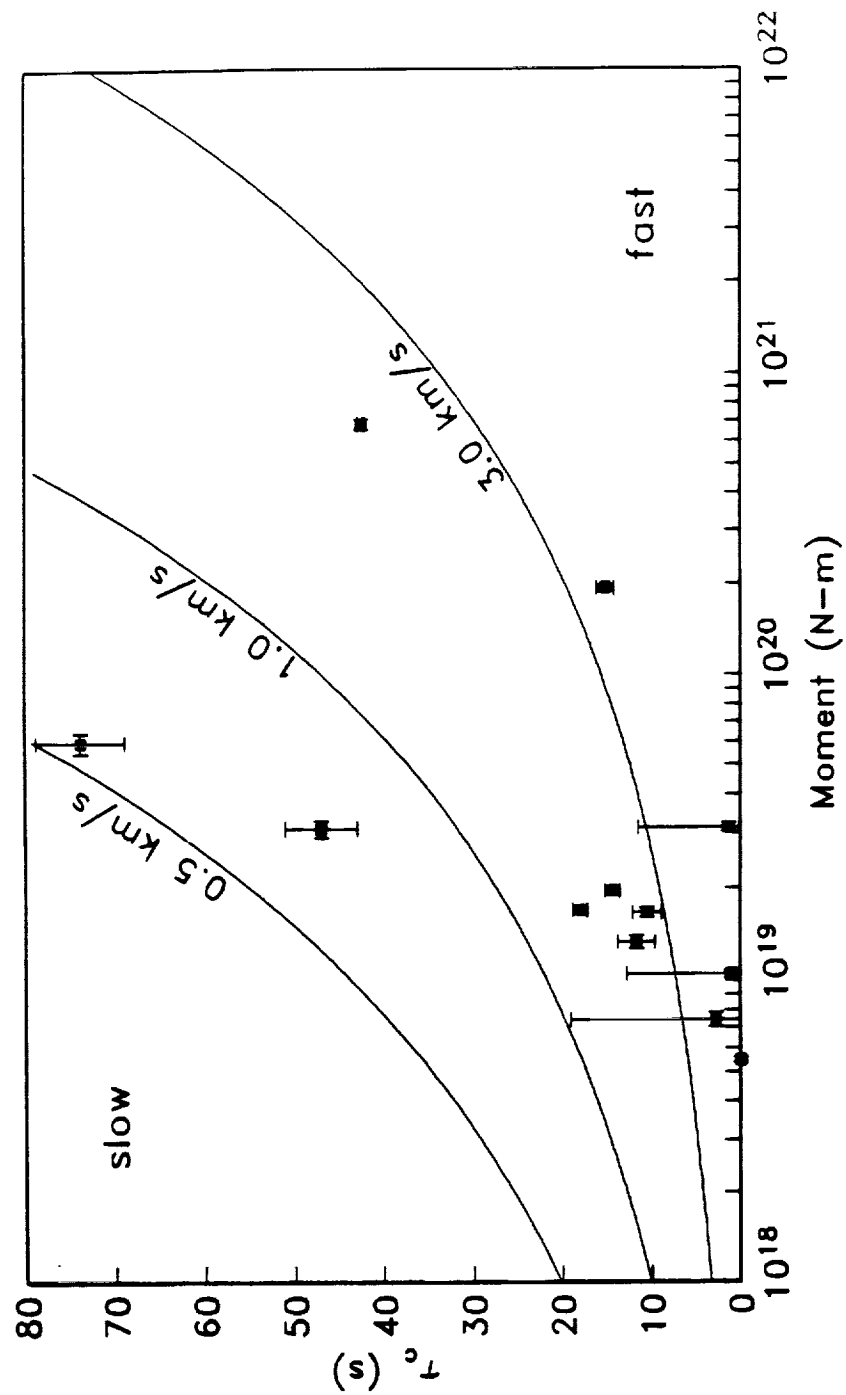


Fig 8.1 -  $M_T^0$  versus  $\tau_c$  diagram. The rupture velocity curves are inferred according to the scaling laws from Kanamori and Given (1981)

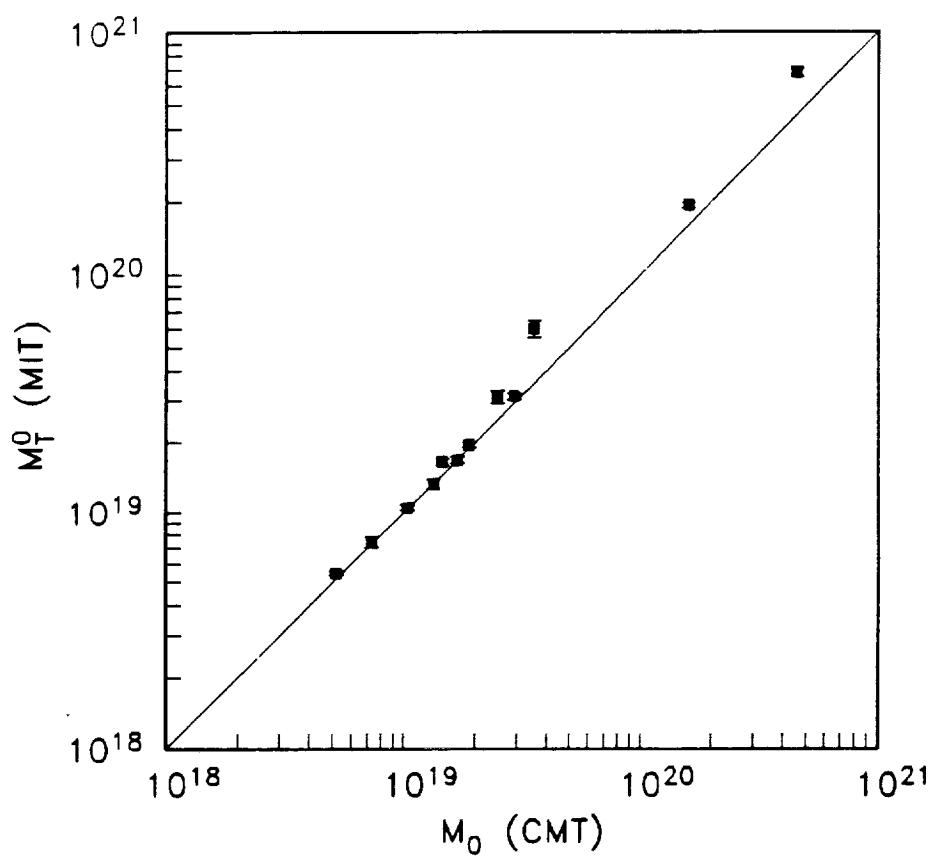


Fig 8.2 -  $M_T^0$  (MIT) versus  $M_0$  (CMT) diagram.

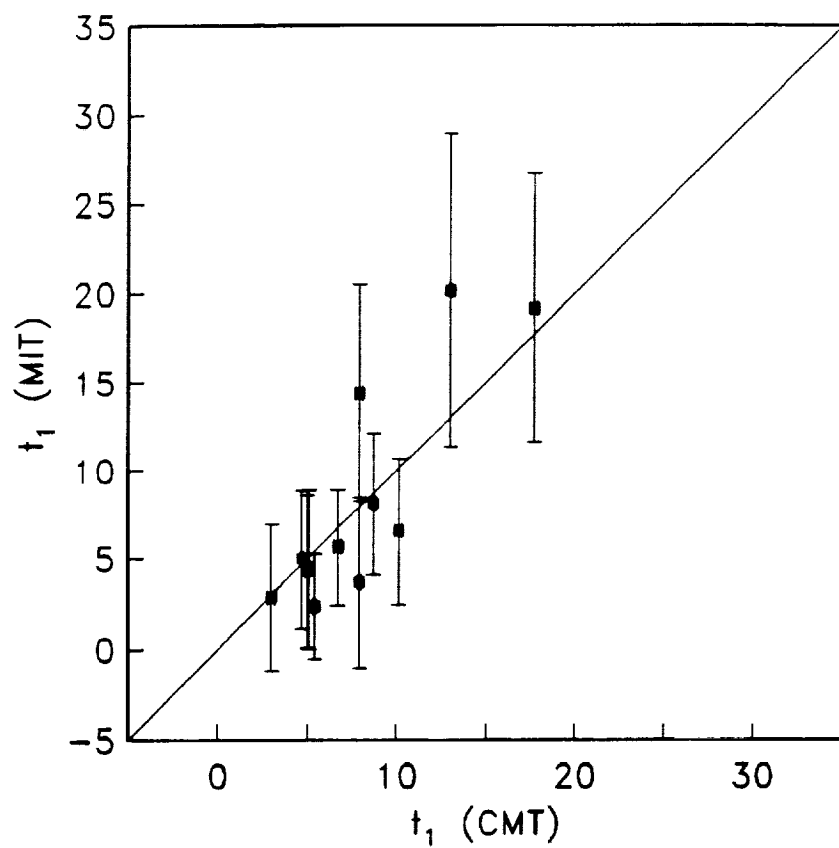


Fig 8.3 -  $t_1$  (MIT) versus  $t_1$  (CMT) diagram.

## REFERENCES

- Agnew, D. C., and J. Berger, Vertical seismic noise at very low frequencies, *J. Geophys. Res.*, 83, 5420-5424, 1978.
- Aki K., Scaking law of seismic spectrums, *J. Geophys. Res.*, 72, 1217-1231, 1967.
- Boschi, E., F. Mulargia, E. Mantovani, M. Bonafede, A. M. Dziewonski and J. H. Woodhouse, The Irpinia Earthquake of November 23, 1980, *EOS, Trans. Am. geophys. Un.*, 62, 330, 1981.
- Bernard, P., and A. Zollo, The Irpinia (Italy) 1980 Earthquake: Detailed Analysis of a Complex Normal Faulting, *J. Geophys. Res.*, 94, 1631-1647, 1989.
- Beroza, G., and T. H. Jordan, Searching for slow and silent earthquakes using free oscillations, *J. Geophys. Res.*, 95, 2485-2510, 1990.
- Brune, J. N., Tectonic stress and the spectra of seismic shear waves from earthquakes, *J. Geophys. Res.*, 75, 4997-5009, 1970.
- Cifuentes, I. L., and P. G. Silver, Low-frequency source characteristics of the great 1960 Chilean earthquake, *J. Geophys. Res.*, 94, 643-663, 1989.
- Dziewonski, A. M., T.-A. Chou, and J. H. Woodhouse, Determination of earthquake source parameters from waveform data for studies of global and regional seismicity, *J. Geophys. Res.*, 86, 2825-2852, 1981.
- Dziewonski, A. M., and F. Gilbert, Temporal variation of the seismic moment tensor and the evidence of precursive compression for two deep earthquakes, *Nature*, 247, 185-188, 1974.
- Dziewonski, A. M., and D. L. Anderson, Preliminary reference Earth model, *Physics of the Earth and Planetary Interiors*, 25, 297-356, 1981.

- Ekstrom, G., A. M. Dziewonski, and J. H. Woodhouse, Centroid-moment tensor solutions for the 51 IASPEI selected earthquakes, 1980-1984, *Physics of the Earth and Planetary Interiors*, 47, 62-66, 1987.
- Fukuyama, E., and K. Irikura, Rupture process of the 1983 Japan Sea (Akita-Oki) Earthquake using a waveform inversion method, *Bulletin of the Seismological Society of America*, 76, 1623-1640, 1986.
- Gilbert, F., Excitation of the normal modes of the Earth by earthquake sources, *Geophysical Journal of the Royal Astronomical Society*, 22, 223- 226, 1970.
- Gilbert, F., Derivation of source parameters from low-frequency spectra, *Phil. Trans. R. Soc. London A*, 274, 369-371, 1973.
- Gilbert, F., and A. M. Dziewonski, An application of normal mode theory to the retrieval of structural parameters and source mechanisms from seismic spectra, *Phil. Trans. R. Soc. London A*, 278, 187-269, 1975.
- Harabaglia, P., P. Suhadolc, and G. F. Panza, Rupture process dynamics from inversion of accelerometric data, in *Irpinia dieci anni dopo, Riassunti degli interventi* (Enzo Boschi, Convenor), Sorrento, Napoli, 73-78, 1986.
- Houston, H., and H. Kanamori, Broadband rupture process and strong motions of large subduction zone earthquakes, *EOS, Trans. Am. geophys. Un.*, 67, 1119, 1986.
- Ihmlé, P. F., Harabaglia, P. and T. H. Jordan, Teleseismic detection of a slow precursor to the great 1989 Macquarie Ridge earthquake, *Science*, submitted, 1993.
- Jordan, T. H., A procedure for estimating lateral variations from low-frequency eigenspectra data, *Geophysical Journal of the Royal Astronomical Society*, 52, 441-455, 1978.
- Jordan, T. H., Far-Field detection of slow precursors to fast seismic ruptures, *Geophysical Research Letters*, 18, 2019-2022, 1991.
- Jordan, T. H., and L. N. Frazer, Crustal and Upper Mantle Structure From Sp Phases, *J. Geophys. Res.*, 80, 1504-1517, 1975.



- Kanamori, H., and J. J. Cipar, Focal process of the great Chilean earthquake, *Physics of the Earth and Planetary Interiors*, 9, 128-136, 1974.
- Kanamori, H., and J. W. Given, Use of long-period surface waves for rapid determination of earthquake-source parameters, *Physics of the Earth and Planetary Interiors*, 27, 8-31, 1981.
- Kanamori, H., and J. W. Given, Use of long-period surface waves for rapid determination of earthquake-source parameters, 2, *Physics of the Earth and Planetary Interiors*, 30, 260-268, 1982.
- Kanamori, H., and G. S. Stewart, Mode of the strain release along the Gibbs fracture-zone, Mid-Atlantic ridge, *Physics of the Earth and Planetary Interiors*, 11, 312-332, 1976.
- Kanamori, H., and G. S. Stewart, A slow earthquake, *Physics of the Earth and Planetary Interiors*, 18, 167-175, 1979.
- Okal, E. A., and L. M. Stewart, Slow Earthquakes along oceanic fracture zones: evidence for asthenospheric flow away from hotspots?, *Earth and Planetary Science Letters*, 57, 75-87, 1982.
- Riedesel, M. A., Seismic moment tensor recovery at low frequencies, Ph.D. thesis, University of California, San Diego, 1985.
- Riedesel, M. A., and T. H. Jordan, Display and assessment of seismic moment tensors, *Bulletin of the Seismological Society of America*, 79, 85-100, 1989.
- Riedesel, M. A., T. H. Jordan, A. F. Sheehan, and P. G. Silver, Moment-tensor spectra of the 19 Sept 85 and 21 Sept 85 Michoacan, Mexico, earthquakes, *Geophysical Research Letters*, 13, 609-612, 1986.
- Scholz, C. H., *The Mechanics of Earthquakes and Faulting*, 439, Cambridge University Press, Cambridge, 1990.
- Silver, P. G., and T. H. Jordan, Optimal estimation of scalar seismic moment, *Geophysical Journal of the Royal Astronomical Society*, 70, 755-787, 1982.

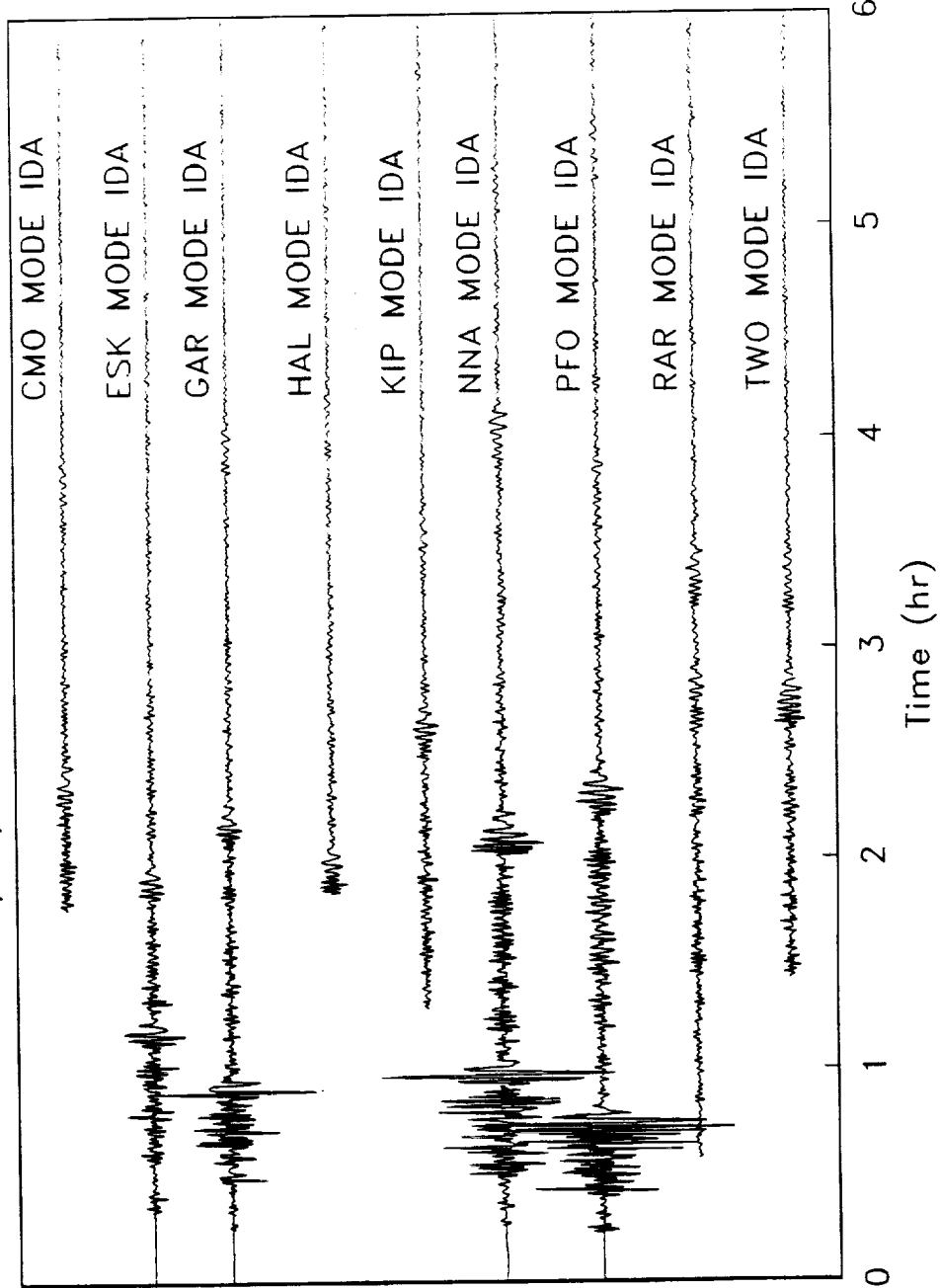
- Silver, P. G., and T. H. Jordan, Total-moment spectra of fourteen large Earthquakes, *J. Geophys. Res.*, 88, 3273-3293, 1983.
- Westaway, R., and J. Jackson, The earthquake of 1980 November 23 in Campania-Basilicata (southern Italy), *Geophys. J. R. astr. Soc.*, 90, 375-443, 1987.
- Widmer, R., G. Masters, and F. Gilbert, Spherically symmetric attenuation within the Earth from normal mode data, *J. Geophys. Res.*, 104, 541-553, 1991.
- Woodhouse, J. H., and A. M. Dziewonski, Mapping the upper mantle: three dimensional modelling of Earth structure by inversion of seismic waveforms, *J. Geophys. Res.*, 89, 5953-5986, 1984.
- Woodward, R.L., A. M. Forte, W.-J. Su, and A. M. Dziewonski, Constraints on the large-scale structure of the earth's mantle *J. Geophys. Res.*, special volume, in press, 1992.

## APPENDIX

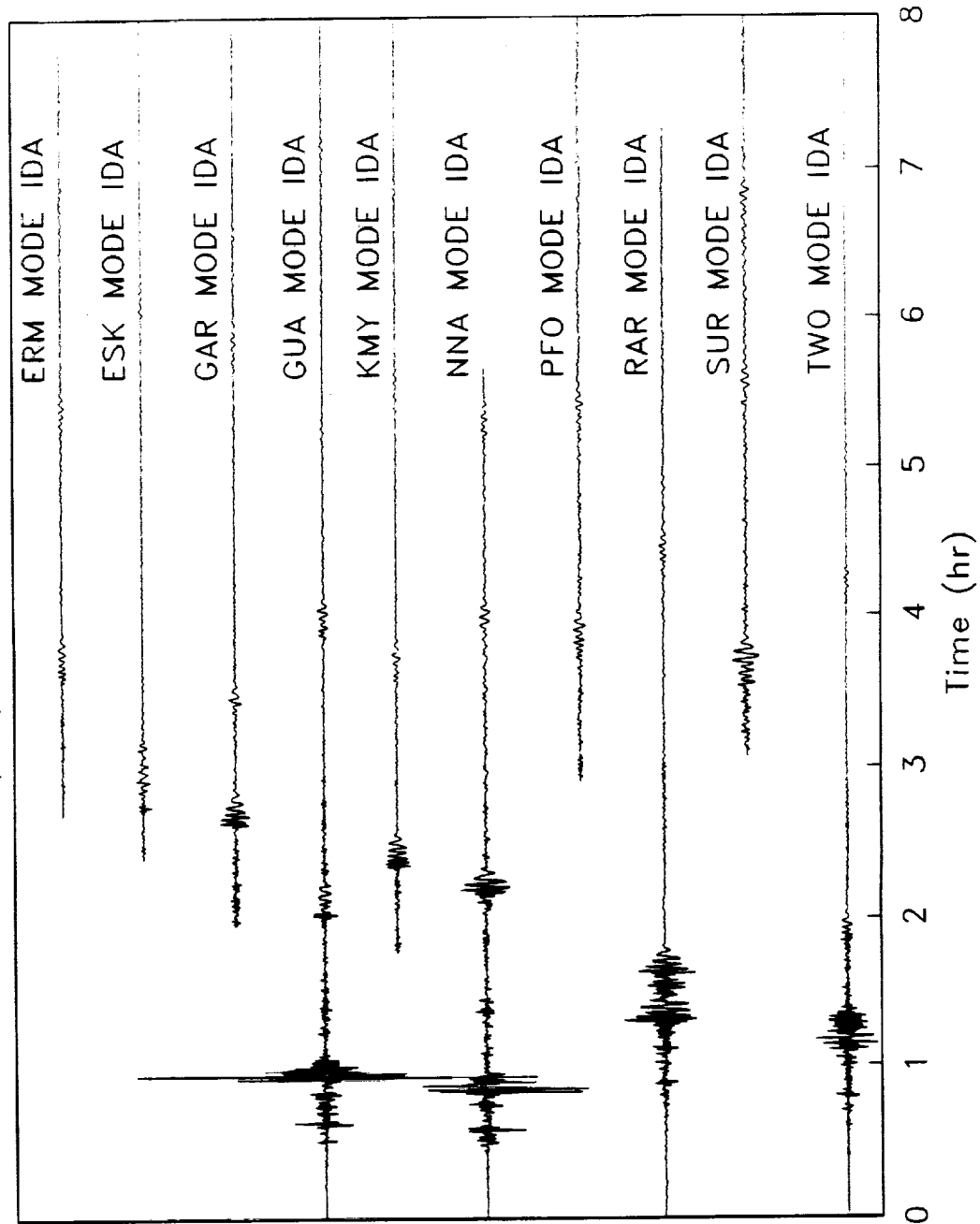
Seismograms used in the inversion.



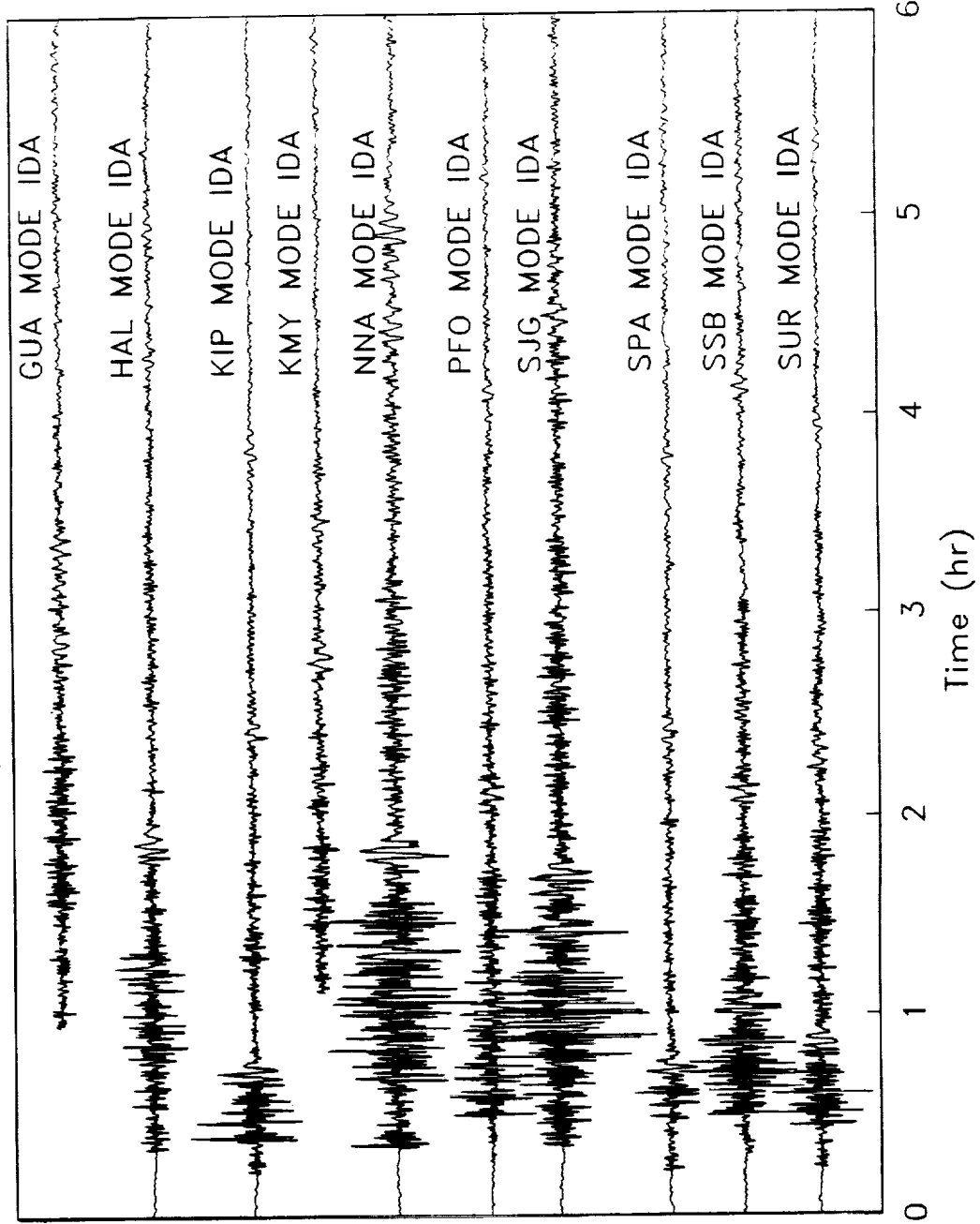
78/09/23 New Hebrides Region



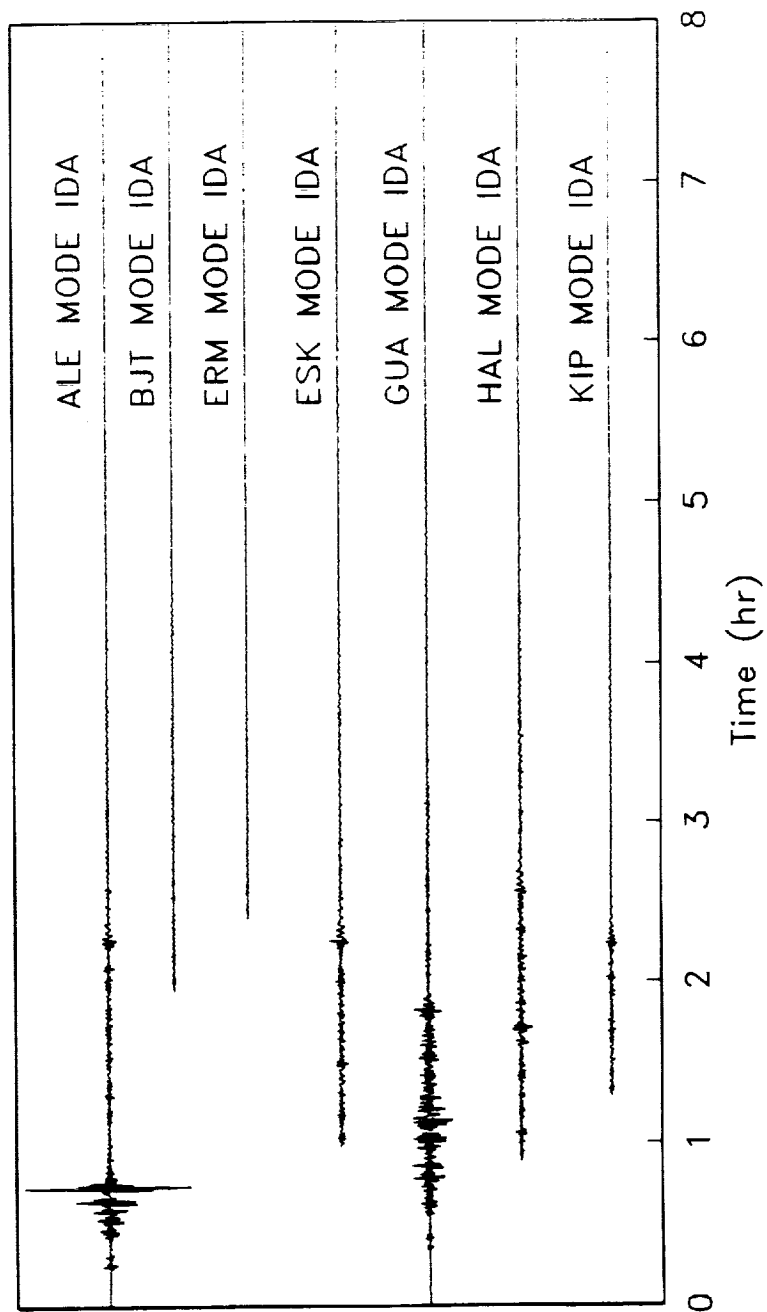
80/11/23 Irpinia, Italy



82/10/07 Banda Sea

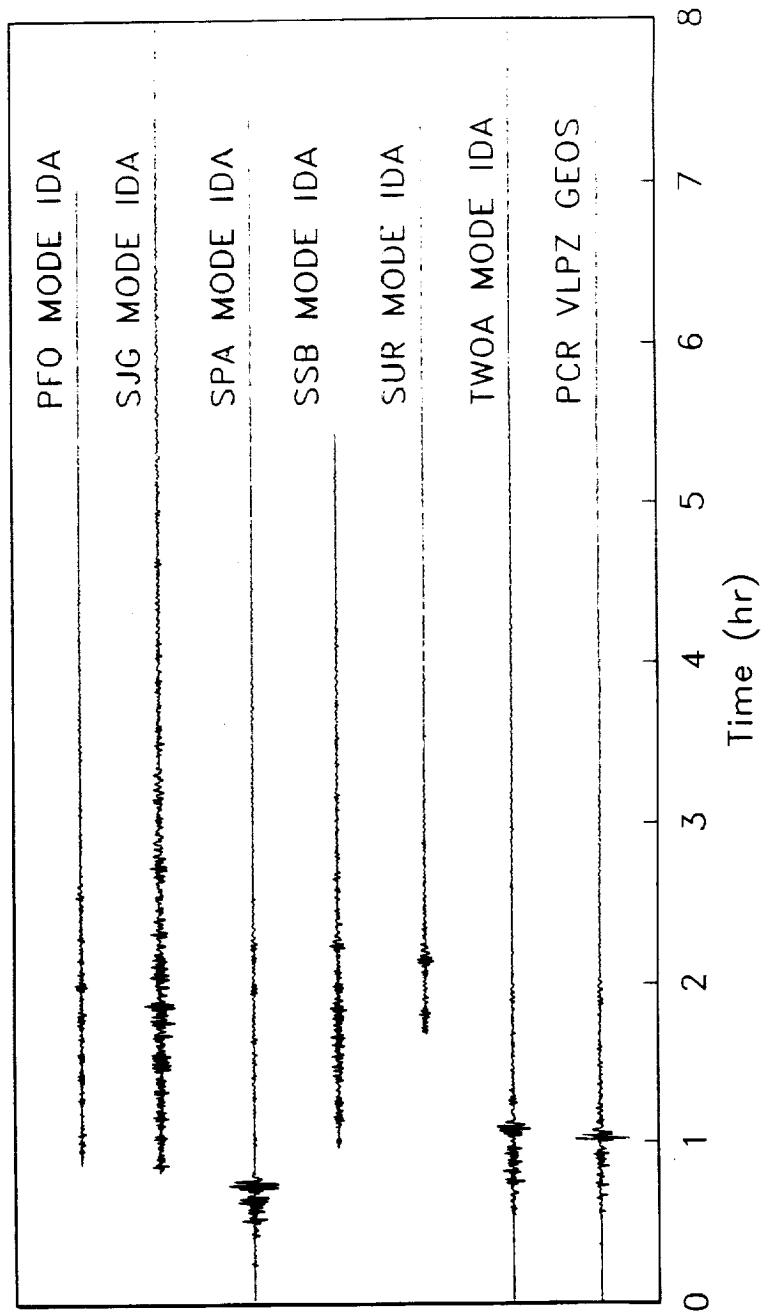


83/04/12 Peru-Ecuador



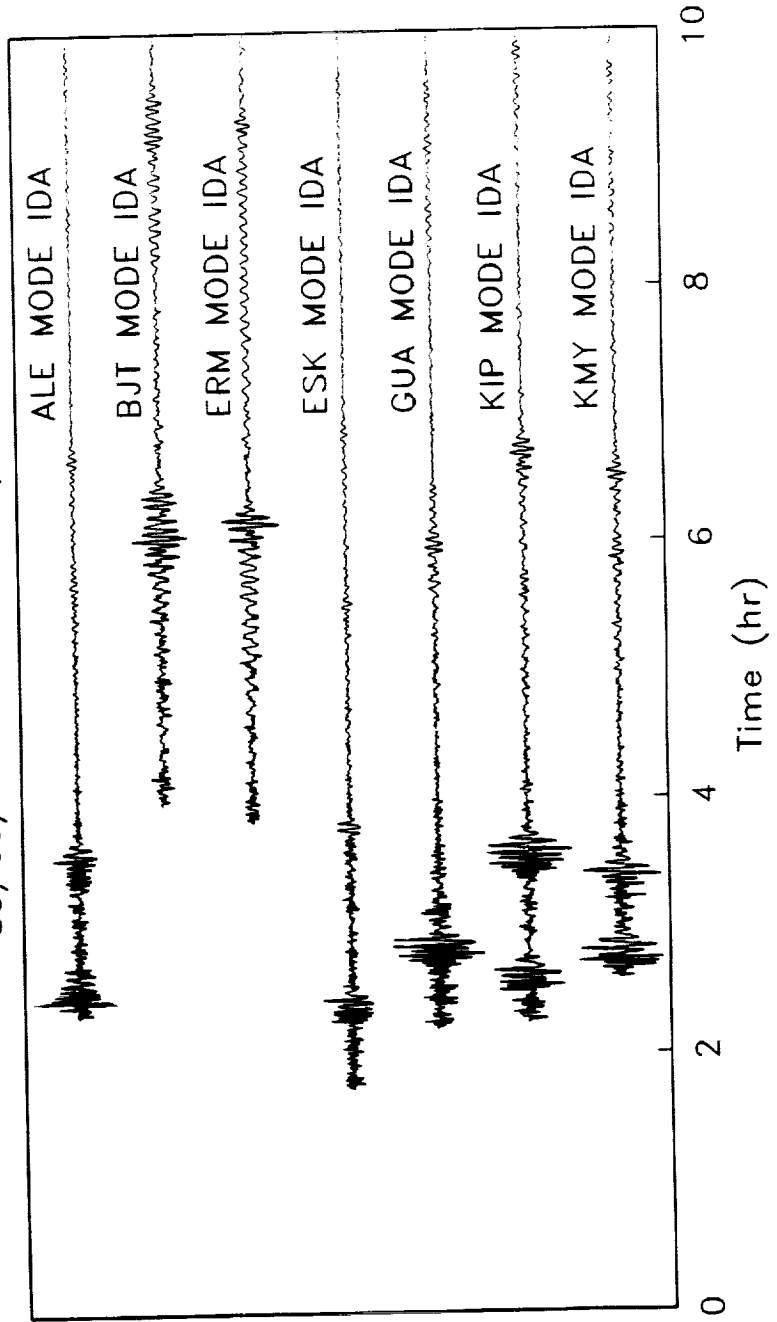


83/04/12 Peru-Ecuador

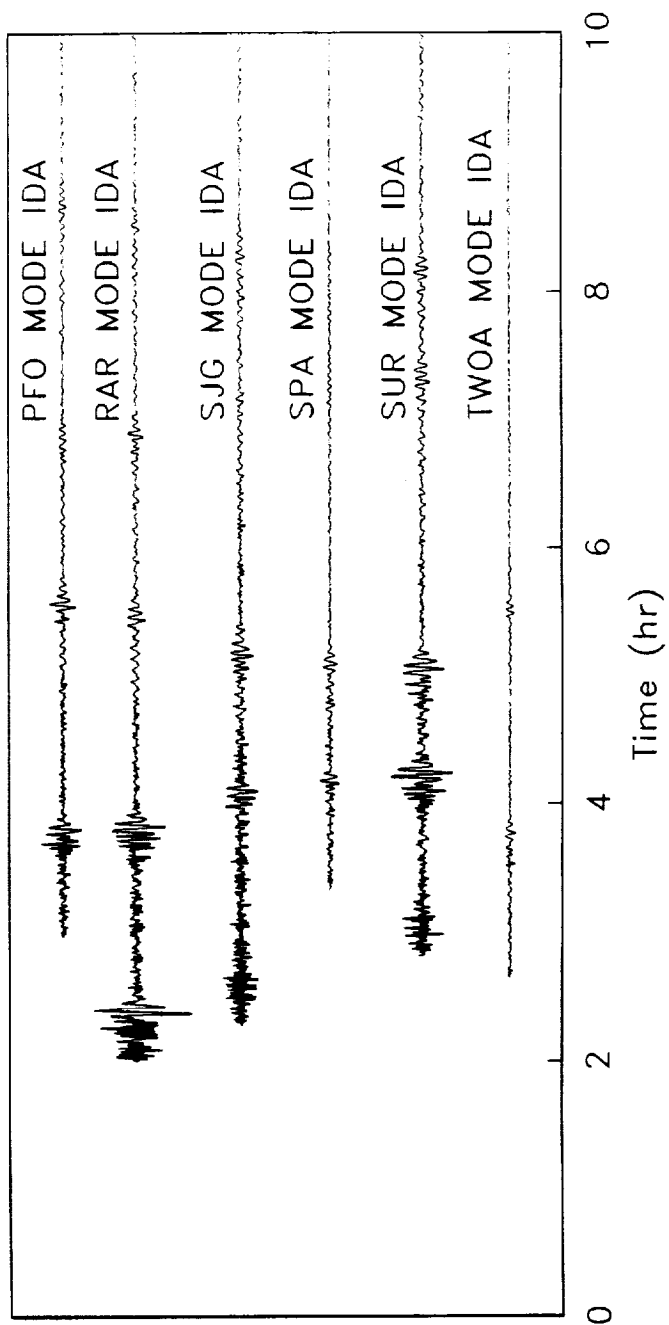


C-2

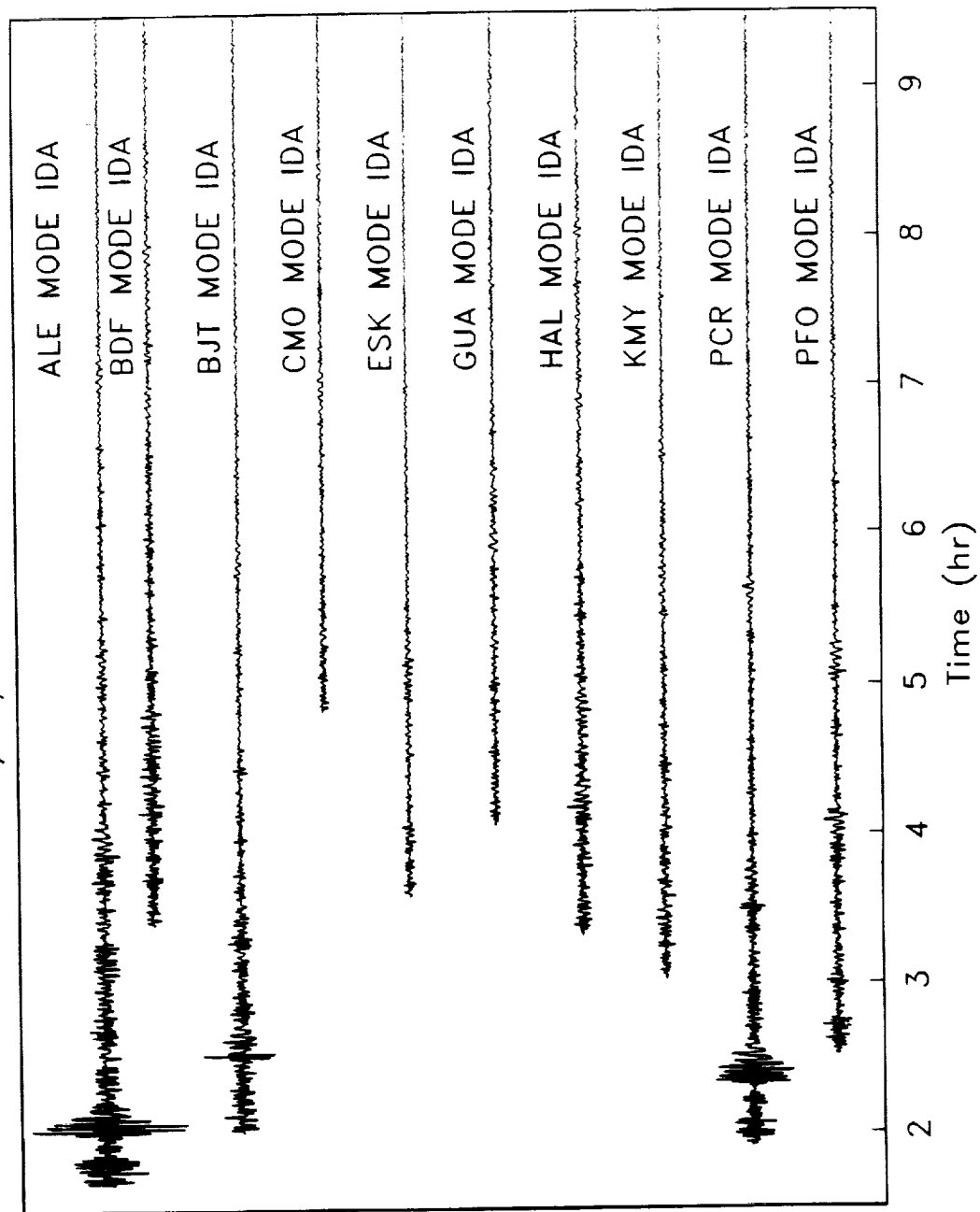
83/05/26 Akita-Oki, Japan



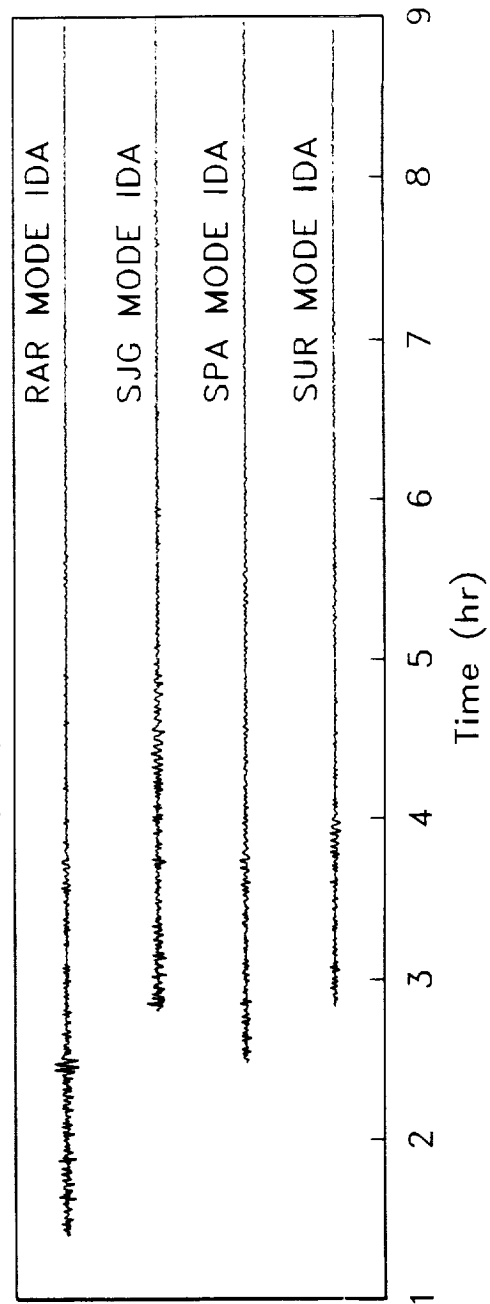
83/05/26 Akita-Oki, Japan



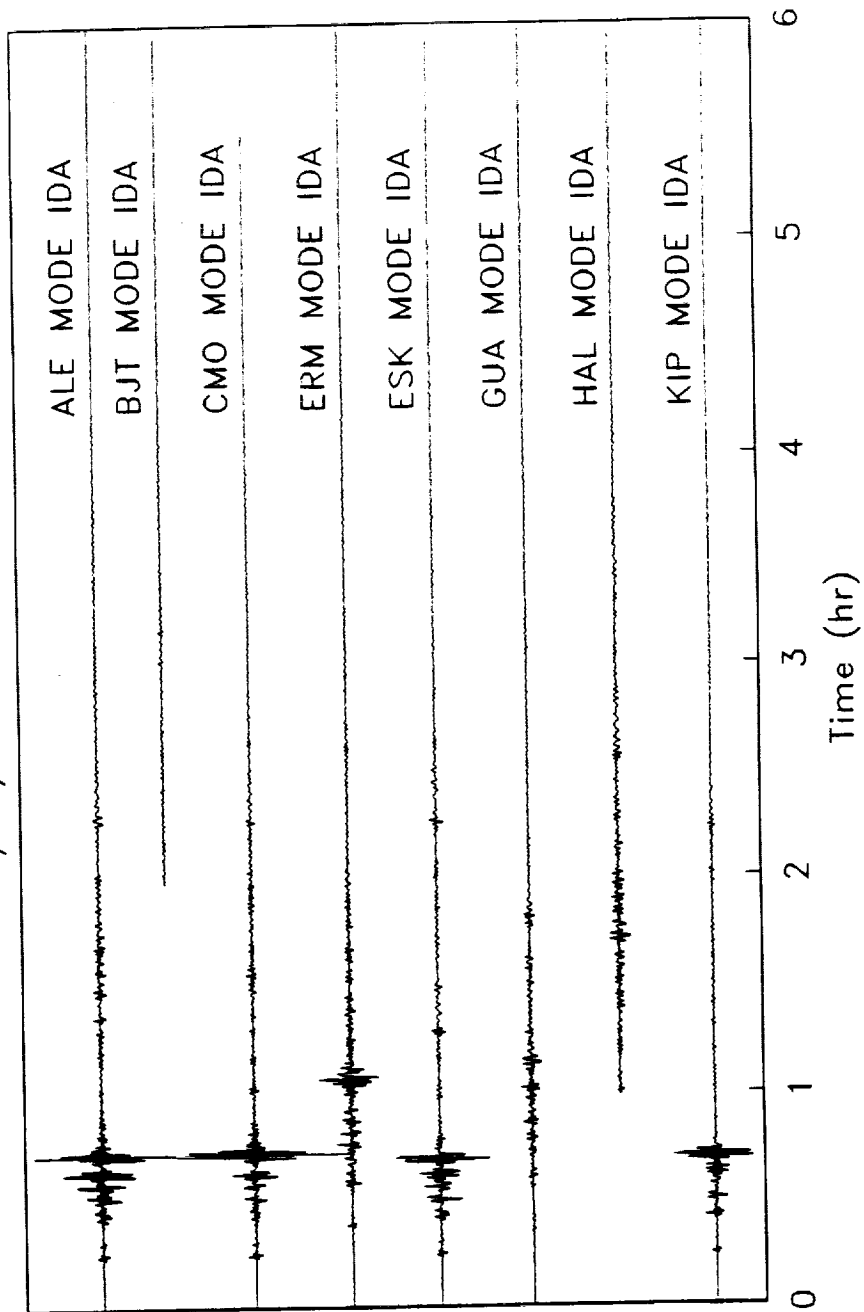
83/11/24 Banda Sea



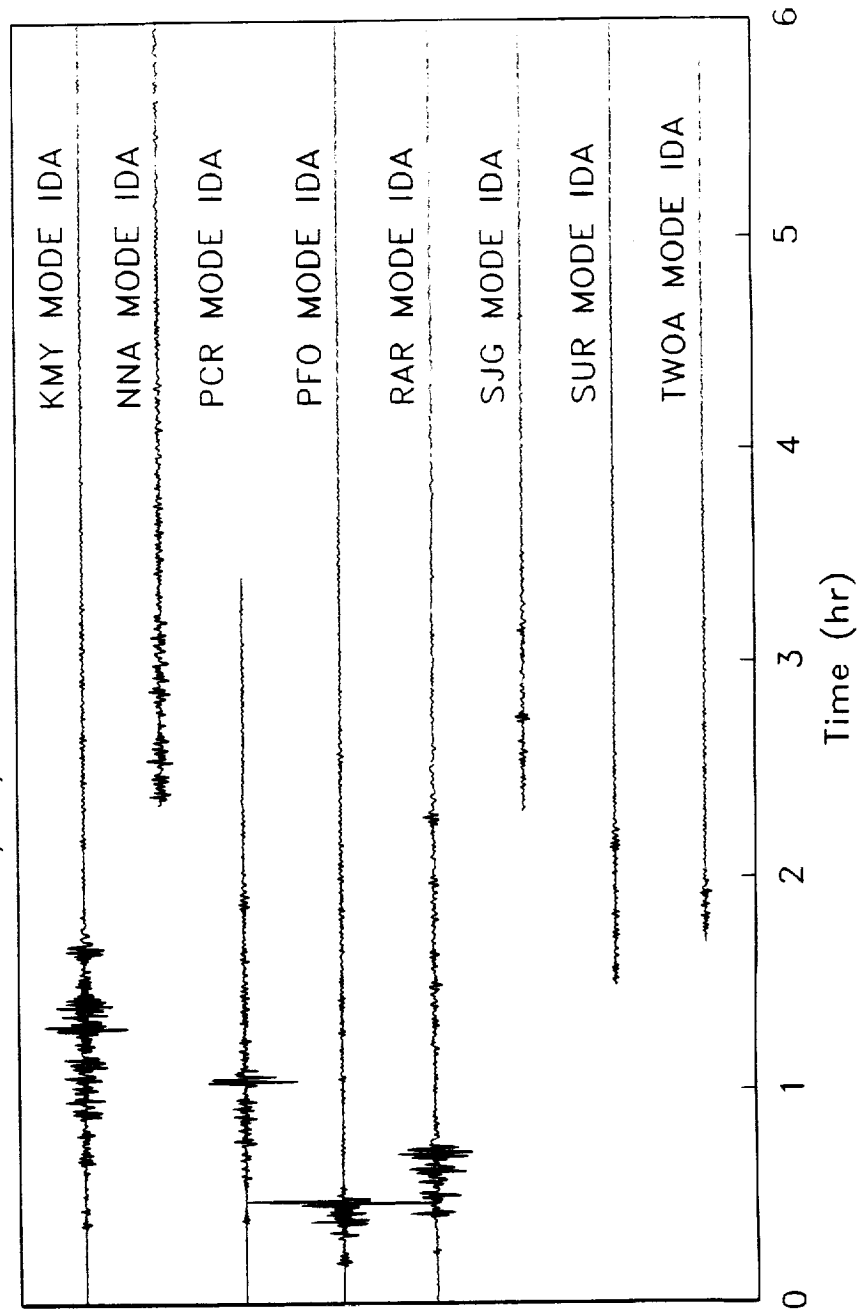
# 83/11/24 Banda Sea



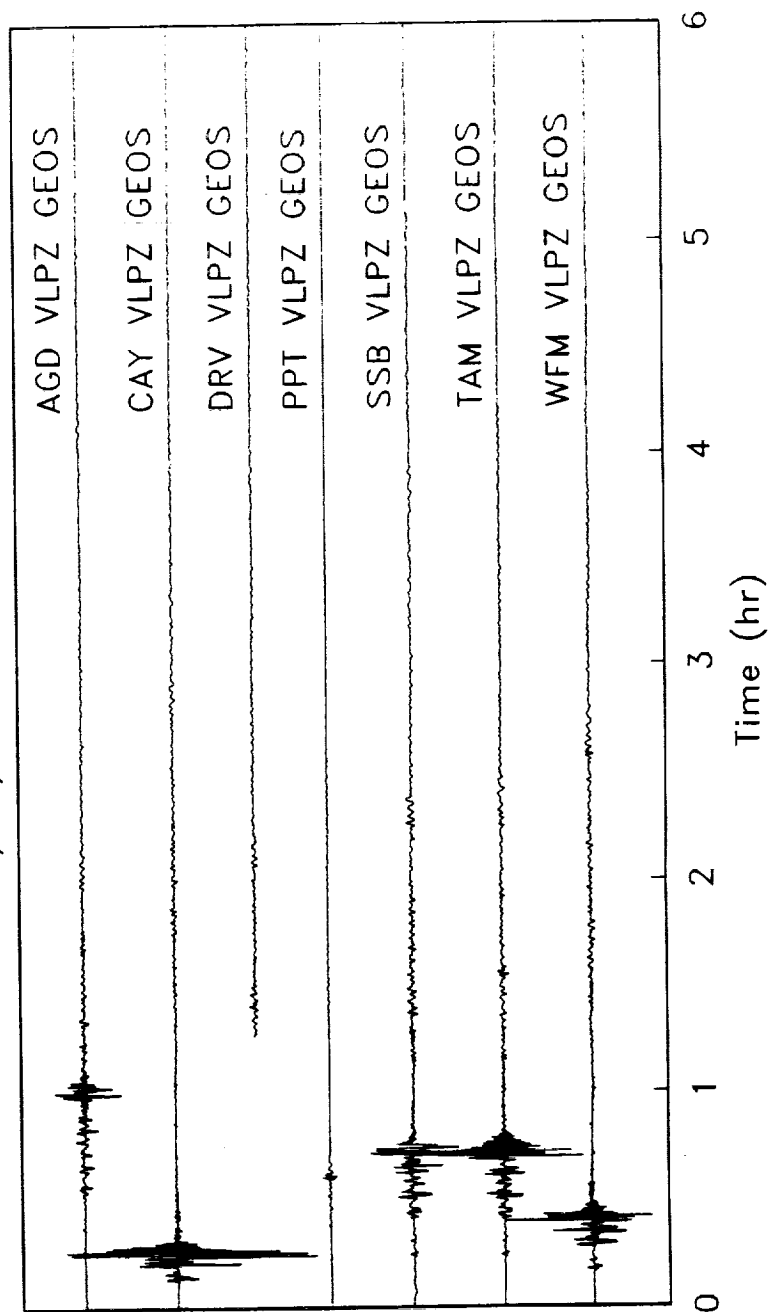
86/11/23 Peru-Ecuador



86/11/23 Peru-Ecuador

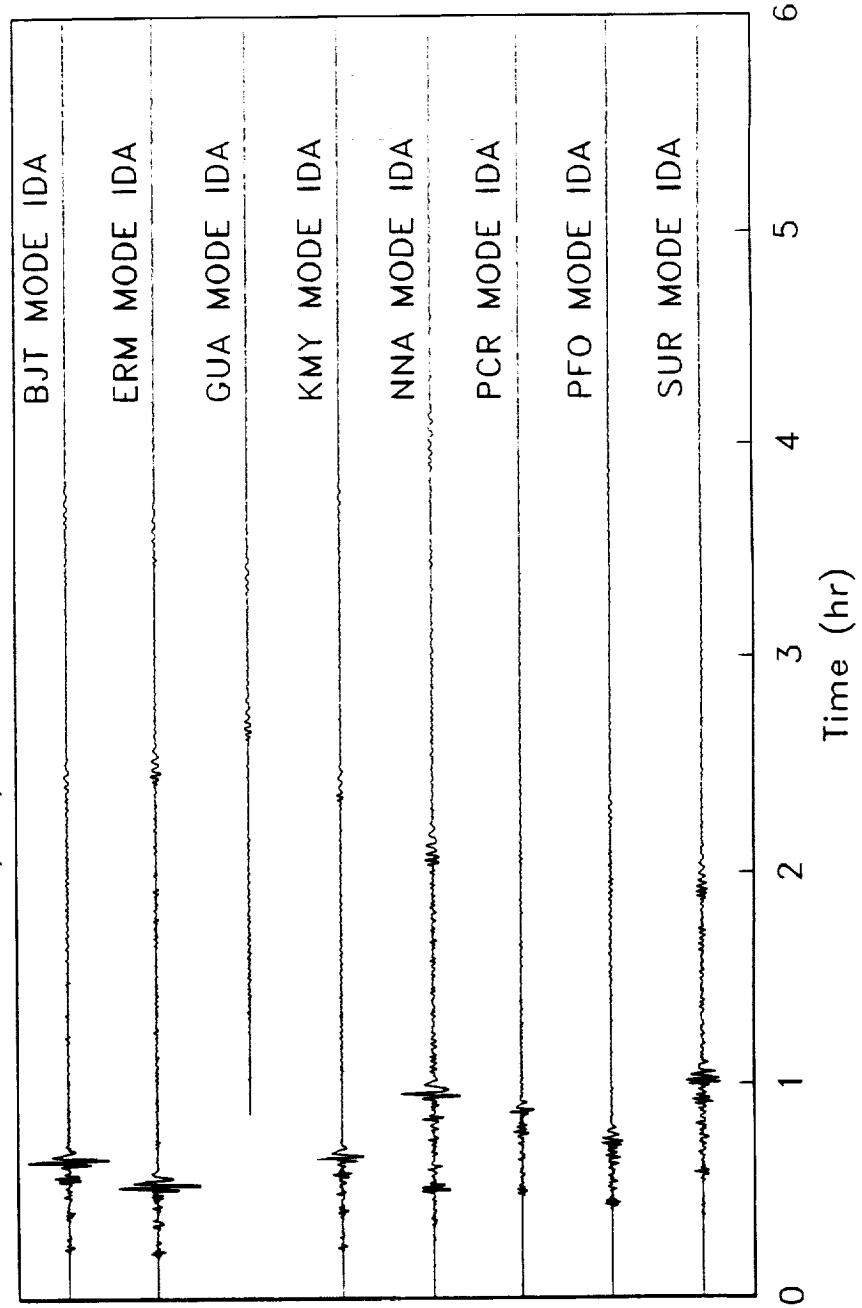


86/11/23 Peru-Ecuador

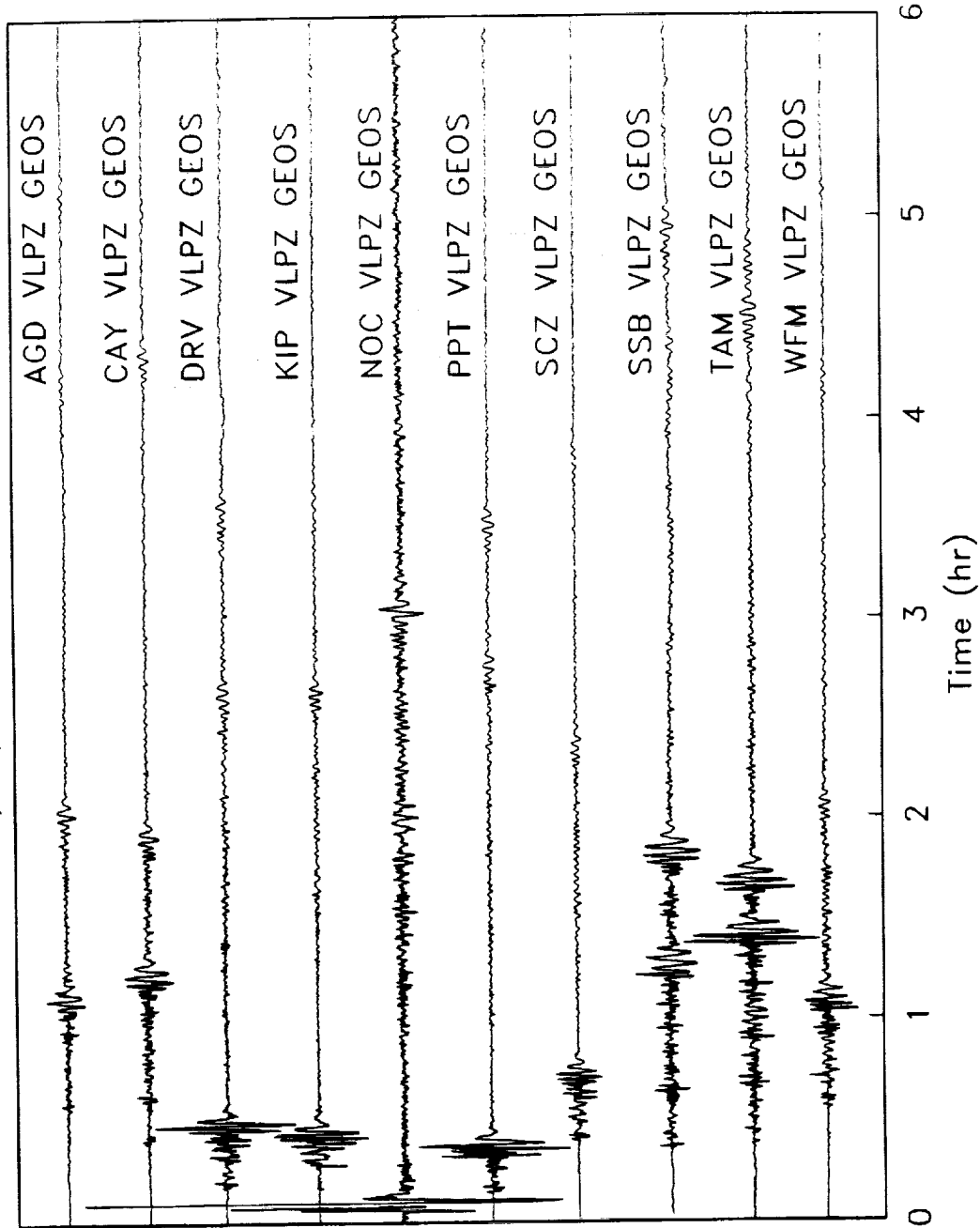




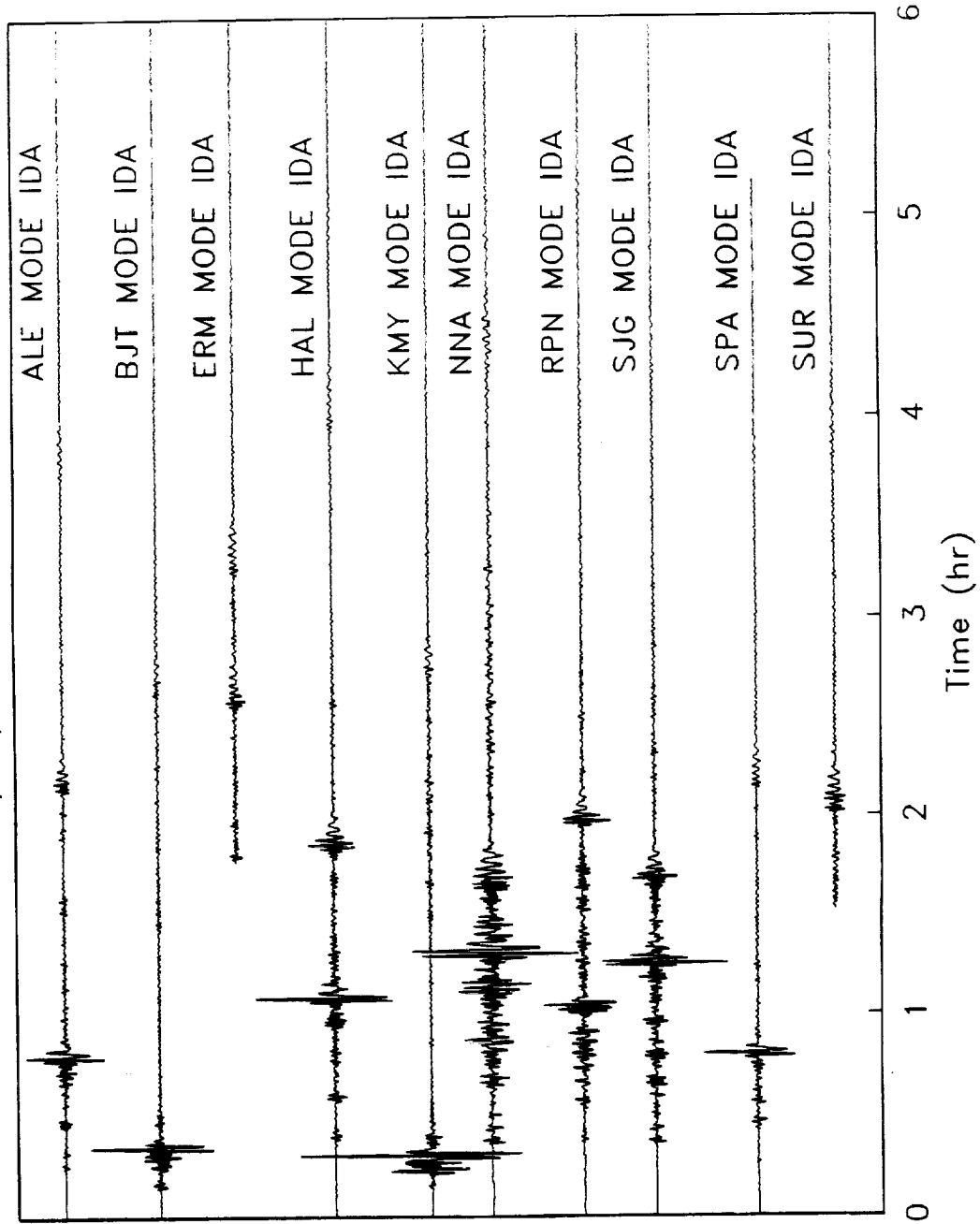
87/02/23 Vanuatu Islands



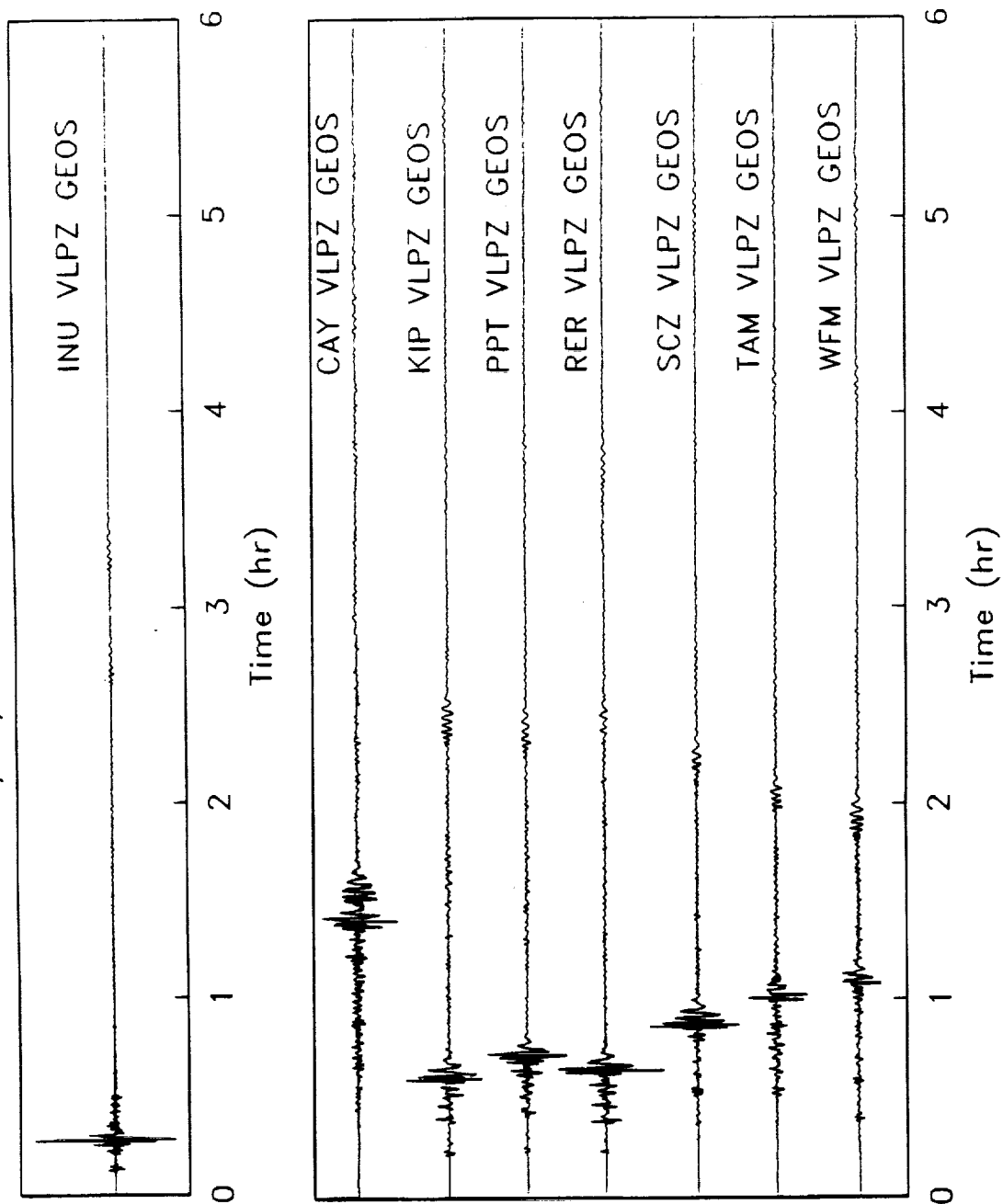
87/02/23 Vanuatu Islands



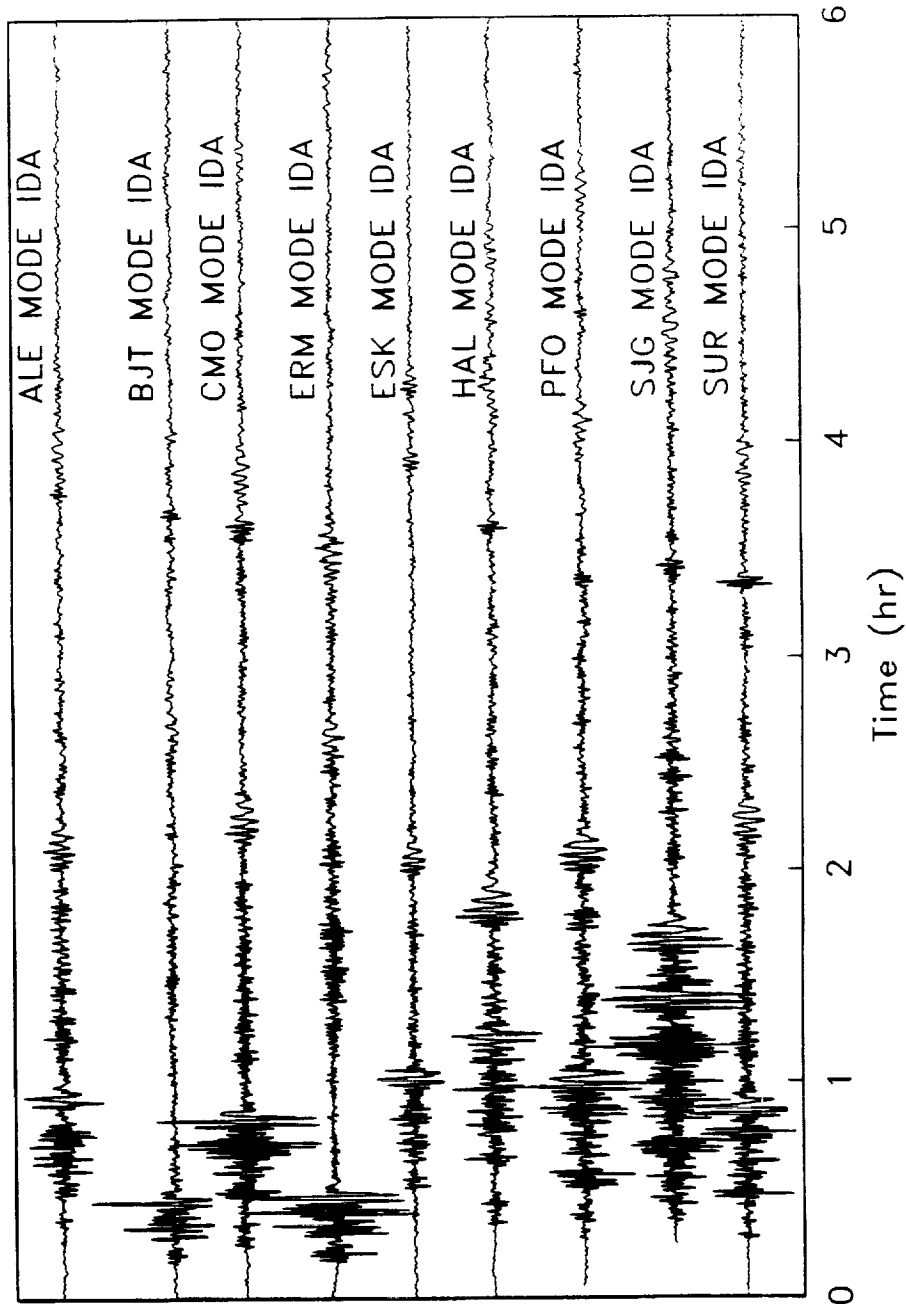
87/10/29 Talaud Islands



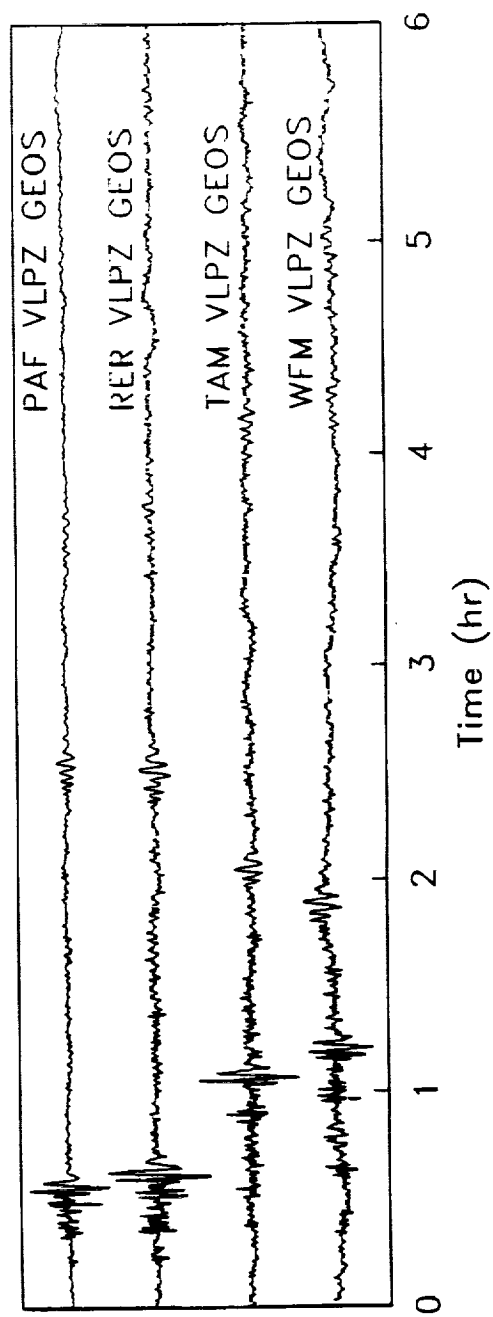
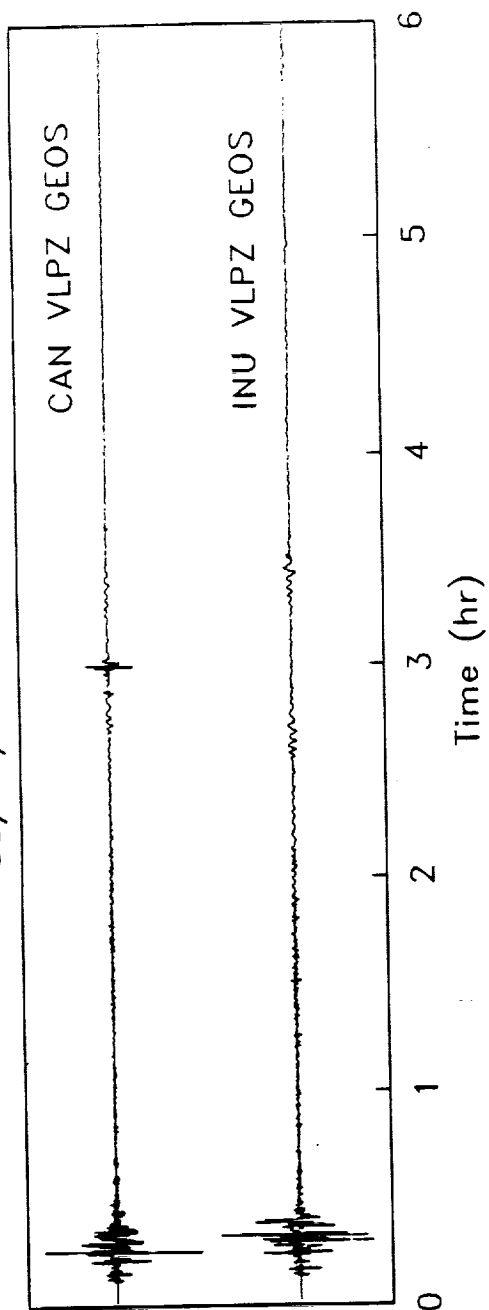
## 87/10/29 Talaud Islands



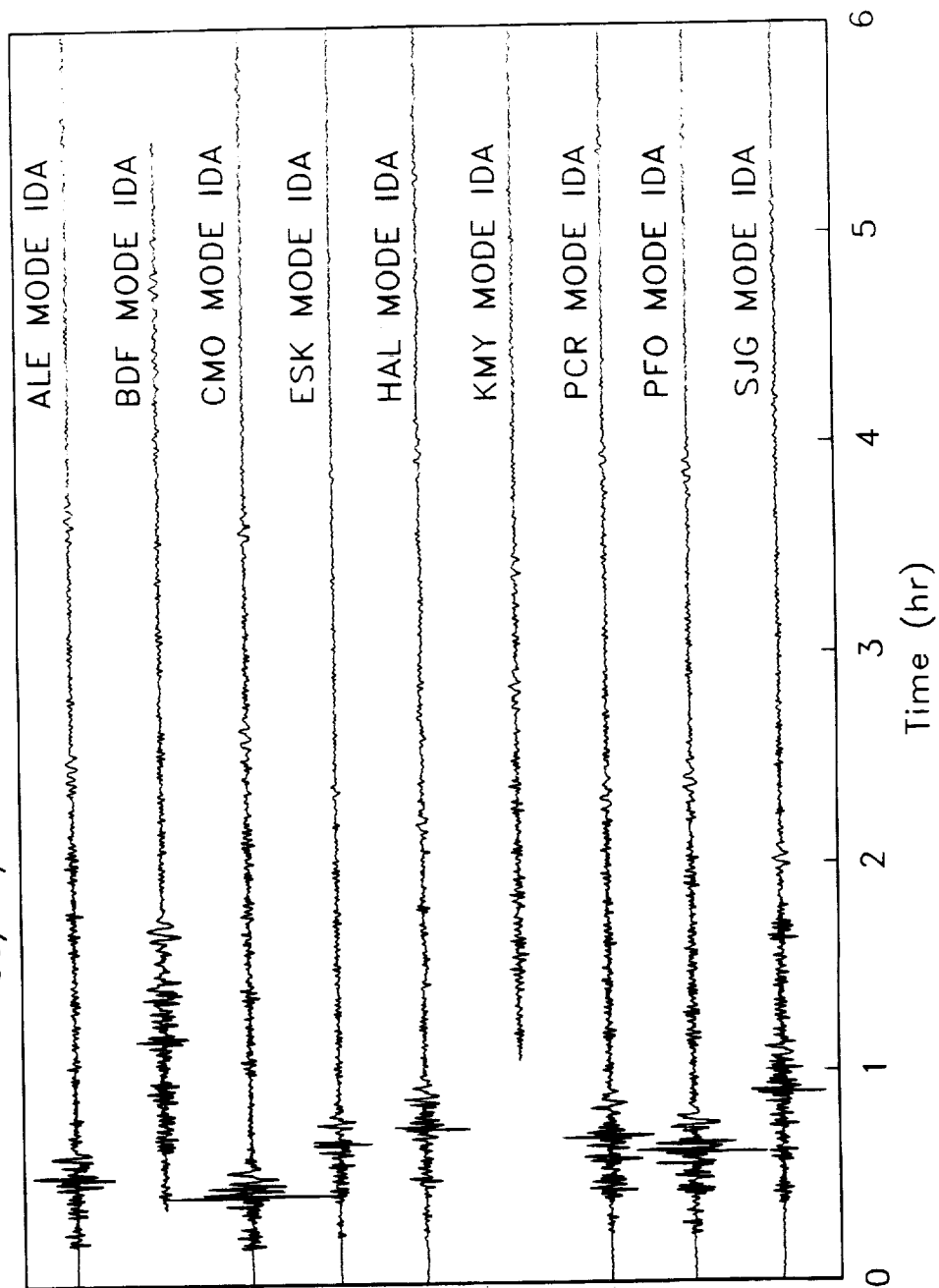
88/02/20 Banda Sea



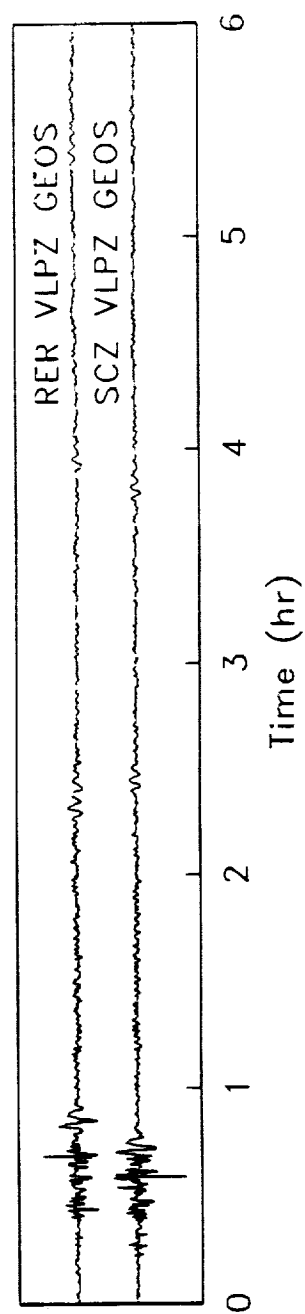
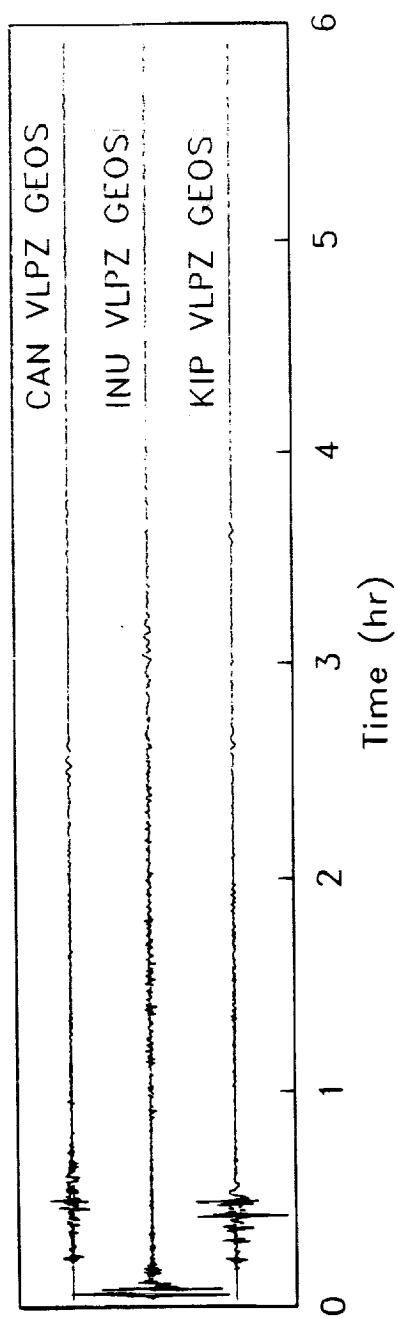
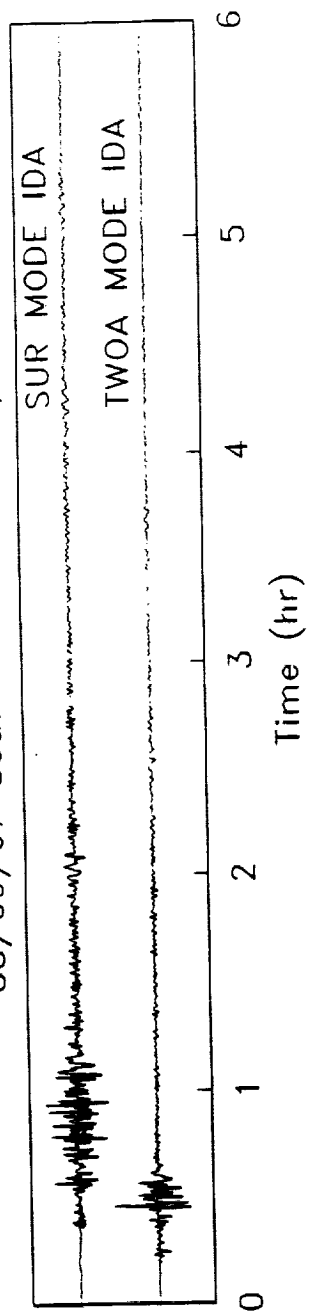
## 88/02/20 Banda Sea



88/09/07 South of Honshu, Japan



88/09/07 South of Honshu, Japan





89/12/03 Peru-Brazil

